King's College London

M.Sc. Programme: Environmental Monitoring, Modelling and Management

Dissertation

Delimiting the Central Business District – A physical analysis using Remote Sensing

by

Martin Klotz
(Student No: 1162118)

Submitted: 2012

Supervision

Prof Dr Martin Wooster
Department of Geography
King's College London

Dr Hannes Taubenböck
DFD - German Remote Sensing
Data Center
DLR - German Aerospace Center

This dissertation is submitted as part of a M.Sc. degree in Environmental Monitoring, Modelling and Management at King's College London.

KING'S COLLEGE LONDON

UNIVERSITY OF LONDON

DEPARTMENT OF GEOGRAPHY

MSc DISSERTATION

I, ……………………………………………………………… hereby declare (a) that this Dissertation is my own original work and that all source material used is acknowledged therein; (b) that it has been specially prepared for a degree of the University of London; and (c) that it does not contain any material that has been or will be submitted to the Examiners of this or any other university, or any material that has been or will be submitted for any other examination.

This Dissertation is ………………………………….words.

Signed: ……………………………………...…………….

Date: ………………...…………………………………….

"The CBD has no fence around it, no wall as there was around the city in Europe in the Middle Ages. You will never see a sign, "You are entering the CBD," although there may be signs directing you to the city's downtown area. However, the district can be conceptualized and its position outlined on a map on the basis of this mental construct. How can this best be done?"

(Raymond E. Murphy, Editor of *Economic Geography*, 1971, p.2)

Abstract

Central Business Districts (CBDs) are important for the functional arrangement of cities and urban risk analysis, however, past research underscores the importance of their spatial delineation. This dissertation presents a conceptual framework to define this urban structure type using physical parameters, and a transferable method to detect and delineate CBDs from a combination of Cartosat-1 high resolution digital surface models and multispectral Landsat images. Applying the method to three European megacities, CBDs are detected with a producer accuracy of 75.71% and spatially delineated with overall accuracies exceeding 82.97%. Cross-city comparison paints a characteristic picture of the spatial CBD configuration.

List of Contents

List of Tables

List of Figures

Glossary

CBD	Central Business District
CBHI	Central Business Height Index
CBII	Central Business Intensity Index
DEM	Digital Elevation Model
DFD	German Remote Sensing Data Center
DLR	German Aerospace Center
DN	Digital Number
DSM	Digital Surface Model
DTM	Digital Terrain Model
EO	Earth Observation
ETM+	Enhanced Thematic Mapper
FIRE	Finance/Insurance/Real Estate
GeoTIFF	Georeferenced Tagged Image File Format
GIS	Geographic Information System
HR	High Resolution
IRS-P5	Indian Remote Sensing Satellite P5
LiDAR	Light Detection And Ranging
LPGS	Level 1 Product Generation System
LPI	Largest Patch Index
MSS	Multispectral Scanner
nDSM	Normalised Digital Surface Model
OSM	Open StreetMap
PAM	Partitioning Around Medoids
PAN	Panchromatic Band
RADAR	Radio Detection And Ranging
RMSE	Root Mean Square Error
SRTM	Shuttle Radar Topography Mission
TM	Thematic Mapper
UN	United Nations
USGS	United States Geological Survey
UST	Urban Structure Type
UTM	Universal Transverse Mercator
VGI	Volunteered Geographical Information
VHR	Very High Resolution

Acknowledgement

1. INTRODUCTION

1.1 The Central Business District in Urban Geography

The Central Business District (CBD) as a concept of Urban Geography has been examined in various contexts. However, definitions of this mental construct are qualitative and no universal theory on its location and spatial extent in complex urban environments exists. Furthermore, few studies on its internal structure have been carried out due to the lack of spatial datasets for this comparatively small geographic zone (Murphey *et al.*, 1955; McDonald and McMillen, 2010). This introduction provides basic characteristics of CBDs, brings the term in line with theories of city structure, and presents existing approaches towards CBD delimitation.

1.1.1 Characteristics of the CBD

One of the most visible features of global cities and their supremacy in national economies are CBDs (Sassen, 2001 and 2002; Drozdz and Appert, 2010). Originating in industrial America, the term CBD was used to describe the downtown of American cities in the 19th century (Pitzl, 2004) but was diffused to the rest of the western world in the following decades. Although settled as a geographic concept, the CBD is difficult to define. Definitions are qualitative such as the CBD is "the nucleus … of an urban area that contains the main concentration of commercial land use" (McColl, 2005, p. 159) or a "unique area of massive concentration of activities and focus for the polarisation of capital, economic and financial activities in cities" (Drozdz and Appert, 2010, p.2). Thus, several authors describe CBDs as areas marked by the various qualitative indicators relative to the surrounding urban environment (Table 1-1).

Tab. 1-1 Qualitative features of CBDs (Murphy, 1971; Waugh, 2000; Haggett, 2001; Heineberg, 2001)

Qualitative feature
- main concentration of commercial land use;
- main concentration of the city's offices and high employment density;
- dominance of tertiary sector activities;
- peak land values;
- tallest buildings within a city;
- high degree of accessibility and traffic density;
- high daytime vs. low night-time population and low resident population.

Literature on the temporal development of CBDs provides recent discussions about the decline of existing CBDs (Coffey *et al.*, 1994) in favour of new business districts in peripheral locations and therefore, functional separation (Baerwald, 1978; Borusso and Prorceddu, 2009). Hence, business districts remain important for the distribution of functional spaces within cities.

1.1.2 Theories of city structure and the CBD

Burgess (1929) was among the first interested in the functional arrangement of cities. In his concentric zone model, the CBD represented the inner core of functional concentric land use zones and the origin of marginal urban growth. Hoyt (1939) advanced this model by the concept of land pricing with maximum values within the CBD and the importance of transportation routes leading to axial urbanisation and sectoral zoning. Contrasting the growth around a single urban core, Harris and Ullman (1945) developed a model of patchy urban form with multiple centres of specialised functions, thus, being an early model very accurate for the description of today's internal configuration of cities (Figure 1-1).
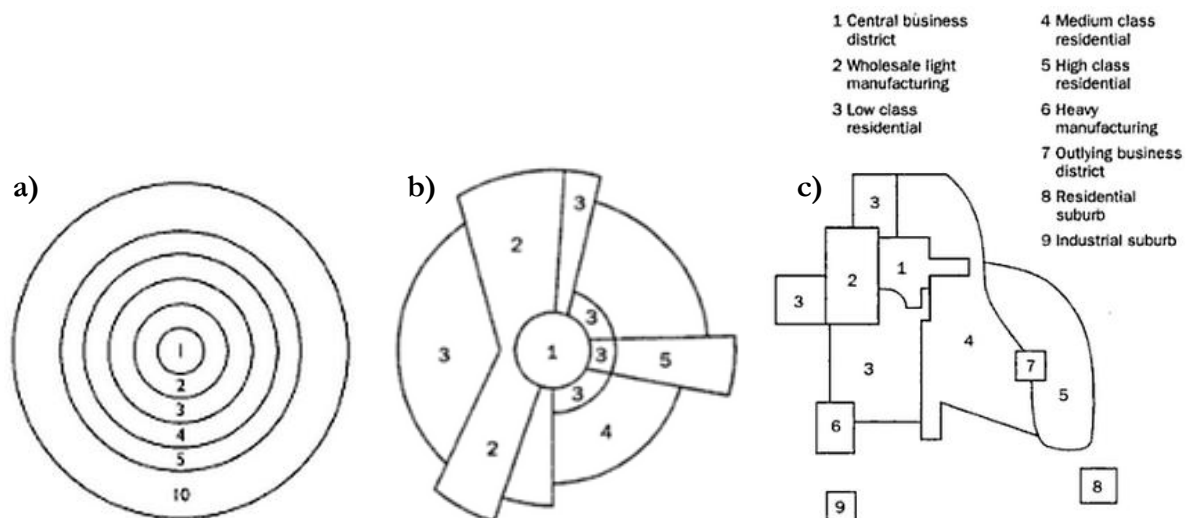
Fig. 1-1 a) Concentric zone model b) sector model, and c) multiple nuclei model (Harris and Ullmann, 1945)

Since the 1960s, more complex theories have been developed. Central places' theory highlights the significance of human activities for the definition of urban hierarchies (Berry and Allen, 1961) with the CBD as the service centre of the highest order within a city. Furthermore, several authors dealt with density functions regarding land use/value or the occurrence of transportation infrastructure decreasing from the CBD towards the urban fringe (Alonso, 1960; Knos, 1962).

In recent years, the scientific discussion on urban form shifted towards mono- versus polycentric urban patterns (Hoch and Waddel, 1993; Waddel *et al.*, 1993) stressing the emergence and

coexistence of new CBDs in peripheral locations (Heikkila *et al.*, 1989; Fogelston, 2001). Prominent examples are the new business districts at Carnary Wharf, London or Lujiazui CBD, Shanghai (Borusso and Prorceddu, 2009). To analyse these emerging spatial patterns, new methods have been employed including geographic information systems (GIS) (Batty and Longley, 1994), remote sensing (Wegmann *et al.*, 2011), and urban modelling (Benenson and Torrens, 2004).

1.1.3 Existing delineation techniques

First studies on the delineation and cartographic representation of CBDs were based on observation and perception (Murphey, 1971). By contrast, Murphey and Vance (1954a) aimed to quantify activities being central to the urban environment using indices of central business height (*CBHI*) and intensity (*CBII*). Defining a set of typical central business land uses, they calculated the two metrics on block level (eq. 1 and 2) and spatially delimited CBDs using distinct thresholds (Figure 1-2). In a study (Murphey and Vance, 1954b), they applied this Central-Business-Index-Technique to compare nine American CBDs in terms of shape and spatial extent.

$$CBHI = \frac{total\ floor\ area\ in\ central\ business\ use}{total\ ground\ floor\ area} \tag{1}$$

$$CBII(\%) = \frac{total\ floor\ area\ in\ central\ business\ use}{total\ floor\ area} x100 \tag{2}$$

In the following years, various indicators of urban centrality have been used for CBD delimitation in case studies: Carol (1960) emphasised the significant difference between day and night-time population whereas Ning (1984) and Erteking (2008) analysed spatial pattern and hierarchical structure of shopping malls. Furthermore, Guillain (2006) and Marguilos (2007) used spatial distributions of employment and real estate to measure centrality.

Due to increased availability of spatial datasets and analytical tools, generation and analysis of density surfaces such as population or commerce have recently gained attention for the detection of urban centres in several GIS-based approaches (Thurstain-Goodwin and Batty, 1998; Borusso and Prorceddu, 2009; Zheng, 2009). For example, Thurstain-Goodwin and Unwin (2000) calculated centrality based on a continuous density transformation of spatial variables such as building density and residential population from geocoded unit postcode data.
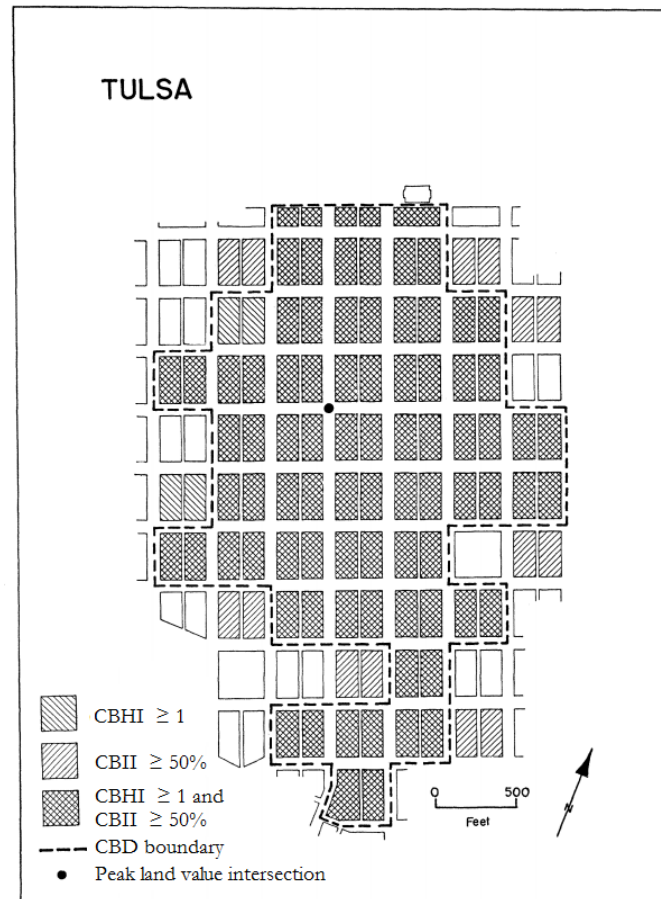
Fig. 1-2 CBD delimitation for Tulsa, Oklahoma (Murphey and Vance, 1954b)

Although a certain amount of research towards CBD delineation has been carried out, no universal method exists. All of the presented methods rely on spatial data availability of socioeconomic variables from land use surveys and therefore, are often limited to small geographic regions regarding their transferability. In this context, remote sensing should be reconsidered as a tool for large-scale urban monitoring and structuring.

1.2 Urban Remote Sensing

1.2.1 Remote sensing of urban environments

In the last decades, the majority of research based on earth observation from space has been applied to natural environments whereas the application of remote sensing to urban areas is relatively new (Weng and Quattrochi, 2007). However, the capabilities of remote sensing for studies on urban environments for reasons of widespread availability of datasets, frequency of update and costs are now widely recognised (Donnay and Barnsley, 2001; Netzband et al., 2007).

Today, not only optical, but also radar (radio detection and ranging) sensors which are capable of acquiring data independent from weather and time of day at very fine spatial resolutions, as well as topographic datasets derived from LiDAR (light detection and ranging) or stereophotogrammetric measurements are used to study urban phenomena, specifically supporting data fusion approaches (e.g. Wurm *et al.*, 2011). Such studies include the detection of urban heat islands (Streutker, 2002), land use change detection (Mas, 1999), population estimation (Wu *et al.*, 2007), or the analysis of urban morphology (Longley and Mesev, 2000). Furthermore, very high resolution (VHR) optical satellite-based sensors of the commercial sector provide crucial information for urban planning on building level (Albertz, 2007; Wurm and Taubenböck, 2010) and exceed the capabilities of traditional pixel-based analysis techniques. Thus, new analytical concepts such as object-based feature extraction have been developed (Wang and Schenk, 2000; Blaschke, 2010; Taubenböck *et al.*, 2010).

Another application of remote sensing is linked to rapid worldwide urbanisation: Cities are projected to absorb almost all of the world's population growth in the future (UN, 2008). In this context, area-wide and up-to-date information for spatiotemporal analysis of urban sprawl is on demand. An indicator for the degree of urbanisation is the urban footprint of a city, i.e. the land covered by impervious surfaces. Taubenböck *et al.* (2012) extracted and comparatively analysed the spatiotemporal development of urban footprints for all global megacities. However, these studies do not allow for the identification of the internal urban structure such as the spatial delineation of CBDs as a physical reflection of a city's temporal evolution (Wurm *et al.*, 2009).

1.2.2 Urban structuring using remote sensing

As already indicated, CBDs are a distinct urban structure type (UST) defined not only by individual buildings, but also by the surrounding urban morphology. Recent research has employed remote sensing to quantitatively describe the spatial structure of urban environments and characterise morphological patterns but has shown strong dependence on data availability and the purpose of structuring (Taubenböck *et al.,* 2008a). For ecological purposes, a straight-forward urban biotope mapping approach has been used (Sukopp and Wittig, 1998; Bochow *et al.*, 2007). A similar approach can be chosen for the structuring of the built-up landscapes into USTs on block level (Wurm *et al.*, 2009). This scale presents statistical reference units that allow classification of a city into areas homogenous in terms of a combination of physical characteristics, land use, and land cover from the heterogeneous arrangement of individual buildings, streets and open spaces. Furthermore, USTs on block level enable a certain degree of

transferability and comparability as they fit into the hierarchical structure of urban administrative units with a direct reference to both the higher level of urban morphology (local districts) and the lower level of individual structure elements (buildings) (Figure 1-3) (Wurm and Taubenböck, 2010).
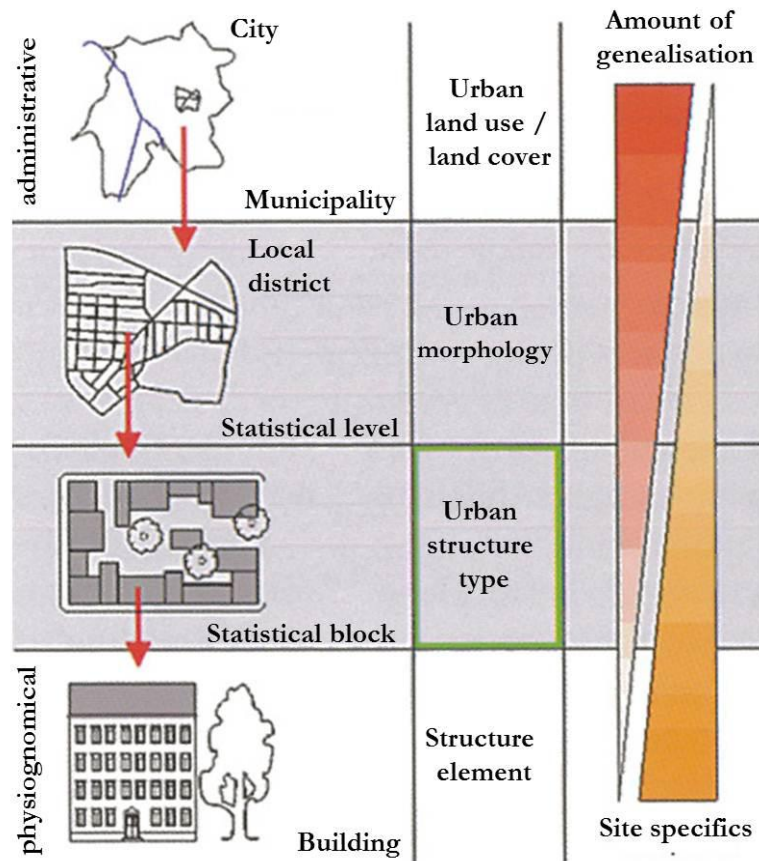
Fig. 1-3 Scale-dependent analysis of USTs (Sukopp and Wittig, 1998)

Various studies on urban structuring using remote sensing have been carried out in the past including methodological concepts such as spatial metrics (Angel *et al.*, 2005; Herold *et al.*, 2002), object-oriented classification using decision trees (Wurm *et al.*, 2009), or supervised classification (Bochow, 2010). In addition, several authors aimed at the delineation of particular USTs such as slums (Netzband *et al.*, 2009). However, most approaches remain on the stage of case studies and are limited in terms of spatial coverage. Exceptions include the study by Herold *et al.* (2003) who used spatial metrics and image texture parameters from VHR Ikonos images to map urban land use in southern California and Wurm *et al.* (2009) who classified the urban structure of two German cities combining VHR Ikonos and LiDAR data from airborne lasercanning. However, these studies require the compilation of relatively costly VHR datasets of high data volume and

are therefore rarely transferable beyond case studies. Although some quantitative descriptions of the physical appearance of CBDs exists (e.g. Pan *et al.*, 2008), no study towards spatial delineation of the UST using earth observation has been carried out before, underscoring the importance of the CBD for the functional arrangement of cities.

1.3 Research objectives

As indicated in this brief introduction, CBDs are a mental construct that does not feature a clear geographic boundary but exhibits certain qualitative characteristics. Based on these characteristics, existing approaches towards CBD delineation either rely on socioeconomic datasets or land use surveys that are rarely available for spatially extensive urban environments, thus, limiting the general transferability of these methodological concepts. Therefore, a distinct research gap towards urban structuring with regard to CBDs in general and transferrable methods for spatial CBD delineation in particular, exists, especially for large-scale and complex urban landscapes.

Overall, the state of the past research does not embrace the importance of the location and spatial extents of CBDs regarding the functional arrangement of cities for urban planning. This knowledge would also benefit applications of urban risk analysis. With regard to natural catastrophe loss modelling, a spatial mismatch exists for hazard data commonly modelled on pixel level, and exposure data often only available for aggregated spatial units (Thieken *et al.*, 2006). Thus, regionalisation techniques such as dasymetric mapping (Holt and Lu, 2011) aim at the spatial disaggregation of exposures to finer spatial resolutions (Kron, 2005; Wünsch *et al.*, 2009). In this context, a valid data basis for land use-based disaggregation of exposure data is on demand, especially for CBDs which concentrate high volumes of asset values on small spatial extents.

In this context, the bird's eye view of remotely sensed data is reconsidered as an independent, area-wide, and consistent data basis for urban monitoring and structuring. Due to capabilities of remote sensing measuring the physical face of cities from space and the aforementioned lack of suitable spatial datasets for CBD delineation, this dissertation aims at identifying characteristic physical features of the built-up environment that define CBDs. Furthermore, a method towards CBD detection and delineation from high resolution (HR) digital surface models (DSMs) for large scale urban agglomerations is developed. Applying the developed method to three

European megacities confidence is gained about the accuracy of results and transferability of this method. In the context of this dissertation, the following research questions (Table 1-2) will be addressed.

Tab. 1-2 Research questions addressed in this study

No.	Research question
(1)	Which physical parameters from the published literature can be used to delineate CBDs as an urban structure type?
(2)	Do CBDs feature physical differences regarding these parameters compared to surrounding urban structures?
(3)	Which remote sensing datasets are suitable for the delineation of CBDs based on physical parameters in large-scale urban environments?
(4)	How can CBDs be delineated from these datasets?
(5)	How accurate are the results regarding spatial delineation and detection?
(6)	Are there differences and analogies in the spatial configuration of CBDs across European megacities?

1.4 Conceptual framework of the study

For a systematic approach towards the overall goal of this study, a conceptual framework consisting of five logical sequences of working stages has been developed (Figure 1-4).

As indicated before, CBDs do not feature distinct physical thresholds or spatial boundaries. Thus, the central hypothesis of this study is based upon qualitative statements on the physical nature of CBDs: In cities that are known to exhibit CBDs, these USTs can be differentiated from the surrounding urban morphology based on physical parameters.

Based on this hypothesis, a quantitative physical analysis and statistical designation of CBDs from the surrounding urban structures is performed. For this purpose, highly detailed 3D city models are compiled from spatial datasets for test sites of three European mega cities that are known to contain CBDs. As literature provides qualitative descriptions of the essential features of CBDs that allow for a physical parameterisation of the UST, the 3D city models are statistically analysed to spatially designate CBDs and derive distinct parameter thresholds.

With these analysis results at hand, the remote sensing analysis focuses on the delineation of CBDs from remotely sensed datasets. This analysis includes the selection of suitable datasets for large-scale urban structuring as well as the implementation of a transferable method. For the implementation of the method, it is resorted to the parameters and thresholds identified in statistical designation procedure.

To assess accuracy and performance of the presented method, a straight-forward approach to quantify spatial delineation and detection accuracies with regard to the statistical reference is put forward resulting in an evaluation of the method and its subproducts. Thus, confidence about the thematic results and the transferability of the methods with regard to the central hypothesis is gained.

Finally, a thematic analysis using spatial metrics in a cross-city comparison to detect analogies and differences of spatial CBD configuration is conducted.
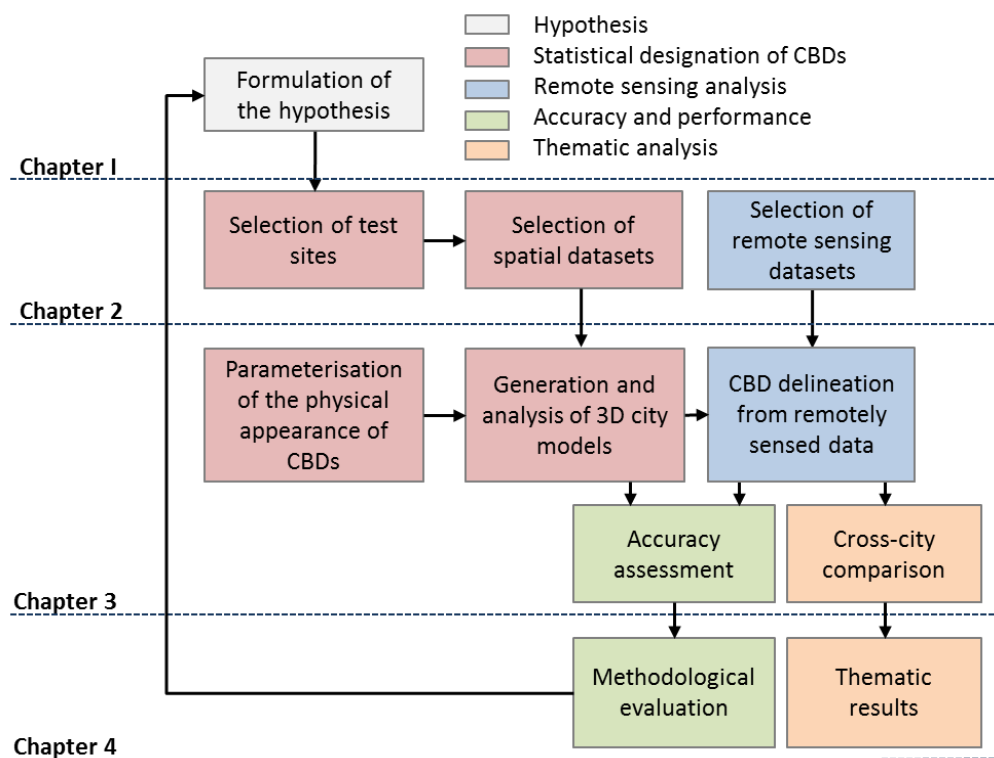
Fig. 1-4 Conceptual framework

2. STUDY SITES AND DATA

2.1 Study sites

According to McColl (2005), most large cities exhibit CBDs, especially global cities where international financial business centres can be found. Therefore, the selection of study sites is straight-forward by reason of three attributes to cover the spatial and thematic spectrum of urban morphology (Table 2-1). Consequently, two European megacities, i.e. conurbations exceeding 10 million inhabitants (UN, 2007), and one city projected to pass this threshold shortly, were selected. All of these cities feature one or more well-described CBDs that are used as city-internal test sites. These will be described in the following sections. Photo impressions of the test sites are shown in figure 2-1.

Tab. 2-1 Study site selection criteria

No	Criterion
(1)	*the size of the city:* based on population numbers;
(2)	*existence of an already identified CBD within the selected city based on the literature*;
(3)	*the age of the CBD:* based on the availability of acquisition dates of the selected remote sensing data sets;

2.1.1 London, Carnary Wharf

London currently inhabits 9.0 million people (UN, 2012a) but is projected to pass the 10-million-threshold by 2025 (UN, 2012b). The city's clustered distribution of specialised industries is unique (GLA, 2008). Representing its international economic competiveness and significance as a global centre for the FIRE (finance/insurance/real estate) sector (Frug and Baron, 2008), the CBD at Carnary Wharf was built in the 1980s and is located about 8km east of London's historical centre in the London Docklands. Contrasting London's traditional financial centre in the City of London, Carnary Wharf was selected as a test site as it - until recently - featured the UK's three highest buildings (Shin, 2008).

2.1.2 Paris, La Defense

With 10.6 million inhabitants Paris is currently the third largest European city (UN, 2012a). Located in the Île-de-France region, Paris features a similar functional separation as London with

a coexistence of CBDs such as the selected test site, La Defense, which presents an internal edge city (Hall and Pain, 2006). Located about 8km west of the historic city centre (Hall and Pain, 2006), La Defense was developed to protect central Paris from modern office development and embrace the demands of international business in 2000 (Trip, 2007). Along with Carnary Wharf, La Defense is one of the most concentrated areas of high-rise buildings in Europe (Shin, 2008).

2.1.3 Istanbul, Levent

Located in a different cultural area, Istanbul is one of the most sprawling global megacities with its current population of 11.3 million inhabitants (Breunig *et al.*, 2009, UN, 2012a). Although being located in an earthquake prone region, the enormous population pressure forces the city towards high-density building and vertical expansion (Taubenböck, 2008c). Istanbul's main business activities developed during the 1980s along the Levent-Maslak-axis (Yigitcanlar *et al.*, 2008), 8km north-east of Istanbul's historic centre. The Levent CBD was chosen as a test site for this study as it exhibits the headquarters of Turkey's major banks with a high vertical dimension of buildings (Seger, 2012).

2.2 Remotely sensed data

2.2.1 Selection of remotely sensed data sets

For the development of a method for spatial CBD detection and delineation, remote sensing provides an independent and cost-effective data basis. According to the requirements of the particular application, a considerate selection of data is crucial for the success of the study. The choice of data is predominantly determined by technical aspects (Table 2-2).

Tab. 2-2 Data selection criteria (Radberger, 2001)

No	Criterion
(1)	extent of the test sites;
(2)	number of aimed land cover classes and their spatial differentiation ;
(3)	length of the study period;
(4)	requirements for accuracy for thematic mapping.

For the application at hand, a continuous surface representation of the studied cities including their artificial objects is needed. In this context, the Indian satellite Cartosat-1 was selected. This

satellite carries a sensor system which allows for the photogrammetric derivation of HR DSMs from stereo scenes. In addition to that, it was opted for an optical sensor of the Landsat series for the classification of the urban footprint of each city as a spatial frame for CBD detection. With regard to table 2-2, these datasets meet the requirements of the application at hand. With their large swath widths both sensor systems cover the areal extents and spatial distribution of large cities that are necessary to describe their urban morphology (Schweitzer and Steinbrink, 1998). Furthermore, providing both spectral and HR topographic information at medium to high spatial resolutions, the associated datasets allow for an accurate extraction of the desired urban attributes (Jensen and Cowen, 1999; Jensen, 2007), i.e. classification of the urban footprint and its CBDs. As this application is not time-sensitive, the length of the study period plays only a minor role.

2.2.2 Landsat data

The Landsat series of sensors (Multispectral Scanner (MSS), Thematic Mapper (TM), Enhanced Thematic Mapper (ETM+)) provide large-scale observations covering spatial extents of up to 185km for large-scale conurbations such as megacities, as well as data continuity due to repetitive and continuous monitoring (Chuvieco and Huete, 2010). In addition, these sun-synchronous sensors are a cost-effective choice as imagery is provided free of charge by the United States Geological Survey (USGS). A further distinct advantage is data comparability due to the arrangement of spectral bands within the same spectral regions. However, the sensors' relatively coarse geometric resolution presents one weakness with regard to classification due to subpixel mixed spectral information. Nevertheless, the particular datasets should allow for the classification of the urban footprint in its correct dimension and form (Taubenböck, 2008b). Technical details of the Landsat sensors are displayed in table 2-3.

Tab. 2-3 Technical details of the Landsat series of sensors (GLCF, 2004)

Satellite	Spectral Resolution (µm)	Band	Spatial resolution (m)	Temporal coverage
Landsat 1-3	**MSS**			1972-1983
	Band 4: 0.50 - 0.60	Green	79	
	Band 5: 0.60 – 0.70	Red	79	
	Band 6: 0.70 – 0.80	Near IR	79	
	Band 7: 0.80 – 1.10	Near IR	79	
Landsat 4-5	**MSS**			1982-2012
	Band 4: 0.50 – 0.60	Green	82	
	Band 5: 0.60 – 0.70	Red	82	
	Band 6: 0.70 – 0.80	Near IR	82	
	Band 7: 0.80 – 1.10	Near IR	82	
	TM			
	Band 1: 0.45 – 0.52	Blue	30	
	Band 2: 0.52 – 0.60	Green	30	
	Band 3: 0.63 – 0.69	Red	30	
	Band 4: 0.76 – 0.90	Near IR	30	
	Band 5: 1.55 – 1.75	Mid IR	30	
	Band 6: 10.4 – 12.5	Thermal	120	
	Band 7: 2.08 – 2.35	Mid IR	30	
Landsat 7	**ETM+**			1999-2003 (SLC on)
	Band 1: 0.450 – 0.515	Blue	30	
	Band 2: 0.525 – 0.605	Green	30	
	Band 3: 0.630 – 0.690	Red	30	
	Band 4: 0.760 – 0.900	Near IR	30	2003-2012 (SLC off)
	Band 5: 1.550 – 1.750	Mid IR	30	
	Band 6: 10.40 – 12.5	Thermal	60	
	Band 7: 2.080 – 2.35	Mid IR	30	
	Band 8: 0.52 – 0.92	PAN	15	

For this study it was opted for imagery recorded by the TM due to technical problems with the ETM+ scan-line corrector (SLC) since 2003. Furthermore, acquisition dates were chosen not to date back before the construction of the CBDs in the selected test sites in case of limited temporal availability for a particular city. Furthermore, minimum cloud coverage was preferred.

Overall, four scenes were selected for this study. Due to the spatial position of the satellites an image mosaic had to be generated from two scenes for study site Istanbul. All scenes were provided processed by the default Level 1 Product Generation System (LPGS) and projected

to the Universal Transverse Mercator projection (UTM). Furthermore, digital numbers (DN) were converted to units of at-sensor radiance applying the method presented by Chander *et al.* (2009) to enhance classification results (Roy *et al.*, 2002). A detailed overview over the acquired datasets is given in table 2-4. The original TM scenes are displayed in appendix 3.

Tab. 2-4 Details of the selected Landsat scenes

City	Sensor Platform	Date / Data source	Cloud cover	Path/Row (WRS 1/2)	Product
London	TM Landsat 5	4 July 2011 USGS (Earth Explorer)	10%	201/24	Level 1 GeoTiff
Paris	TM Landsat 5	30 June 2006 USGS (Earth Explorer)	<10%	199/26	Level 1 GeoTiff
Istanbul	TM Landsat 5	7 March 2003 USGS (Earth Explorer)	0%	180/31	Level 1 GeoTiff
	TM Landsat 5	7 March 2003 USGS (Earth Explorer)	0%	180/32	Level 1 GeoTiff

2.2.3 Cartosat-1 data

HR DSMs present the central datasets used for CBD delineation in this study. DSMs belong to the group of digital elevation models (DEMs) which are defined as continuous representations of surface elevation (Miller, 20004). In this context, DSMs present the earth's surface including all features of the landscape such as vegetation and artificial objects (Jensen, 2007), whereas digital terrain models (DTMs) are a representation of the bare-earth surface.

The DSMs used in this study were derived from stereo scenes provided by Cartosat-1. This Indian Remote Sensing Satellite P5 (IRS-P5) was launched in 2005 by the Indian National Remote Sensing Agency to provide imagery for large-scale cartographic applications (Jensen, 2007). According to the specifications listed in table 2-5, this satellite, orbiting the earth sun-synchronously at an altitude of 618km with a repeat cycle of 126 days, is equipped with two PAN cameras sensitive in the 500-850nm spectral wavelength region. Featuring a geometric resolution of 2.5m, these sensors simultaneously acquire images in stereo mode, one looking forward at 26° and one looking aft at -5°. Due to the relatively large swath width of 26km large urban agglomerations can be fully captured during one or two paths. With these specifications, Cartosat-1 provides HR stereo scenes which are well suited for the creation of large-scale DSMs (D'Angelo *et al.*, 2010).

Tab. 2-5 Cartosat-1 a) orbit and b) payload specifications (Gianinetto, 2008)

b) *Characteristic*	*Specification*
Camera inclination (°)	
Fore	+26
Aft	-5
Spatial resolution across-track x along-track (m)	
Fore	2.50 x 2.78
Aft	2.22 x 2.23
Spectral resolution	
No. of bands	1
Bandwidth (nm)	500-850
Radiometric resolution	
Saturation radiance (mw/cm2/str/mm)	55
Quantisation (bits)	10
Signal-tp-noise ratio (SNR)	345

a) *Characteristic*	*Specification*
Nominal altitude (km)	617.99
Number of orbits per day	15
Orbital repetivity cycle (days)	116
Nominal wait time to acquire adjacent path (days)	11
Max. wait time for revisit (days)	5
Local time for equatorial crossing	10:30 AM

Swath (km)	
Stereo mode acquisition	30
Mono mode acquisition (fore and aft combined)	26.855

Orbital parameters	
Semi-major axis (km)	6,996.13
Eccentricity	0.001
Inclination (°)	97.87

Charge-coupled device (CCD) parameters	
No. of detectors per camera	12,000
Detector element size (mm)	7 x 7
Odd-even spacing (mm)	35 (staggered)

Attitude and orbit control system	
Attitude pointing accuracy of all axes (°)	0.05
Attitude drift (°/s)	5×10^{-5}
Attitude determination accuracy (°)	0.01
Ground location accuracy (m)	< 220

Optics	
No. of mirrors	3
Effective focal length (mm)	1,980
F-number	4.5
Field of view (°)	± 1.08
Integration time (ms)	0.336

Tab. 2-6 Details of the selected Cartosat-1 scenes

City	No. of stereo pairs	Aerial coverage	Sensor / Year Platform	Date / Data source	Cloud cover	Path/Row	Product
London	2	1,521	PAN Fore PAN Aft	19 May 2010 Euromap	<10%	86/162	Standard GeoTiff
			PAN Fore PAN Aft	19 May 2010 Euromap	<10%	86/163	Standard GeoTiff
			Cartosat-1 (IRS-P5)				
Paris	4	2,505	PAN Fore PAN Aft	29 June 2011 Euromap	0%	104/174	Standard GeoTiff
			PAN Fore PAN Aft	29 June 2011 Euromap	<10%	104/175	Standard GeoTiff
			PAN Fore PAN Aft	3 July 2011 Euromap	0%	105/174	Standard GeoTiff
			PAN Fore PAN Aft	3 July 2011 Euromap	0%	105/175	Standard GeoTiff
			Cartosat-1 (IRS-P5)				
Istanbul	2	1,403	PAN Fore PAN Aft	20 January 2009	0%	256/210	Standard GeoTiff
			PAN Fore PAN Aft	28 May 2010 Euromap	0%	257/210	Standard GeoTiff
			Cartosat-1 (IRS-P5)				

An overview of the Cartosat-1 scenes selected for this study is given in table 2-6. These data were provided within the scope of the DLR scientific data pool by Euromap GmbH, which holds the rights for commercial distribution of IRS-P5 data in Europe. High quality DSMs were generated by the DFD from the available scenes by fully automated semi-global image matching (D'Angelo *et al.,* 2009 and 2010) using mutual information of the acquired images (Hirschmüller, 2008). This method is based on general principles of stereo photogrammetry, i.e. the reconstruction of 3D physical objects from picture coordinates of two or more overlapping scenes with a known viewing geometry and computer stereovision techniques (Albertz, 2007; Jensen, 2007), and has been tested against independent ground truth measurements for 18 stereo pairs with a mean lateral and vertical accuracy of 6.7m and 5.1m, respectively (D'Angelo, 2010). The final DSMs and the input Fore PAN images for the cities under study are presented in figures A4-1 to A4-3 of appendix 4. Aerial DSM maps of the test sites including photo impressions are displayed in figure 2-1.

Due to the 5m grid spacing of the final DSMs, the datasets can be classified as HR products (Taubenböck *et al.*, 2012), although they do not allow for extraction of individual objects on building level due to spatially varying of quality. For areas occluded from the sensors' field of view due to building density or cloud cover, no height data exists. These holes are filled by interpolated 30m resolution digital elevation information from the Shuttle Radar Topography Mission (SRTM) using the delta fill algorithm developed by Grohman *et al.* (2006). In combination with spatial resolution induced artefacts, this procedure results in a loss of sharpness in building edges (Sirmarcek *et al.*, 2010 and 2012) and spatial variation of data quality. This, so-called Christo-effect (Fritsch, 1999), is exemplified in figure 2-2 by both profile lines as well as DSM views of different locations in Paris.

Although Cartosat-1 derived DSMs are not flawless and do not feature microscopic detail on building level, they present a valuable data source for the application at hand. The decisive advantage of this dataset is the large-scale aerial coverage at a high spatial resolution, allowing the detection of significant physical urban structures such as CBDs in relation to the large-scale built environment.
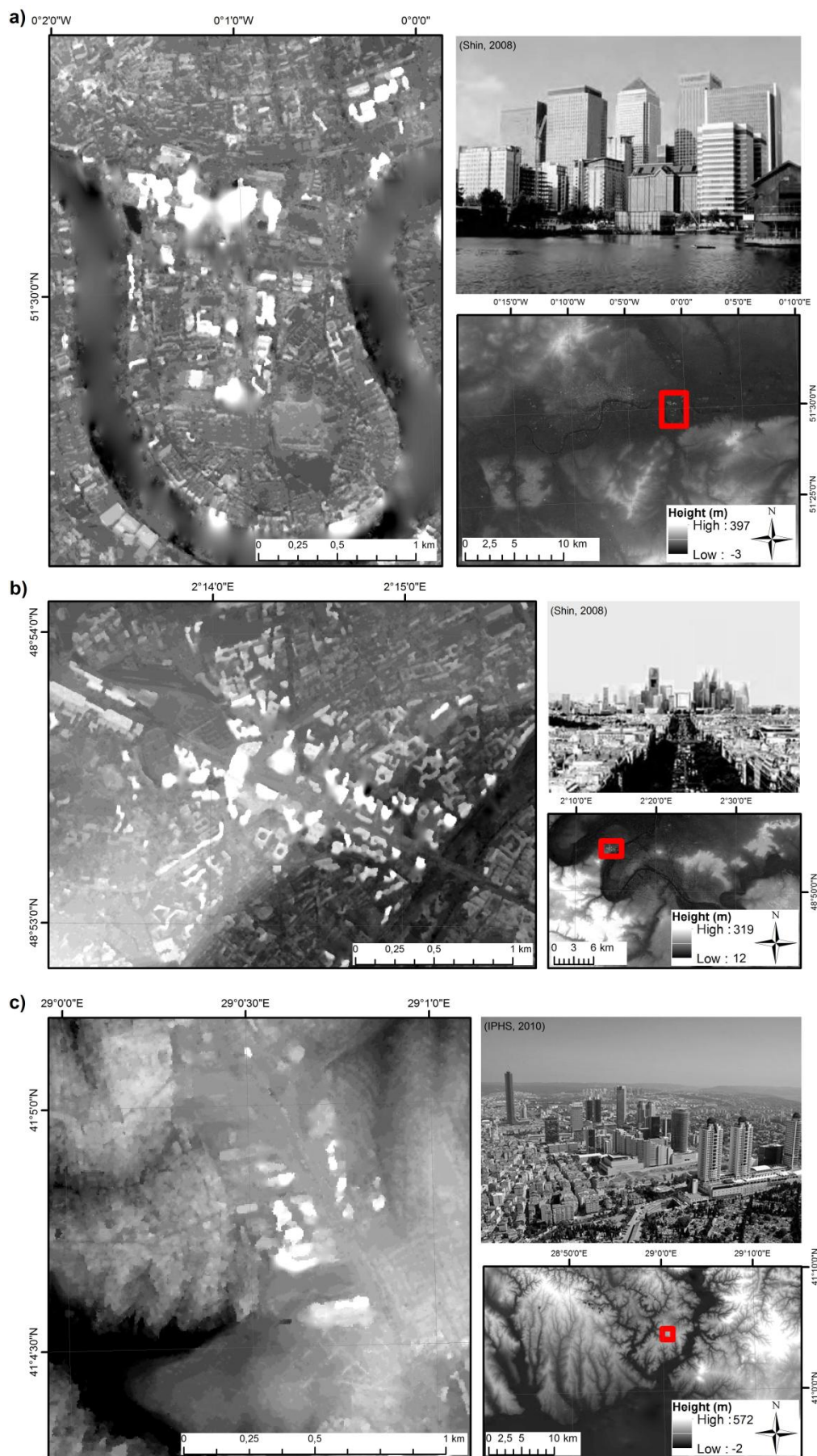
Fig. 2-1 Cartosat-1 DSM and photo impression of the three test sites in a) London, b) Paris, and c) Istanbul
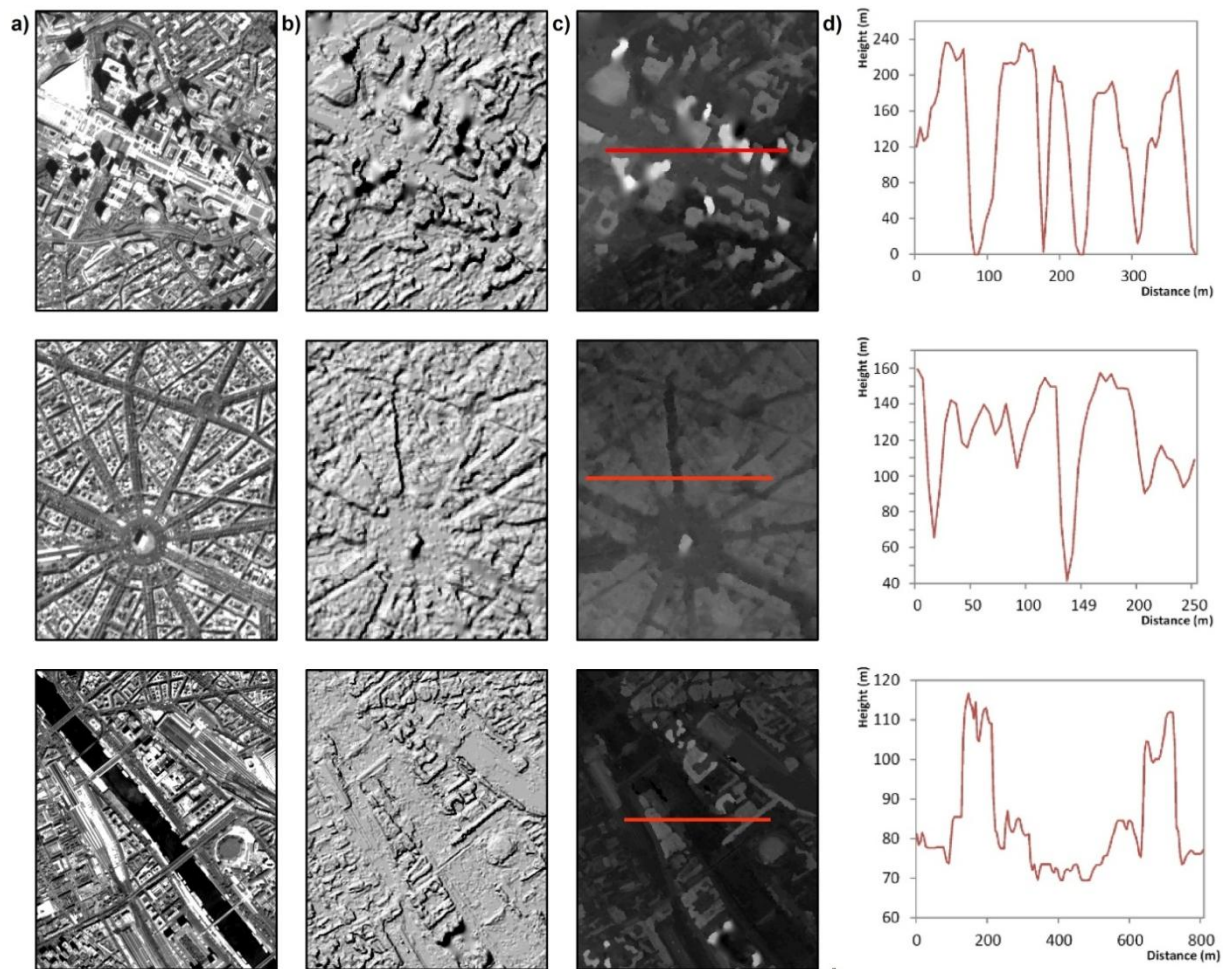
Fig. 2-2 Cartosat-1 a) PAN fore image (2.5m), b) DSM hillshade view, c) DSM, and d) sample profile graphs of different locations in Paris

2.3 Spatial data sets

To statistically designate CBDs from the surrounding urban structures by physical building parameters a highly detailed building reference is needed. In this context, 3D city models have proven useful in a variety of urban planning applications (Frueh and Zakhor, 2003). However, such models are usually expensive due to the costs of airborne laserscanning campaigns necessary and work-intensive maintenance of these datasets, especially for large-scale urban areas (Benner *et al.*, 2005). Therefore, it is opted for a combination of spatial datasets with a focus on open source availability that allow for a straight-forward compilation of 3D models for the selected inner-city test sites (Figure 2-3).
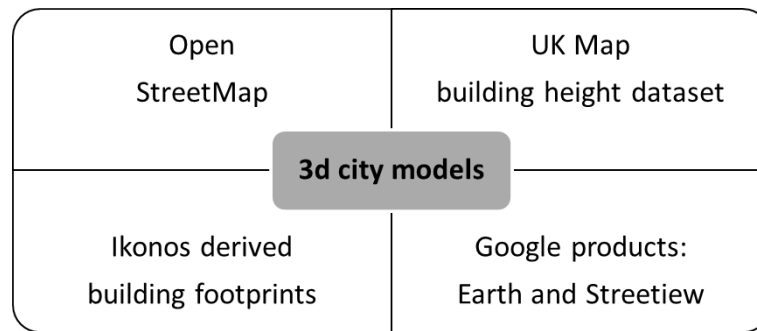
Fig. 2-3 Overview of spatial datasets used for 3D city model generation

2.3.1 Open StreetMap

In the context of detailed urban mapping, crowdsourcing of geospatial data using informal social networks and web technology has gained attention in the past decade (Haklay and Weber, 2008). Although the accuracy, availability, and completeness of volunteered geographical information (VGI) depend on the individual mappers, Open StreetMap (OSM) presents a valuable and cost-effective data source (Goodchild, 2007). Providing both street networks and information on building level – a large databasis exists especially for Paris -, OSM data (2012) is used for the determination of building blocks and acquisition of building footprints. Furthermore, significant buildings of the urban landscape commonly contain useful height information.

2.3.2 UKMap building height dataset

In the case of London, a very detailed building dataset is already openly available. LiDAR-derived building shapefiles containing detailed height attributes with a vertical accuracy with 95% confidence limits of 0.5m for the entire London area are provided by the Geoinformation Group of the University of Manchester for teaching, learning, and research purposes (Kitmitto *et al.*, 2000) (UKMap © The Geoinformation Group, 2012).

2.3.3 Ikonos-derived building footprints

Unfortunately, not for every city a detailed building database exists. In the case of Istanbul, a Ikonos image from 2005 provided by Taubenböck (2008c) is employed as reference for mapping the building inventory of the test site. As this VHR optical sensor acquires multispectral resolution in four bands and an additional panchromatic band (PAN) at a spatial resolution of 4m and 1m, respectively, it is very suitable for the derivation of building footprints based on cognitive perception (Figure 2-4).

Fig. 2-4 True-color Ikonos composite for the test site Levent

2.3.4 Google products: Earth and Streetview

In the context of 3D city model building, Google products (Google Inc., 2012) are used to fill gaps of data availability and inconsistencies due to temporal deviation of the aforementioned datasets from the Cartosat-1 acquisition dates. This includes digitalisation of missing building footprints from aerial imagery and systematic building height estimation procedure from floor counts using Google Streetview which provides area-wide imagery on street level (Dulong *et al.*, 2010).

3. METHODOLOGY

With regard to the conceptual framework presented, the methodological workflow of this dissertation is subdivided into five modules: (1) Physical parameterisation of CBDs, (2) compilation and analysis of 3D city models, (3) CBD delineation from remotely sensed data, (4) accuracy assessment, and (5) cross-city comparison (Figure 3-1). In general, the literature as well as earth observation (EO) data and the external spatial datasets described in chapter 2 are used as inputs.

In a first stage, physical building parameters that characteristically describe the physical face of CBDs are logically derived from the published literature (section 3.1). Subsequently (section 3.2), 3D city models are generated from the aforementioned external spatial data sources to build a reference for statistical CBD designation. This GIS-based procedure includes the compilation of building footprints and systematic height estimation. For structural analysis, an additional street layer is integrated to determine statistical reference units, in this case building blocks. Subsequently, this higher spatial scale is used as an aggregation level for the identified building parameters. Calculated on block level, these parameters allow for a statistical differentiation using dissimilarity clustering into two characteristic physical classes. These classes are thematically described as CBDs and Non-CBD areas and allow for a further structural analysis to examine the physical differences by use of within-group and between-group variance as a check for the central hypothesis. Furthermore, quantitative thresholds between the two classes are identified.

In the remote sensing analysis (section 3.3), the aforementioned EO datasets and the results from structural analysis are used to implement a method for CBD detection and delineation based on physical parameters. This modular procedure includes object-based urban footprint classification from Landsat scenes and delineation of CBDs from Cartosat-1 DSMs based on a stepwise procedure of morphological filtering, hierarchical segmentation and fuzzy-logic classification.

To gain confidence about the transferability and accuracy of the developed method, CBD delineation results are assessed using pixel-based confusion matrices for all test sites. Furthermore, the spatial detection accuracy is quantified on urban footprint level by a straight-forward visual comparison using Google Earth. In this context, also the associated subproducts are assessed (section 3.4).

Finally, the spatial configuration of the detected CBDs is analysed on urban footprint level using a set of spatial metrics to detect differences and analogies of CBD configuration across cities (section 3.5).
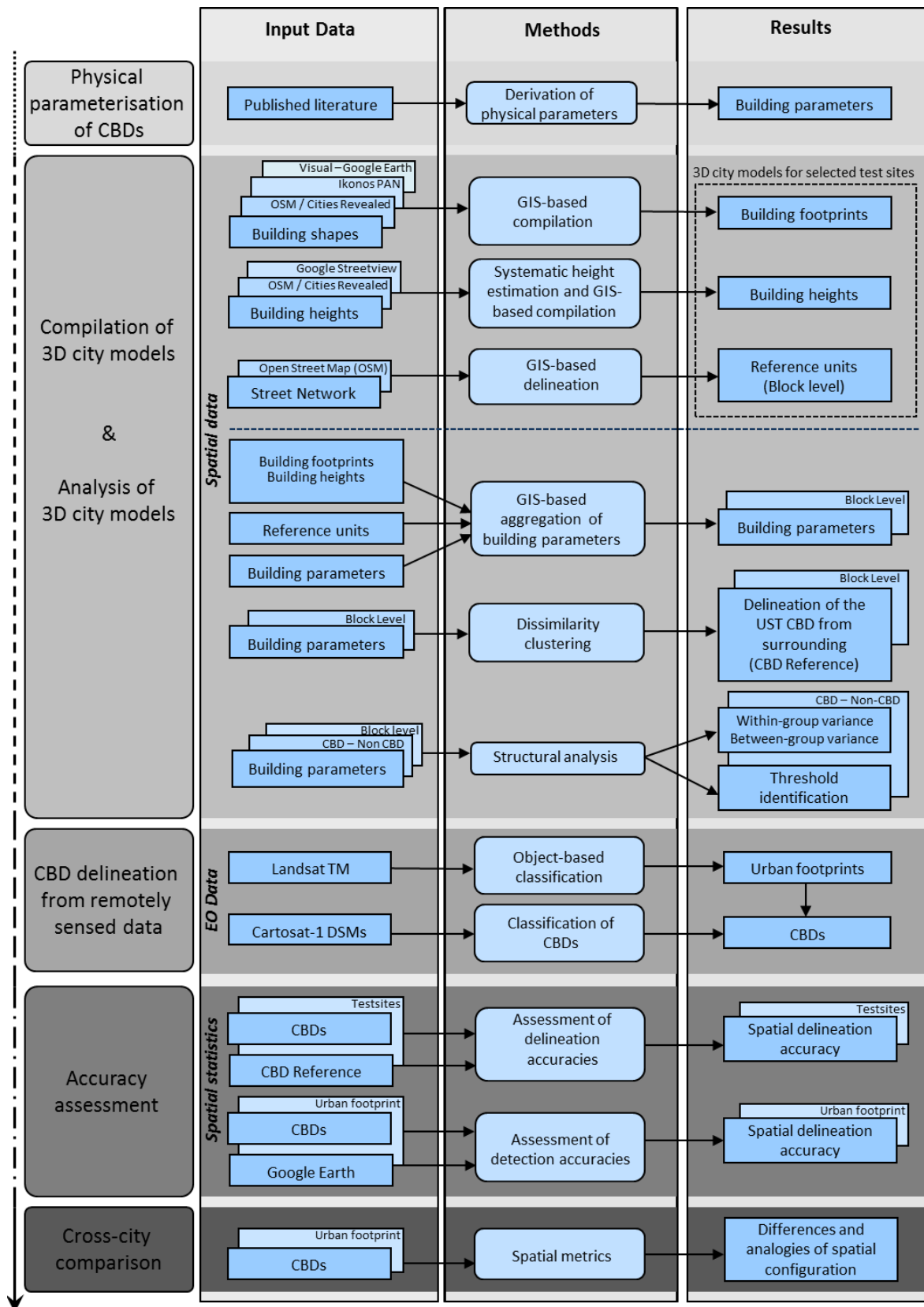
Fig. 3-1 Methodical workflow of this study

3.1 Literature review – physical parameterisation of CBDs

Large cities are too complex for a universal and holistic structural definition (Taubenböck, 2011). For instance, some authors describe the CBD as the most central region of a city (Galster *et al.*, 2000), whereas others argue that CBDs have long ago abandoned downtown locations and are only central in terms of their functional land use (Borruso and Porceddu, 2009). Thus, this study focuses on physical features to delineate CBDs. In this context, it is important to first understand what makes CBDs different from the surrounding USTs in terms of their morphology. Although physical definitions in literature are rather vague and pre-defined thresholds do not exist, qualitative statements that characteristically describe the physical face of CBDs can be used to logically derive a physical parameterisation on block level.

Most authors who dealt with this concept of urban geography describe the CBD as the part of the city which features peak land values and employment densities and thus, the highest buildings (e.g. Haggett, 2001; McColl, 2005; Pacione, 2005). In this context, the maximum building height presents a distinct indicator for central business land use (Heiken *et al.*, 2003) and can be supplemented by the maximum building volume which is commonly highly correlated (Shin, 2008). Further qualitative statements imply that the CBD is an aerial unit formed by a group of buildings, not by an individual object (e.g. Murphey, 1971). Thus, average values of the aforementioned measures present a logical addition to the parameter set.

Another parameter commonly used for urban structuring is building density (Wurm and Taubenböck, 2011). Although CBDs are generally not recognised to be more densely built-up than other parts of the city due to a maximum concentration of transport infrastructure (Heineberg, 2001), they do feature a unique density of high-rise buildings, known as the skyline (Ford, 1976). Finally, high floorspace densities have been found to be a typical physical feature of CBDs (Pan *et al.*, 2008).

This set of parameters reflects the essential physical features of CBDs and is summarised in table 3-1. Besides these, an additional land cover based feature of CBDs is the fraction of impervious surfaces which has been found to be maximal for this type of urban land use (Figure 3-2) (Ridd, 1995; Wu and Murray, 2003).

Tab. 3-1 Overview of the selected building parameters and their calculation on block level

Building parameter	Equation		Variables
Average building height (m)	$\overline{B_h} = \dfrac{\sum_{n=1}^{n_{R_u}} B_{h_n}}{n_{R_u}}$	(3)	
Maximum building height (m)	$B_{h_{max}} = \max_{n \in R_u}(B_{h_n})$	(4)	B_a = Building area; B_d = Building density; B_h = Building height; B_v = Building volume;
Average building volume (m³)	$\overline{B_v} = \dfrac{\sum_{n=1}^{n_{R_u}}(B_{h_n} \times B_{a_n})}{n_{R_u}}$	(5)	FSD = floorspace density; n = number of buildings; f = floor count per building;
Maximum building volume (m³)	$B_{v_{max}} = \max_{n \in R_u}(B_{h_n} \times B_{a_n})$	(6)	R_u = reference unit; A = area of the reference unit;
Floorspace density	$FSD = \dfrac{\sum_{n=1}^{n_{R_u}}(f_n \times B_{a_n})}{A_{R_u}}$	(7)	$high$ = high-rise building (exceeding 14 floors/50m or defined by CTBUH (2011))
Building density of high-rise buildings (%)	$B_{d_{high}} = \dfrac{\sum_{n=1}^{n_{R_u}} B_{a_{high_n}}}{A_{R_u}}$	(8)	
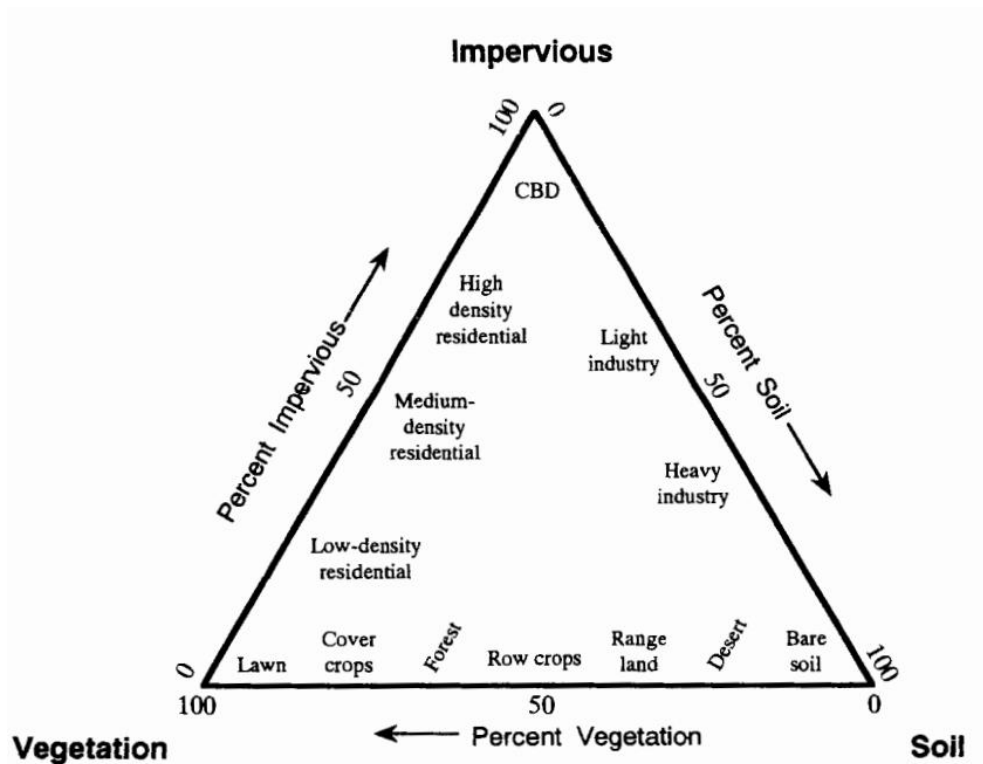
Fig. 3-2 Arrangement of urban land use types in the Vegetation-Impervious Surface-Soil model (Ridd, 1995)

3.2 Generation and analysis of 3D city models

3.2.1 Generation of 3D city models

This section covers the generation of 3D models as physical reference datasets for the selected test sites. As this part of the study focuses on the statistical designation and detailed structural analysis of CBDs vs. Non-CBD areas, the spatial extents of the models were chosen to cover not only the CBDs but also surrounding urban structures. Subsequently, the stepwise procedure of GIS-based (ESRI, 2011) 3D model building is described.

3.2.1.1 Compilation of building footprints

For the test sites in London and Paris, rich building inventories from the UKMap height dataset and OSM exist. However, these are not complete or fully consistent. Therefore, the associated building footprints were randomly checked against up-to-date Google Earth imagery resulting in the elimination of incorrect footprints and digitalisation of missing buildings. In the case of Istanbul's test site Levent, building footprints were extracted by manual digitising based on cognitive perception of the interpreter. This method features shortcomings in terms of repeatability and consistent quality in and across cities (Sliuzas *et al.*, 2008). However, in contrast to automated extraction of building objects which is difficult to apply in high-density urban environments (Netzband and Rahman, 2009), this form of visual interpretation provides a flexible approach when following a standardised digitising protocol. Thus, the high spatial resolution and multispectral information provided by Ikonos allowed for the straight-forward derivation of one polygon per building (Figure 3-3). Same as for the other test sites, these footprints were supplemented by missing buildings from Google Earth-based digitising.
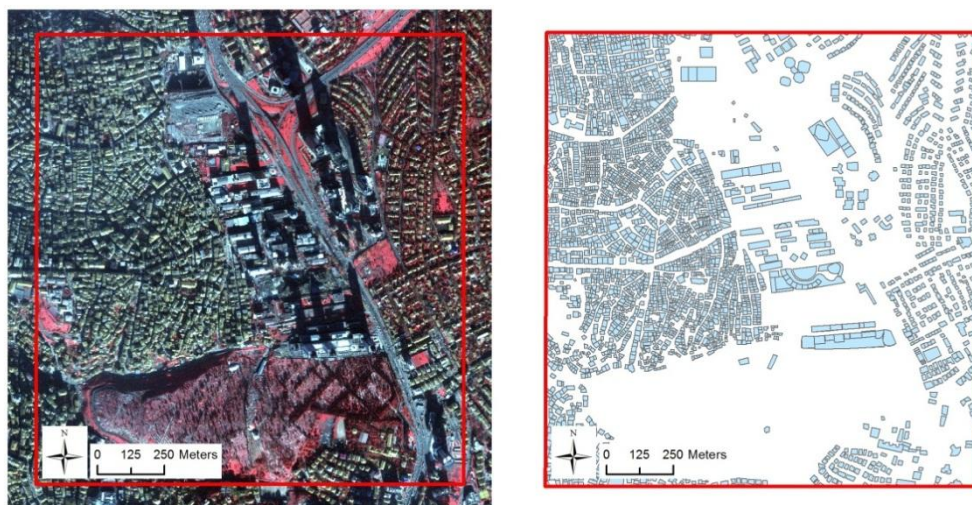
Fig. 3-3 Ikonos false-color composite and digitised building footprints, Levent

3.2.1.2 Building height estimation

To supplement the described building footprints by the third dimension, systematic height estimation was conducted for buildings not attributed by height information so far. Herein, Google StreetView (Google Inc., 2012) which provides aerial views of building façades on street level was employed. The indirect derivation of the absolute building height is based on floor counts from these views which are directly attributed to the footprints of building façades visible from the street view path. In the case of total occlusion, building footprints were attributed with the rounded mean floor count of the particular block in which they are located (Figure 3-4).

Fig. 3-4 Example of the systemic height estimation for a building block in Paris

In the following, floor counts were converted to values of absolute building height using the empirical correlation (r=0.864) found by Wurm *et al.* (2011) for housing inventories of two European cities:

$$y = 5.59 \times x^{0.73} \tag{9}$$

where y is the absolute building height and x the number of floors.

3.2.1.3 Building block determination

The determination of building blocks presents a crucial step due to the employment as statistical reference units in subsequent analyses. The designation is based on the concept of homogeneous land-use regions that are made up from the arrangement of individual buildings and open spaces (land cover objects) presenting a specific land use type (Zhan *et al.*, 2002; Herold *et al.*, 2002 & 2003). Streets have been identified as crisp geographic boundaries of these man-made structures (Couclelis, 1992; Wurm *et al.*, 2010). Therefore, the determination of building blocks is primarily oriented on the street network as the structuring element provided by OSM (Figure 3-5). Further criteria are the aerial coverage of Google Streetview to maximise the value of the available imagery for height estimation and the visual homogeneity at obvious structural change-overs.
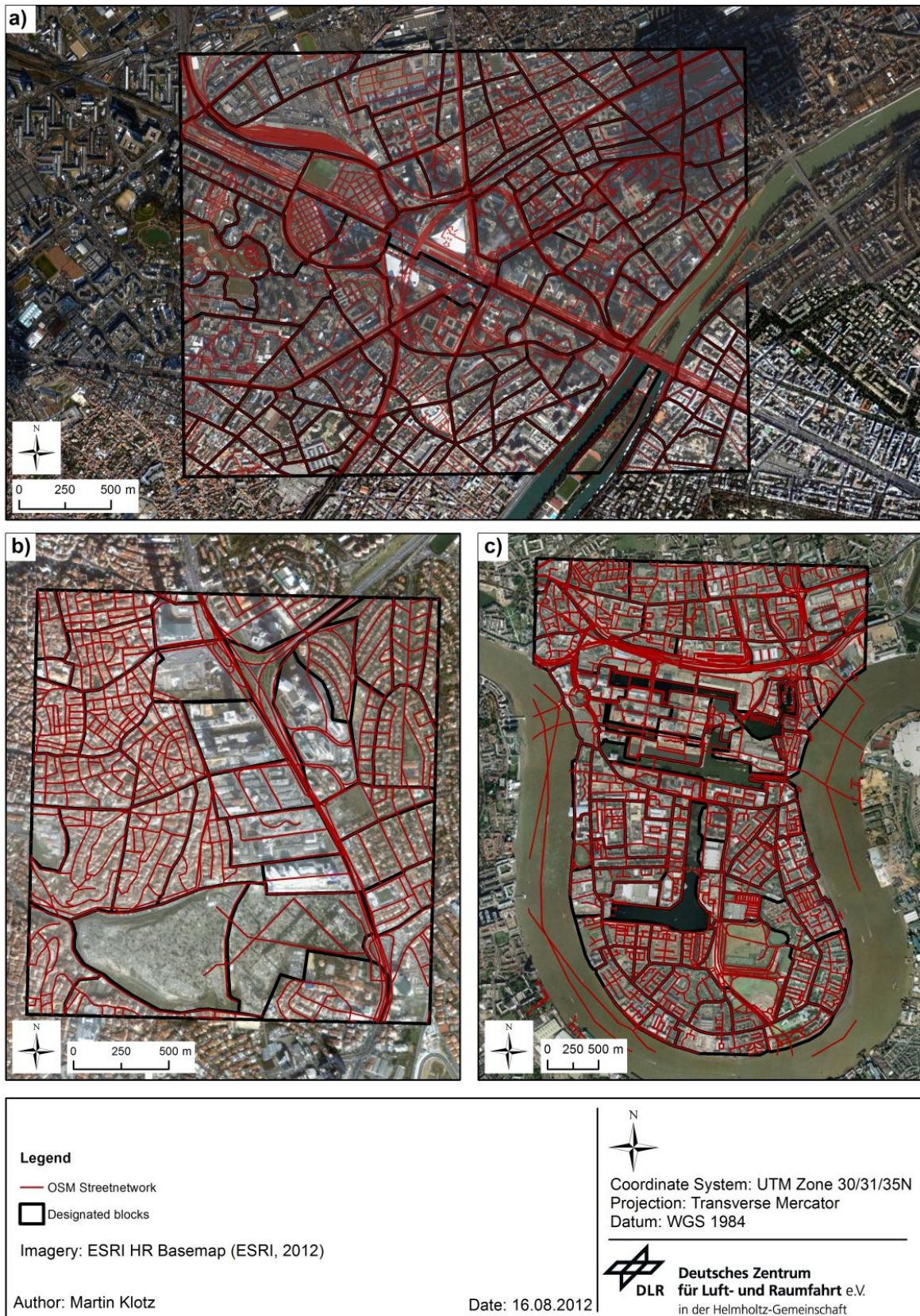
Fig. 3-5 Designated building blocks for a) La Defense, b) Levent, and c) Carnary Wharf

With regard to the presented procedure, the generated 3D models are not 100% accurate since they depend to a high degree on visual interpretation and cognitive perception of the mapper. However, they present a close-to-realistic image of the detailed physical real-world structure of the test sites and allow for the differentiation of CBDs relative to the surrounding urban morphology. Finally, table 3-2 sums up the process of model generation with respect to the spatial datasets used and figure 3-6 displays a final 3D block model of La Defense.

Tab. 3-2 Summary of 3D city model building

	Carnary Wharf	La Defense	Levent
No. Of buildings from:			
Open StreetMap		4,900	
UKMap building height dataset	1,835		
Digitisng (Ikonos)			3,695
Digitising (Google Earth)	169	888	34
Total No. of buildings	2,004	5,788	3,729
Total No. of height estimations	169	3,819	3,729
(= buildings not containing height attributes from UKMap or OSM)			
Total No. of blocks	81	143	42
Test site area (km²)	6.23	7.09	2.67
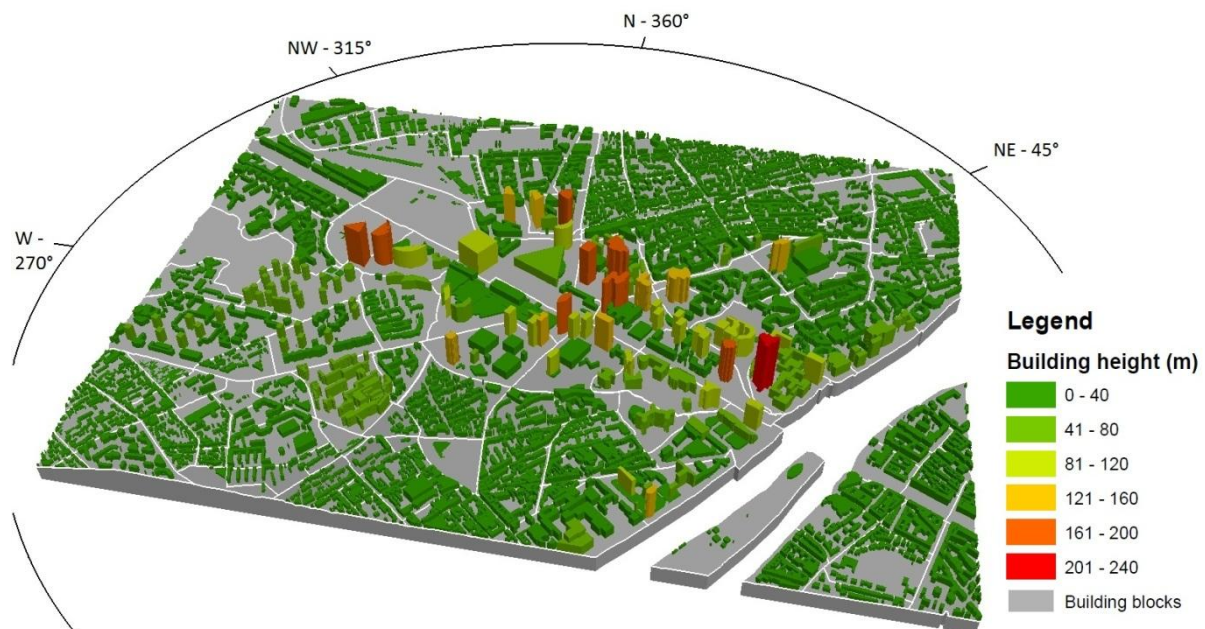
Fig. 3-6 3D perspective view on the building model of La Defense

3.2.2 GIS-based aggregation of building parameters

To allow for a statistical designation and systematic structural comparison of the USTs CBD vs. Non-CBD, the identified physical parameters are aggregated on a higher spatial level of statistical reference units. Based on the designated building blocks and 3D city models presenting a high-detail physical reference of the test sites, building parameters from section 3.1 are calculated on block level using GIS-based spatial join operations. The resulting aggregated parameters are exemplified in figure 3-7 for the test site La Defense.
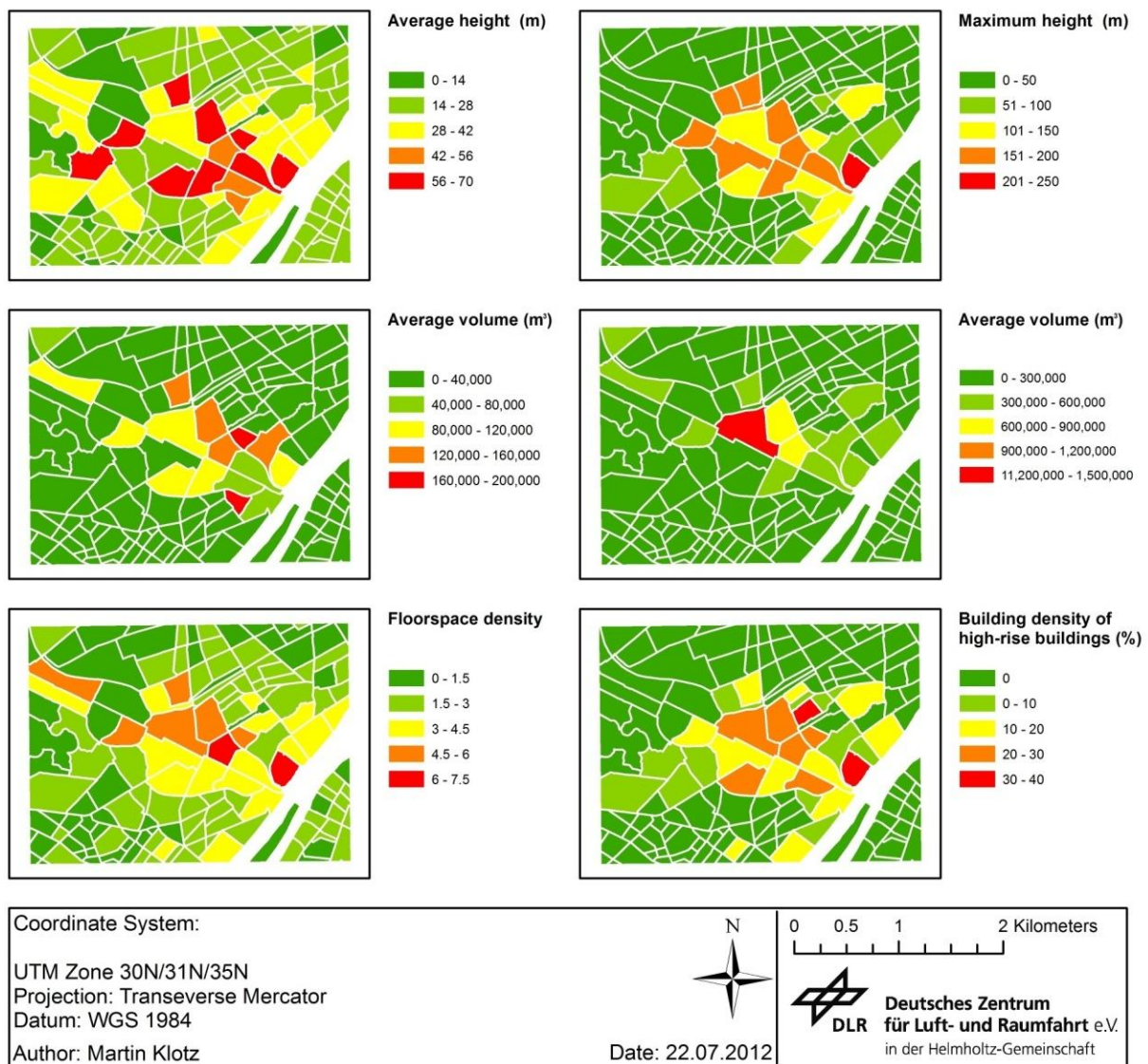
Fig. 3-7 Aggregated building parameters on block level, La Defense

3.2.3 Dissimilarity clustering

For physical differentiation of CBDs vs. Non-CBD areas, cluster analysis based on the observations from the 3D city models, i.e. the aggregated physical building parameters, is used. This step is based on the central hypothesis from chapter 1 that CBDs show significant differences regarding their morphology compared to other urban structures. In this context, cluster analysis is the assignment of a set of observations to groups, called clusters, so that observations in the same cluster show a high degree of similarity (Richards and Jia, 2006). With this statistical approach, it is aimed at spatial differentiation within the test sites based on physical parameters and the identification of typical thresholds for each class.

Partitioning around medoids (PAM) is used to differentiate the two classes CBD and Non-CBD on block level. This hierarchical clustering method is advantageous compared to other algorithms as it aims to minimise the sum of dissimilarities within clusters based on the structure of the data (Reynolds *et al.*, 2006). To obtain comprehensive thresholds between the two thematic classes, the clustering is executed across the whole set of building parameters and test sites. In a first step, the aggregated data are standardised to avoid dependence on the choice of measurement units according to Thomas and Hugget (1980) (eq. 10):

$$z_i = \frac{x_i - \mu}{\sigma} \tag{10}$$

where z_i is the new value of any sample observation x_i, μ is the sample mean, and σ is the standard deviation of the sampling distribution. Subsequently, a dissimilarity matrix is generated which presents the distances between all pairs of observations i and j with the coordinates $(z_{i1...}z_{ip})$ and $(z_{j1...}z_{jp})$ in the 6-dimensional feature space ($p=6$) based on the Euclidean norm (eq. 11) (Kaufmann and Rousseeuw, 1990):

$$d(i,j) = \sqrt{\left(z_{i1} - z_{j1}\right)^2 + \left(z_{i2} - z_{j2}\right)^2 + \cdots + \left(z_{ip} - z_{jp}\right)^2} \tag{11}$$

In the following, the PAM algorithm iteratively determines representative objects for the thematic classes. These so-called medoids are meant to present the optimal configuration of objects in the feature space by minimising the total dissimilarity within groups (Kaufmann and Rousseeuw, 1990). Thus, two clusters are designated by assigning each object (block) to the nearest medoid creating groups which can be thematically described as CBD and Non-CBD. This clustering procedure was implemented in the statistical computing platform R (Appendix 5).

3.2.4 Structural comparison and threshold identification

The straight-forward methodology to delineate CBDs from the surrounding urban structures based on cluster analysis implies that a significant difference within the input parameters exits on class level. However, the analysis of derived physical characteristics allows for a deeper insight into the physical face of CBDs. As a check whether the central hypothesis is generally true, i.e. if the CBD can be differentiated from the surrounding urban morphology based on physical parameters, the available information allows for a systematic structural comparison on different geometric levels: (1) The analysis of structural differences at test site (district) level and (2) the analysis of within-group and between-group variance at the level of the spatial areas differentiated as the USTs CBDs and Non-CBDs (Figure 1-3). For this reason, the parameters identified in section 3.1 are visualised as boxplots on test site and thematic class level. These plots include the median, the interquartile range and whiskers as defined by Tukey (1977). Furthermore, parameter thresholds are directly derived from class level and visualised using range plots for employment in the remote sensing analysis part of this study.

3.3 Object-based CBD delineation from remotely sensed data

Following this detailed structural analysis, this section presents the method for CBD detection and delineation from a combination of Landsat imagery and HR Cartosat-1 DSMs as the central part of the remote sensing analysis. This method was implemented using the object-based image analysis software eCognition Developer (Trimble GmbH, 2011b) and can be subdivided into four basic modules: (1) Urban footprint classification, (2) morphological filtering, (3) hierarchical segmentation, and (4) fuzzy-logic classification. In the following, these modules are described in sequence.

3.3.1 Urban footprint classification

Due to the high impervious surface fractions found in CBDs, it is a reasonable decision to use the urban footprint of a city as a spatial frame for CBD delineation. However, the high spectral variability due to the complex mixture of urban surfaces makes it an explicitly difficult land cover to delineate (Jensen, 2007; Weng, 2008) (Figure 3-8).
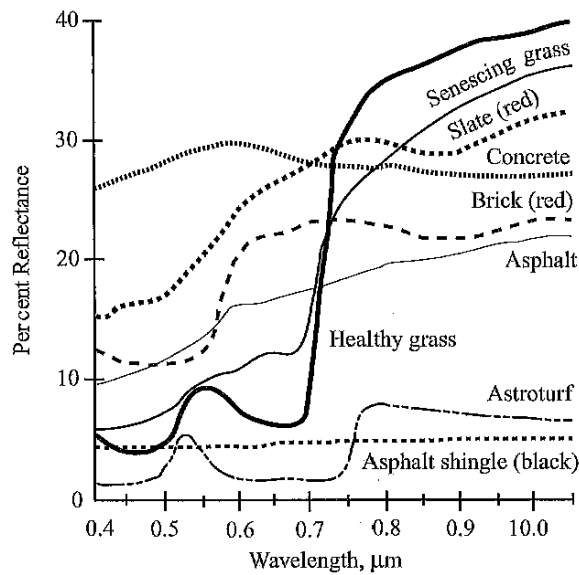
Fig. 3-8 Reflectance characteristics of common urban surfaces (Jensen, 2007)

For urban footprint classification of the Landsat TM scenes a semi-automatic impervious surface classification procedure using decision trees was employed. This has been implemented by Abelen *et al.* (2011) as a fixed processing chain in eCognition Architect consisting of a bottom region growing technique for the generation of image objects (Benz *et al.*, 2004) and hierarchically structured land use classification using a pre-defined feature set (Figure 3-9). Since the urban footprint classification is not the central scope of this study, for a detailed description of this procedure implemented as an interactive graphical user interface (GUI) it is referred to Abelen (2009).
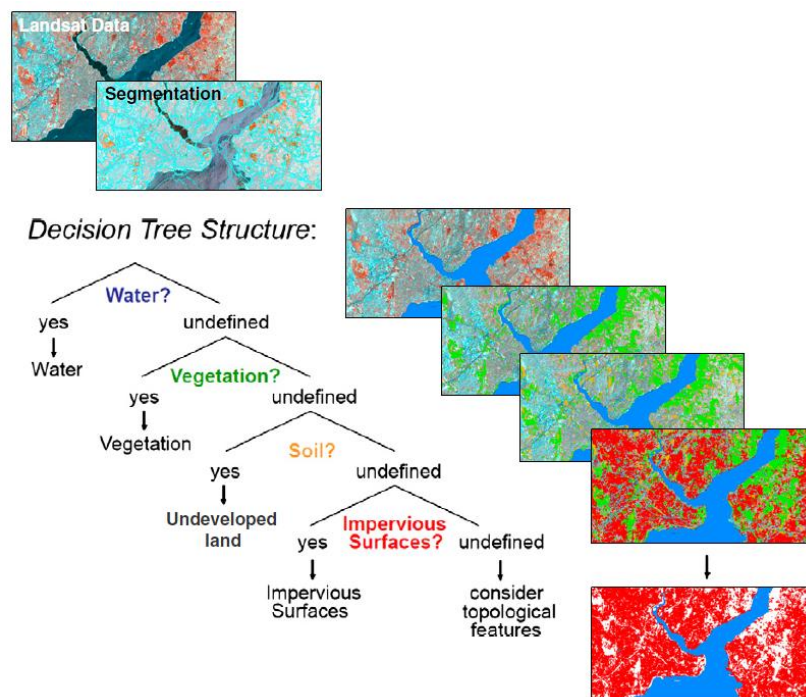
Fig. 3-9 Schematic overview of the step-wise hierarchical land cover classification (Taubenböck, 2012)

At the geometric level of urban footprints a further thematic differentiation is beyond the data's capabilities. Thus, the following sections describe the extraction of the essential features for classification of CBDs from the HR DSMs.

3.3.2 Morphological filtering

Cartosat-1 DSMs have been tested for the extraction of individual buildings by several segmentation procedures including contrast-split, multi-resolution, and canny edge segmentation (Trimble GmbH, 2011a). However, due to fuzzy building edges presented in the DSMs, sharp building outlines are impossible to detect with high accuracies. Thus, the DSMs do not provide a reference for an analysis of physical parameters derived from building level, but are suitable for the delineation of CBDs based on the dimension of their physical features relative to the surrounding urban environment on pixel level.

In this context, a morphological pre-processing is executed to obtain an accurate measure of the above-ground building volume. A classic morphological filtering algorithm to create a normalised DSM (nDSM), i.e. a surface representation of objects lying above-terrain, is the morphological opening (Haralick *et al.* 1987; Bochow, 2009). This algorithm is based on the sequential execution of a kernel window-based minimum (erosion) and maximum (dilatation) filter *s(i,j)* (eq. 12 and 13) on pixel level of the DSM *I(x,y)* (Brenner, 2000) followed by an additional median filter to derive a smoothened DTM surface. Consequently, the nDSM is calculated as the difference between the DSM and the DTM (Figure 3-10) (Figure 3-10).

$$(I \ominus s)(x, y) = \min_{(i,j) \in s} \{I(x + i, y + j)\} \tag{12}$$

$$(I \oplus s)(x, y) = \max_{(i,j) \in s} \{I(x + i, y + j)\} \tag{13}$$
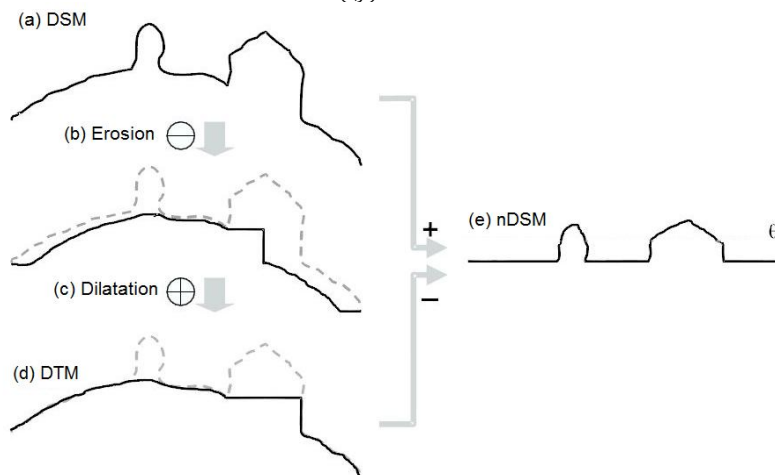
Fig. 3-10 Scheme of the morphologic operations for nDSM generation

As the morphological filtering results are sensitive to the kernel size of the moving window (Arefi *et al.*, 2009) (Figure 3-11), several kernel sizes are tested in the context of the quality assessment of the DTM subproduct by the use of profile lines and basic measures error such as the root mean square error (RMSE) compared to a spatial reference.
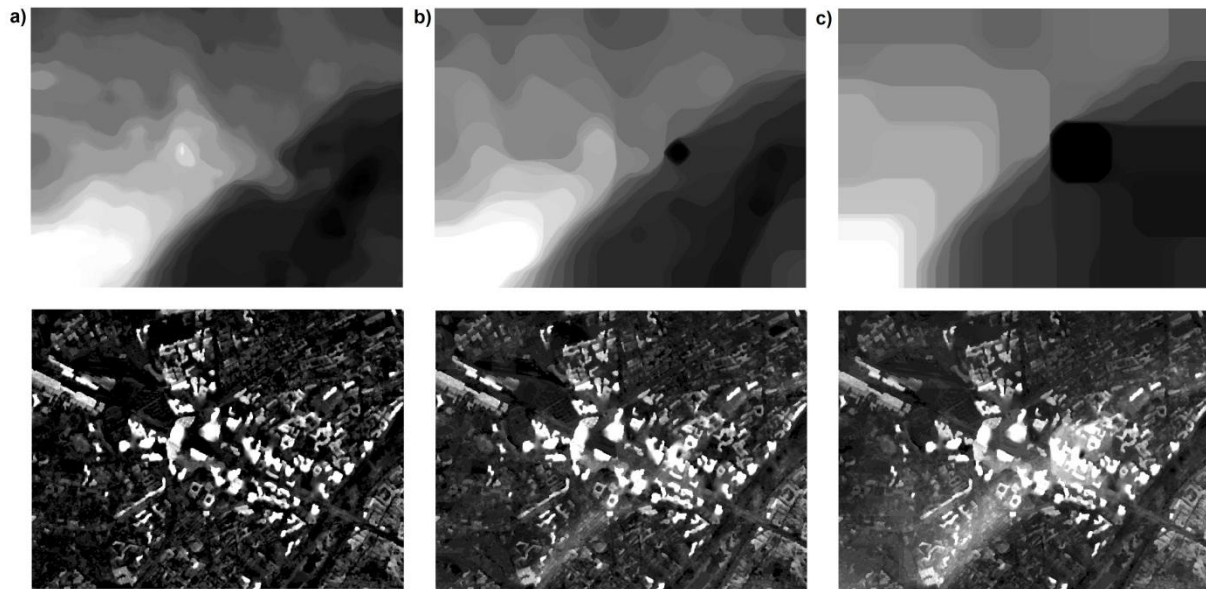
Fig. 3-11 Effect of varying kernel size on the DTM (top) and nDSM (bottom) generation, La Defense; a)-c) kernel sizes of 10x10, 50x50, and 100x100 pixels

3.3.3 Hierarchical Segmentation

The object-based delineation of CBDs underlies a top-down segmentation structure (Figure 3-12) (Taubenböck *et al.*, 2010) which reflects the hierarchical structure of cities presented in section 1.2.2. Starting on pixel level of the nDSM, the highest spatial scale is presented by the urban footprint level (L1) which is generated by embedding the urban footprint classification as a thematic layer into the segmentation process (1).

Below, the aggregation level (L2) presents the spatial scale of statistical reference units. In contrast to the 3D city models, the problem encountered here is that OSM street networks do not present a feasible databasis for transferable designation of building blocks beyond test site level due to the manual editing tasks involved. Furthermore, a gap regarding availability of alternative datasets of administrative units such as land parcels or inner-city districts still exists for European cities (INSPIRE, 2012). Against this background, a chessboard segmentation was chosen to create square reference units of 200m cellsize (2). Although not independent from the

urban morphology (Herold *et al.*, 2003), these artificial units present the best possible practice with regard to the choice of a representative cellsize for building blocks.

By the execution of a further chessboard segmentation, the subobject level (L3) is reached (3). This level equals the pixel level and is classified into pixel objects that represent urban structures and terrain pixels. Subsequently, this multi-level approach allows for the straight-forward aggregation of physical parameters on block level from individual pixel values by the use of relational features between those levels (4) (Trimble GmbH, 2011a). In this connection, the area classified as built-up on L1 presents the reference for area-dependent measures such as floorspace density, whereas subobject terrain pixels present the physical above-ground building volume. As mentioned before, Cartosat-1 DSMs do not allow for classification based on physical parameters aggregated from individual buildings. Thus, substitutes for the selected building parameters on pixel level are used for aggregation on L1 (Table 3-3). Although some of these substitutes only present proxies and are associated with a certain information loss, they reflect the typical physical features of CBDs.
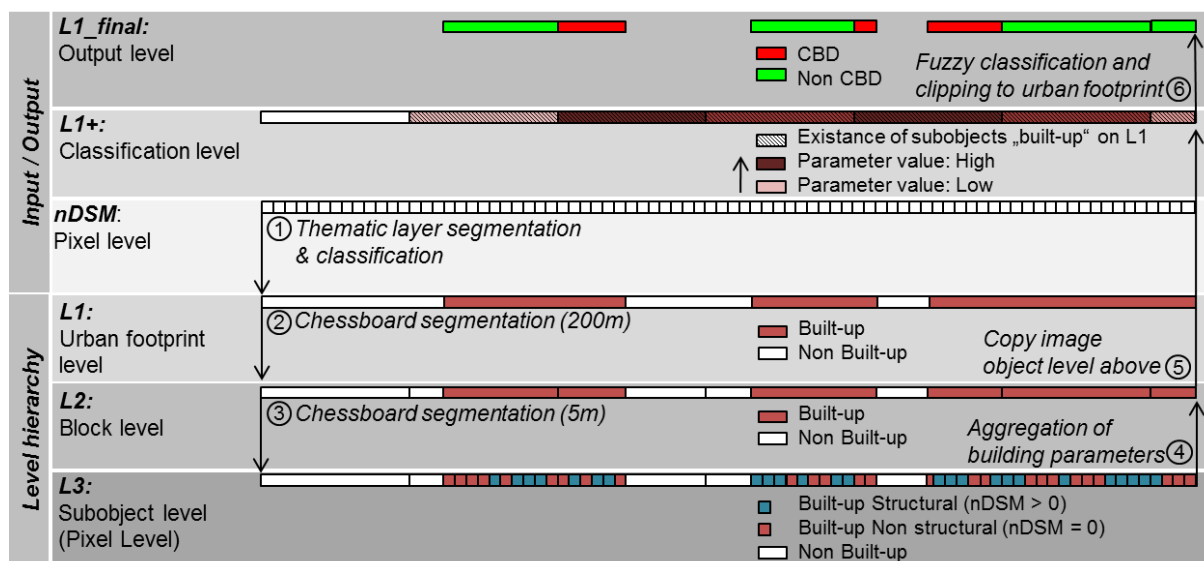
Fig. 3-12 Scheme of hierarchical segmentation

By transferring the aggregation level (5), a separate classification level (L1+) is created which contains all aggregated parameter values as well as a reference to the urban footprint level in the form of an attribute on the existence of subobjects classified as built-up on L1.Subsequently, a fuzzy-logic classification procedure is executed to delineate CBDs. This procedure is described in the next section. Finally, classification results are clipped to limit the occurrence of CBDs to the urban footprint extent (6).

Tab. 3-3 Substitute relational features of physical parameters derived from pixel level

Building parameter	Pixel-based substitute	Equation		Variables
Average building height (m)	Pixel-based average pixel height (m)	$\overline{P_h} = \dfrac{\sum_{n=1}^{n_{R_u}} P_{h_n}}{n_{R_u}}$	(14)	P_a = Pixel-based area;
Maximum building height (m)	Pixel-based maximum height (m)	$P_{h_{max}} = \max\limits_{n \in R_u}(P_{h_n})$	(15)	P_d = Pixel-based density; P_h = Pixel-based height; P_v = Pixel-based volume; FSD = Pixel-based floorspace density;
Average building volume (m³)	Pixel-based average volume (m³)	$\overline{P_v} = \dfrac{\sum_{n=1}^{n_{R_u}}(P_{h_n} \times P_{a_n})}{n_{R_u}}$	(16)	n = number of pixels classified as built-up structural on L3;
Maximum building volume (m³)	Pixel-based maximum volume (m³)	$P_{v_{max}} = \max\limits_{n \in R_u}(P_{h_n} \times P_{a_n})$	(17)	c_f = floor height constant; R_u = reference unit; U = area of the reference unit classified as built-up on L1;
Floorspace density	Pixel-based floorspace density	$FSD = \dfrac{\sum_{n=1}^{n_{R_u}}(\frac{P_{h_n}}{c_f} \times P_{a_n})}{U_{R_u}}$	(18)	$high$ = pixels exceeding a height of 14 floors or 50m as defined by
Building density of high-rise buildings (%)	Pixel-based density of high-rise buildings (%)	$P_{d_{high}} = \dfrac{\sum_{n=1}^{n_{R_u}} P_{a_{high_n}}}{U_{R_u}}$	(19)	CTBUH (2011))

3.3.4 Fuzzy-logic classification

As mentioned before, a fuzzy-logic approach (Stolz, 1998) is used to classify CBDs on block level (L1+). By the use of fuzzy sets, i.e. classes with continuous grades of membership, membership values are added to the final classification result (Yager, 1987). For this purpose, it is referred to the class thresholds on building and pixel level identified from the structural analysis of the 3D city models, as these values represent the comprehensive physical differences of the structure type CBD compared to the surrounding's urban morphology. Here, it is pre-empted that class change-overs are not distinct but exhibit a fuzzy transition range between the two classes defined by distinct lower and upper thresholds. This is due to the holistic approach of parameter combination that makes up the physical face of CBDs. The basic scheme of fuzzy-logic classification applied here consists of two rules combined by a logical minimum (AND) operator (Figure 3-13):

(1) The *a priori* knowledge about the urban footprint extent is employed as a criterion of exclusion by using the existence of subobjects classified as built-up on urban footprint level as a hard thresholding rule. (2) Physical parameters aggregated on block level from pixel object level are combined via a second minimum operator. In between the identified lower and upper thresholds of the transition range, the CBD membership value increases according to a fuzzy sigmoidal membership function from zero to one, thus, returning an individual membership value for each parameter. To combine these values, again, hard thresholding is used based on the logical decision that all blocks must at least meet the lower threshold of the transition range for each parameter to be classified as CBD. Finally, the class membership value of each block classified as CBD is returned as the minimum membership value of each physical parameter.
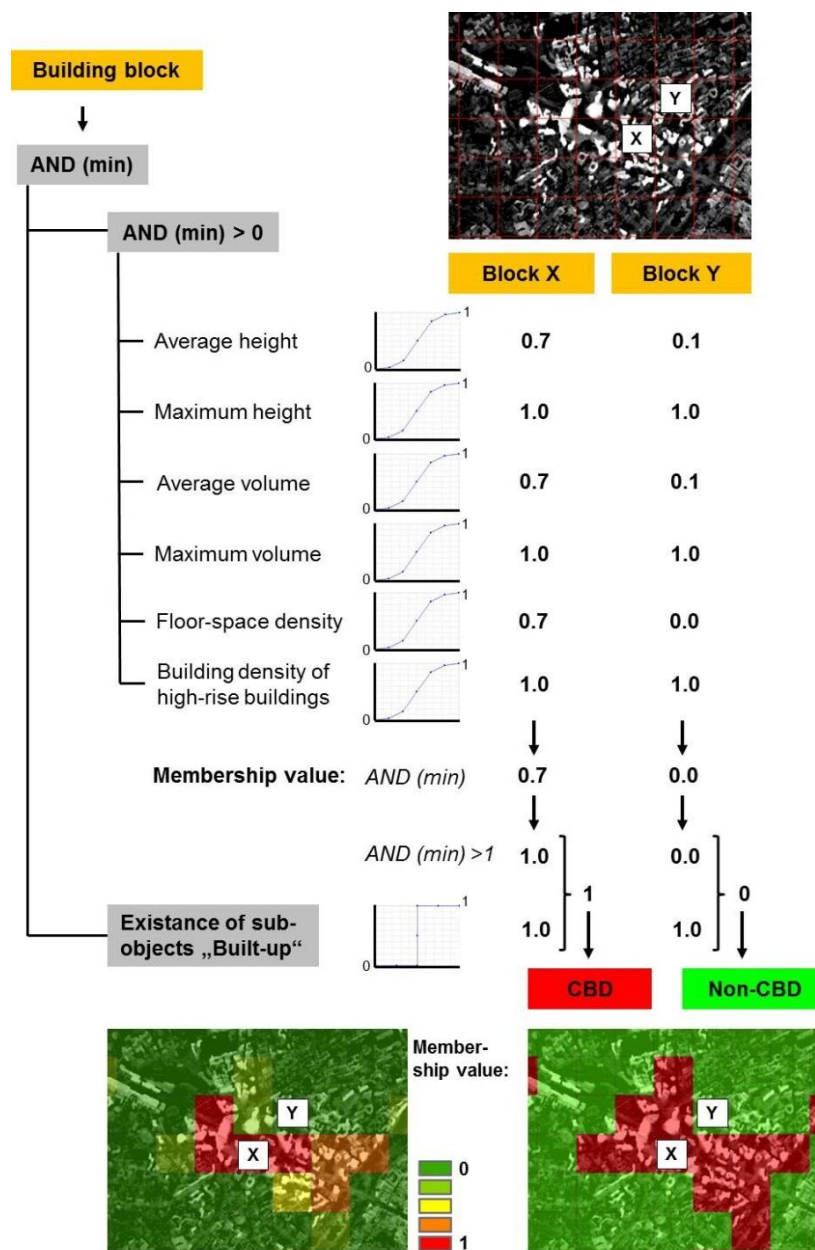
Fig. 3-13 Scheme of fuzzy-logic classification

3.4 Accuracy assessment

In order to assess the transferability of the presented methods, the final CBD delineation and its associated subproducts are assessed.

3.4.1 Urban footprint classifications

To provide a consistent spatial reference for CBD detection, the accuracy of the urban footprint as an important subproduct is assessed. Commonly, classification accuracy is determined by comparing the classification results with ground-truth data (Richards and Jia, 2006). Since such data are not available, the classification accuracy was alternatively assessed by random distribution of 100 checkpoints within each class (Built-up/Non built-up/Water) and visual verification using Google Earth. The resulting confusion matrices include common measures of accuracy such as the Kappa-Index which compares the agreement of the confusion matrix with a chance agreement (eq. 20) (Congalton and Green, 2009):

$$K = \frac{N\sum_{i=1}^{r} x_{ii} - \sum_{i=1}^{r}(x_{i+}x_{+i})}{N^2\sum_{i=1}^{r}(x_{i+}x_{+i})} \tag{20}$$

with N being the total of checkpoints, r the number of rows, x_{ii} the value of row i and column i, and x_{+i} and x_{i+} the row and column totals.

3.4.2 CBD delineation and detection

As the final product of the presented method, the accuracy of CBD classification is assessed. In this context, it is differentiated between spatial delineation and detection accuracy:

The former aims at quantifying the spatial precision of CBD delineation within the three city-internal test sites. As for the urban footprint, the accuracy is assessed by standard pixel-based confusion matrices for the two thematic classes (CBD/Non-CBD) with regard to the statistically designated building blocks from analysis of 3D city models. In contrast, the spatial detection accuracy reflects the correctness of large-scale CBD localisation on urban footprint level. For this purpose all blocks classified as CBDs are visually compared to the urban structures presented by Google Earth imagery and 3D models (Google Inc., 2012) to quantify the user accuracy. However, this procedure does not allow for the calculation of the producer accuracy.

3.5 Cross-city comparison

For cross-city analysis of CBD configuration, a set of spatial metrics, i.e. quantitative, aggregated measures that can be used to describe the spatial pattern of cities (Herold *et al.*, 2005; Huang *et al.*, 2007; Taubenböck *et al.*, 2009), is employed. In this context, adjacent correctly detected blocks are merged since they thematically represent one CBD and the selected metrics are calculated using GIS (ESRI, 2011).

For straight-forward quantitative comparison, the number of CBDs (*n(CBD)*), the absolute (*AA*) and relative total CBD area (*RA*) compared to the spatial extent of the urban footprint are analysed. Furthermore, the largest patch index (*LPI*) as a measure for the dominance of the largest CBD is calculated (McGarigal and Marks, 1995). To compare the spatial configuration of CBDs across cities (Table 3-4), the mean CBD-to-CBD distance (*MD*) in combination with the nearest neighbour distance (*MNND*) are analysed as measures of spatial dispersion. Furthermore, the CBD density within the historic urban core (*CBD-D5*) and the mean CBD-to-centre distance (*MDC*) reflect geographic centrality of CBD distribution. For reason of across-city comparability, these measures of spatial configuration are normalised by the dimension of the largest urban patch of the particular city (Figure 3-14). Finally, spider-charts are used for comparative analysis.

Tab. 3-4 Overview of spatial configuration metrics

Metric	*Abbrev. (unit)*	*Equation*		*Normalisation variables*	*Further variables*
Relative mean CBD-to-CBD distance	MD (%)	$= \dfrac{\frac{\sum_{i=1}^{n} \frac{\sum_{j=1}^{n} d_{ij}}{n}}{n}}{D_{max}}$	(21)	D_{max} = Max. urban footprint extent;	A_{CBD} = Total area covered by CBDs; n = number of CBDs detected;
Relative mean CBD-to-CBD nearest neighbour distance	MNND (%)	$= \dfrac{\frac{\sum_{i=1}^{n} d_{min_i}}{n}}{D_{max}}$	(22)	D_{max} = Max. urban footprint extent;	d_{min} = Nearest Neighbour CBD-to-CBD distance;
CBD density in relation to the built-up area in a 5km circle around the historic centre	CBD-D5 (%)	$= \dfrac{A_{CBD-5km}}{A_{UFP-5km}}$	(23)	$A_{UFP-5km}$ = Built-up area within the 5km radius;	d_c = CBD-to-centre distance;
Relative mean CBD-to-centre distance	MDC (%)	$= \dfrac{\frac{\sum_{i=1}^{n} d_{c_i}}{n}}{D_{c-max}}$	(24)	D_{c-max} = Max. centre-to-urban footprint edge distance;	d_{ij} = distance between CBD i and CBD j; $i/j = 1,…,n$ CBDs

a)
$$MD = \frac{\frac{\sum_{i=1}^{n} \frac{\sum_{j=1}^{n} d_{ij}}{n}}{n}}{D_{max}}$$

b)
$$MNND = \frac{\frac{\sum_{i=1}^{n} d_{min_i}}{n}}{D_{max}}$$

c)
$$CBD - D5 = \frac{A_{CBD-5km}}{A_{UFP-5km}}$$

d)
$$MDC = \frac{\frac{\sum_{i=1}^{n} d_{c_i}}{n}}{D_{c-max}}$$

Legend

● CBD
● Urban footprint edge point
● Historic centre
  - Trafalger Square, London
  - Hagia Sofia, Istanbul
  - Place de la Concorde, Paris

— Normalisation distance measures
--- Other distance measures
   (CBD-to-CBD/CBD-to-centre)
↘ 5km buffer
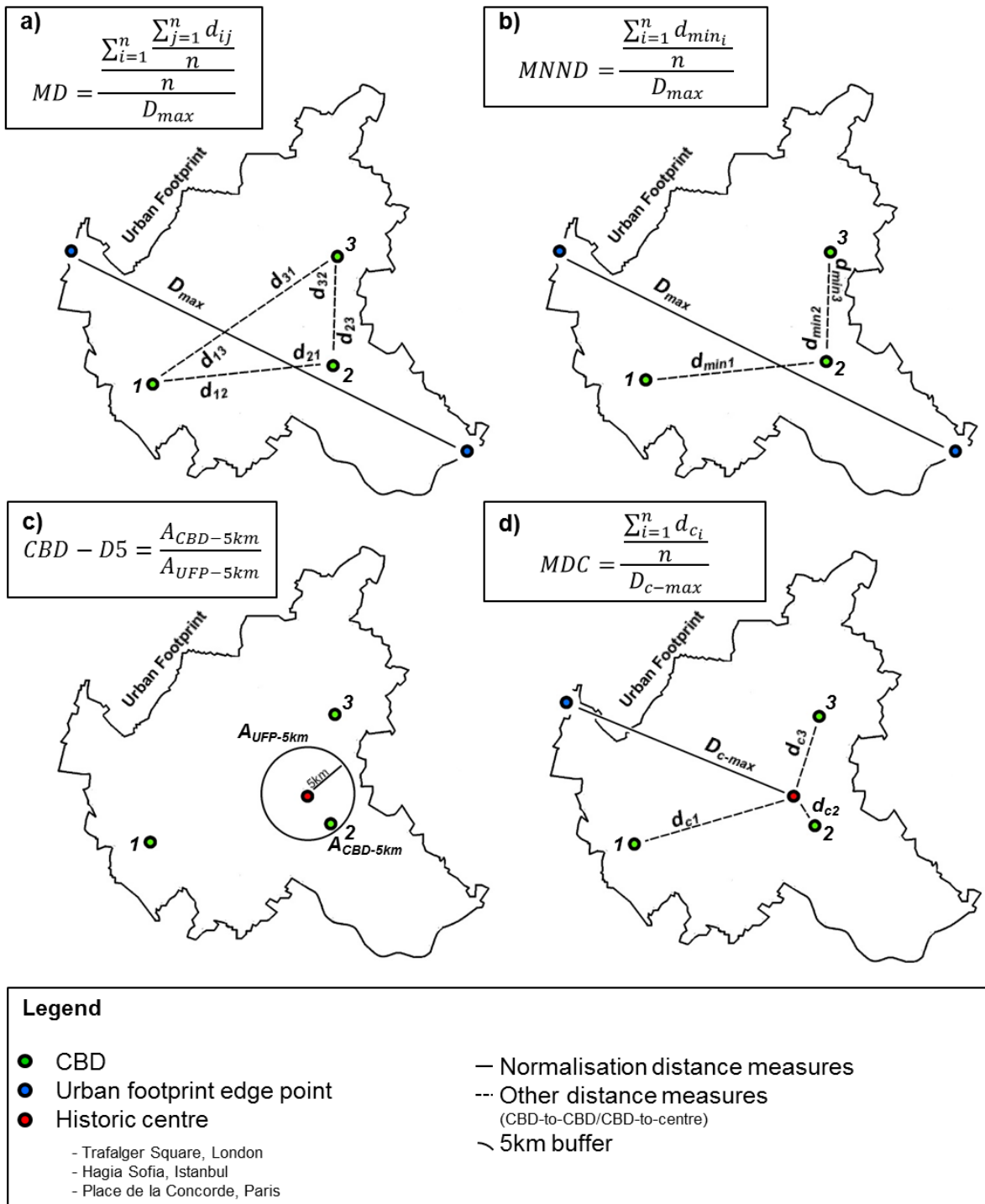
Fig. 3-14 Calculation scheme of spatial configuration metrics

4. ANALYSIS AND RESULTS

This chapter presents the analysis and results of this study which are subdivided into two sections: Thematic results of section 4.1 include the analysis of the 3D city models and final classification products from remote sensing analysis, as well as the cross-city comparison. To gain confidence about the transferability of the presented methods and the consistency of the thematic results, the methodological evaluation of section 4.2 covers the accuracy assessment of CBD delineation from remotely sensed data and the related subproducts.

4.1 Thematic results

4.1.1 Analysis of 3D city models

The results from analysis of the 3D city models (Figure 4-2) present not only a high-detail physical reference for the remote sensing analysis but also a test for the central hypothesis, and thus, the conceptual foundation of this study. These results originate from the statistical differentiation of the classes CBD and Non-CBD on block level (Figure 4-1) and include the structural comparison, as well as the identification of parameter thresholds on class level.
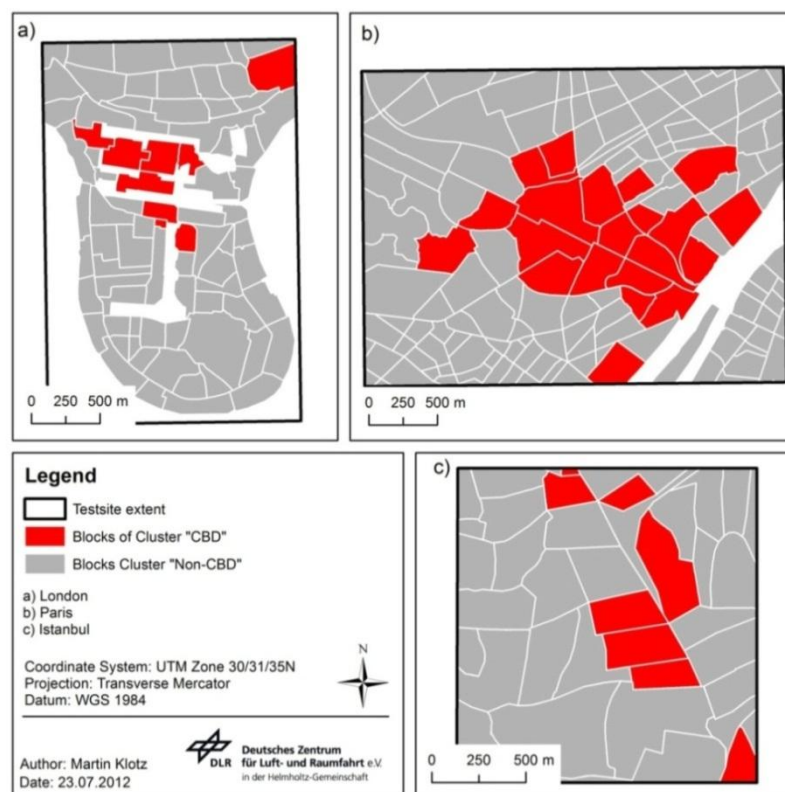
Fig. 4-1 Clustering results on block level
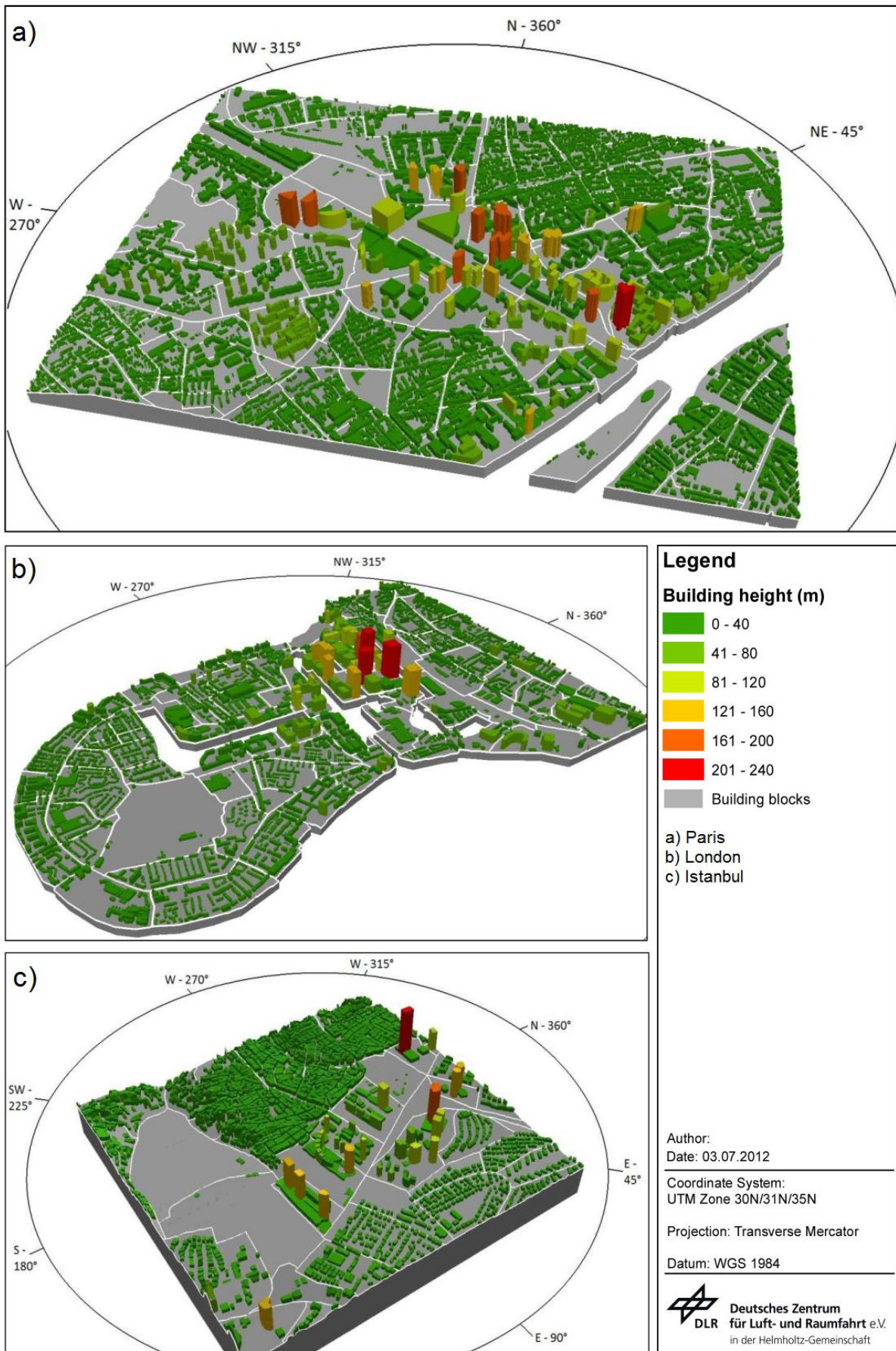
Fig. 4-2 3D perspective on the building models for the three test sites

4.1.1.1 Structural comparison

The differentiation of CBDs and Non-CBD areas by dissimilarity clustering on block level implies a significant difference between the six building parameters selected. However, not only do the derived physical characteristics allow for a deeper insight into the physical face on CBDs and the identification of quantitative thresholds but they also present a test for the central hypothesis of this study. Thus, the subsequent analysis compares the classes CBD and Non-CBD based on the selected parameter set using within- and between-group variance across test sites.

Maximum/average height (Figure 4-3): These parameters do not show considerable differences across test sites. However, CBDs feature significantly higher building heights compared to the urban surrounding. The within-group variability is lower among Non-CBD areas revealing a higher degree of homogeneity of the surrounding urban morphology and underscoring the variance between the two classes. Beyond this, CBDs exhibit a high vertical variability with peak values of average and maximum height at Carnary Wharf.
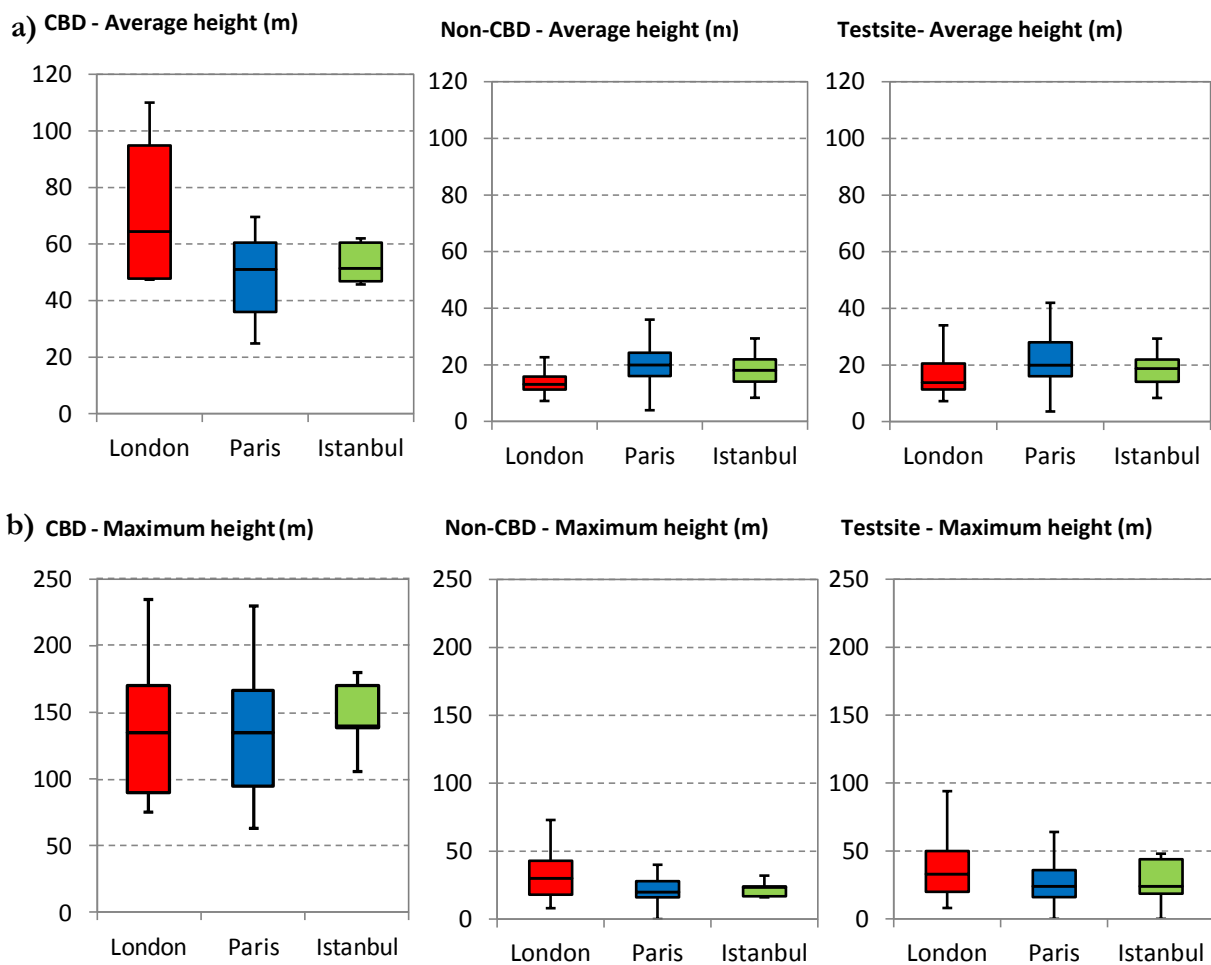
Fig. 4-3 Boxplots illustrating a) average and b) maximum building height on class and test site level

Maximum/average volume (Figure 4-4): Due to high correlation of building height and volume, maximum and average volume show homogenous distributions similar to those of the aforementioned parameters across test sites. Significantly higher building volumes are found in CBDs of all sites, whereas lower within-group variabilities of Non-CBD areas are significantly exceeded by the variance between the two classes. Furthermore, the highest variability and absolute values of the average volume are found for Carnary Wharf and La Defense owing to the high spatial accumulation of voluminous buildings within these CBDs (Figure 4-2).
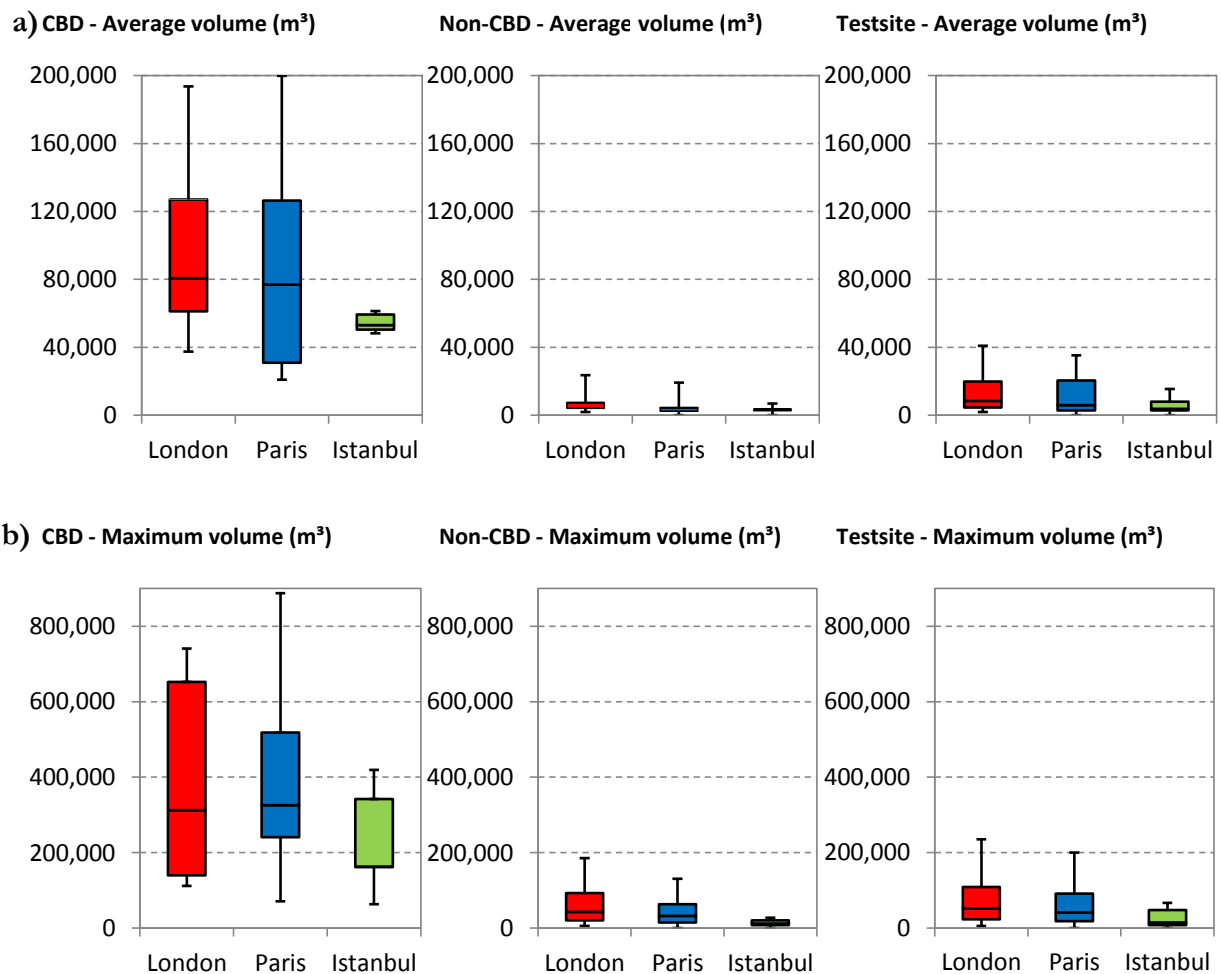
Fig. 4-4 Boxplots illustrating a) average and b) maximum building volume on class and test site level

Floorspace density/density of high-rise buildings (Figure 4-5): Again, this pair of parameters are very homogenous across the test sites with the lowest values identified for Levent due to the more disperse spatial distribution of high-rise buildings (Figure 4-2). On class level, considerable higher values of both parameters are found in CBDs of all sites due to the concentration of high buildings with large floorspaces. Besides that, the distinctly lower within-group variability of Non-CBD areas is clearly exceeded by the between-group variance of these parameters.
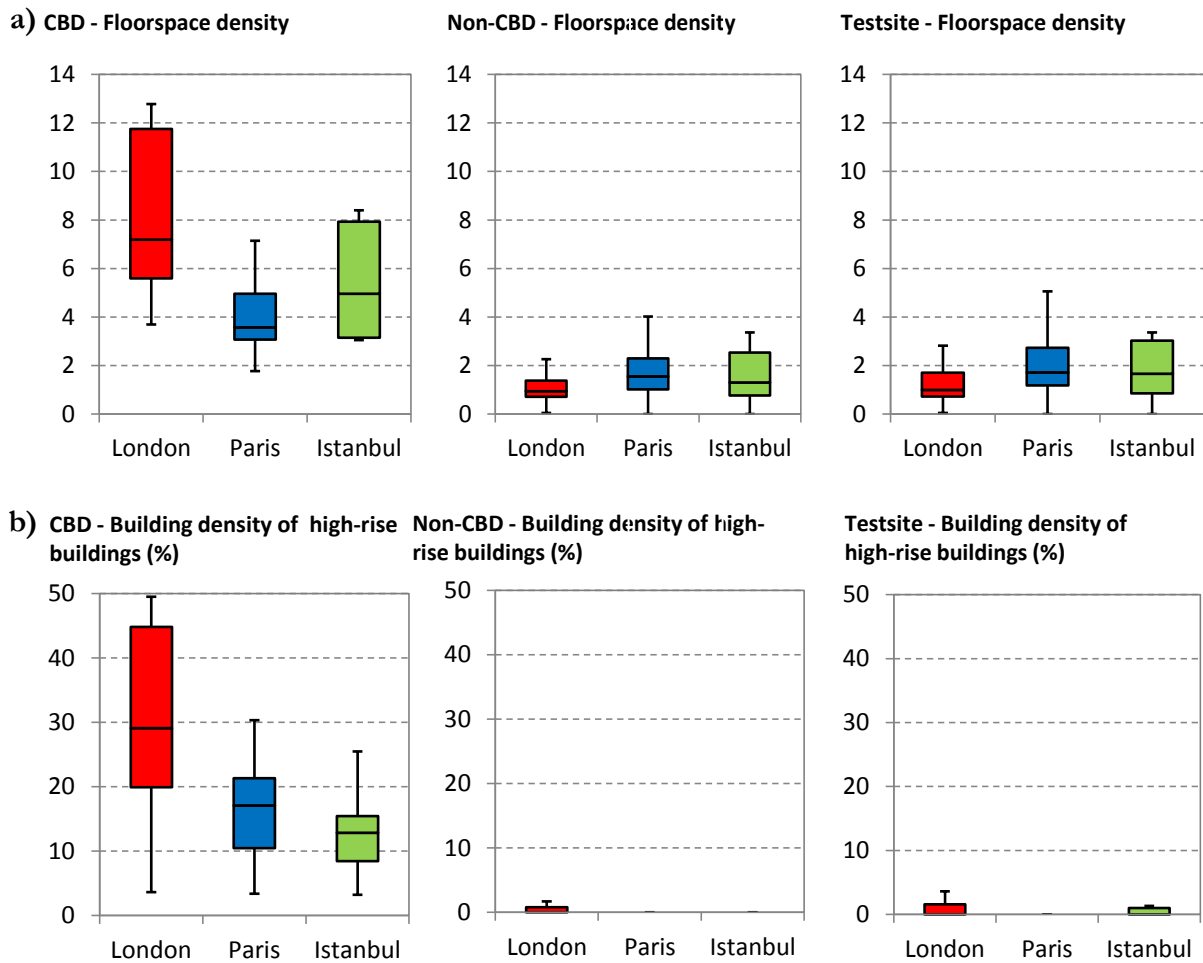
Fig. 4-5 Boxplots illustrating a) floorspace density and b) density of high-rise buildings on class and test site level

These structural analyses support the central hypothesis of this study by comparison of the classes CBD and Non-CBD. Although CBDs are by no means homogenous due to high within class variabilities, a constantly higher between-group variance compared to the within-group variance of the surrounding urban structures is obvious. This means that CBDs are more similar to each other across cities than to the more homogenous urban surrounding.

4.1.1.2 Threshold identification

By applying the two-class unsupervised clustering process to all observations across cities, comprehensive quantitative thresholds for object-based CBD delineation from remote sensing data are approximated. Due to the complexity of urban morphology, a holistic approach of parameter combination was preferred instead of consideration individual parameters that illuminate only a part of the complete picture of CBDs. As a consequence, the between-class transition of parameter values is not entirely disjunct (Figure 4-6), encouraging the decision for a fuzzy-based classification approach. The presented plots include the extrema of each parameter with regard to class range as well as the transition range representing the area of overlap. As Cartosat-1 DSMs do not allow for an analysis on the level of individual buildings, further thresholds for substitute physical parameters were derived from pixel level of each class.

In line with the high similarity of CBDs across cities, all transition ranges where found to be smaller than the absolute range of the class CBD. However, the range of transition varies across parameters as some, such as average height or floorspace density, feature more distinct class change-overs than others. Table 4-1 summarises the lower and upper values of the transition range for each building parameter and its pixel-based substitute. Except for physical volumes, only minor deviations exist between values derived from pixel and building level for the lower thresholds that are decisive for the classification of CBDs. Overall, the uniform criteria derived from the analysis of 3D city models should allow for a transferable and thus, comparable localisation of CBDs on urban footprint level.

Tab. 4-1 Upper and lower thresholds of the transition range derived from building and pixel level

	Building level		Pixel level	
	Lower Threshold	*Upper Threshold*	*Lower Threshold*	*Upper Threshold*
Average height (m)	24.78	42.00	24.37	59.82
Maximum height (m)	36.00	126.00	36.00	126.00
Average volume (m³)	20,996	93,635	609	1,495
Maximum volume (m³)	74,948	541,422	900	3,150
Floorspace density	1.77	4.53	1.75	4.02
Density of high-rise buildings (%)	2.30	17.94	2.30	17.94
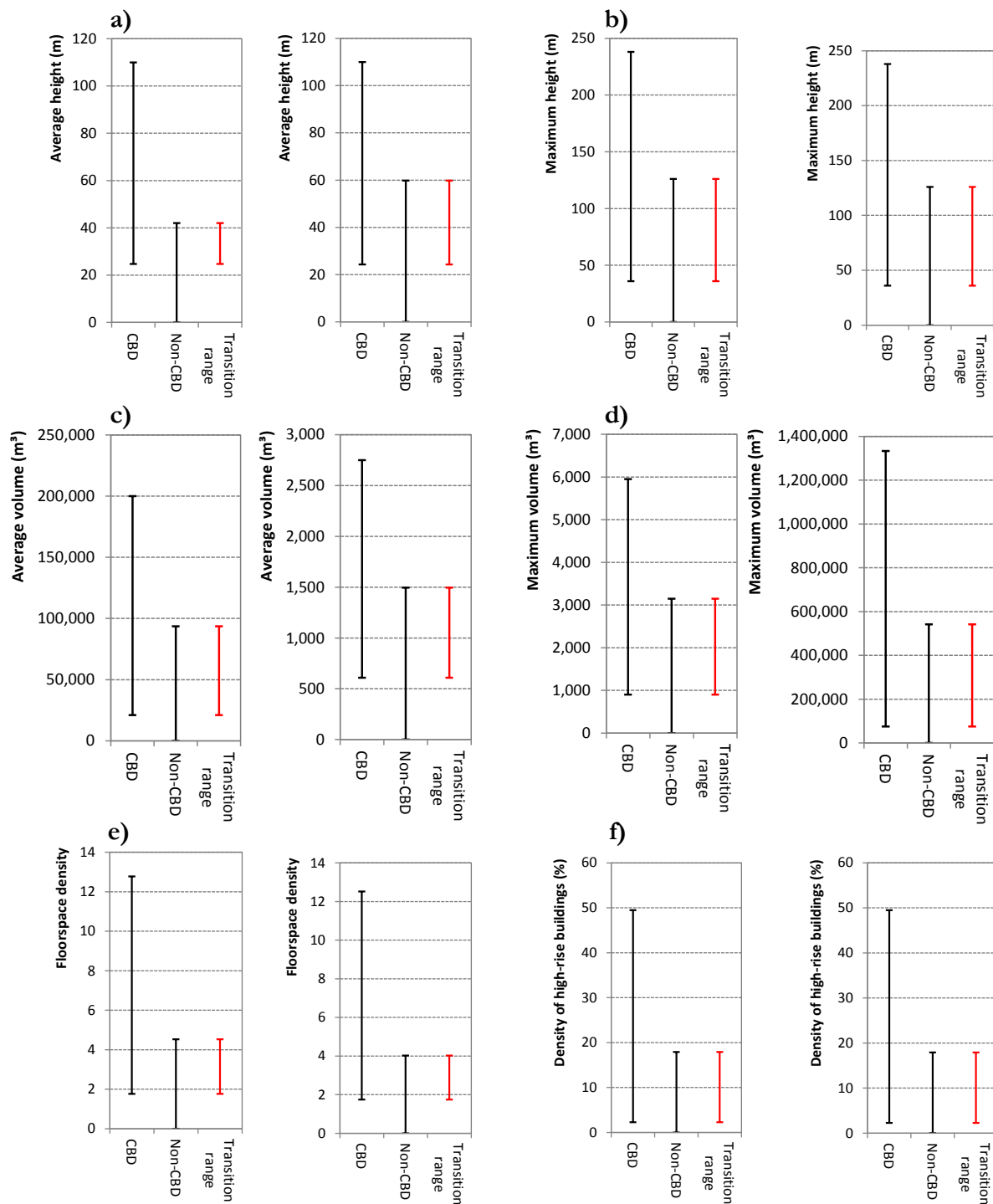
Fig. 4-6 Range plots showing the absolute and the transition range (red) of a) average height, b) maximum height, c) average volume, d) maximum volume, e) floorspace density, and f) density of high-rise buildings of both thematic classes derived from building (left) and pixel level (right)

4.1.2 CBD delineation results

The final delineation results based on the aforementioned parameter thresholds on urban footprint level are displayed in figure 4-7. The determined membership values for each block are shown in figure 4-8 as the minimum of membership of all physical parameters. The maps show that for all cities the CBDs of the selected test sites are detected with maximum membership

values identified for La Defense and Carnary Wharf. With regard to the thematic interpretation, the accuracy of these results needs to be assessed in terms of their spatial delineation and detection (section 4.2.3).
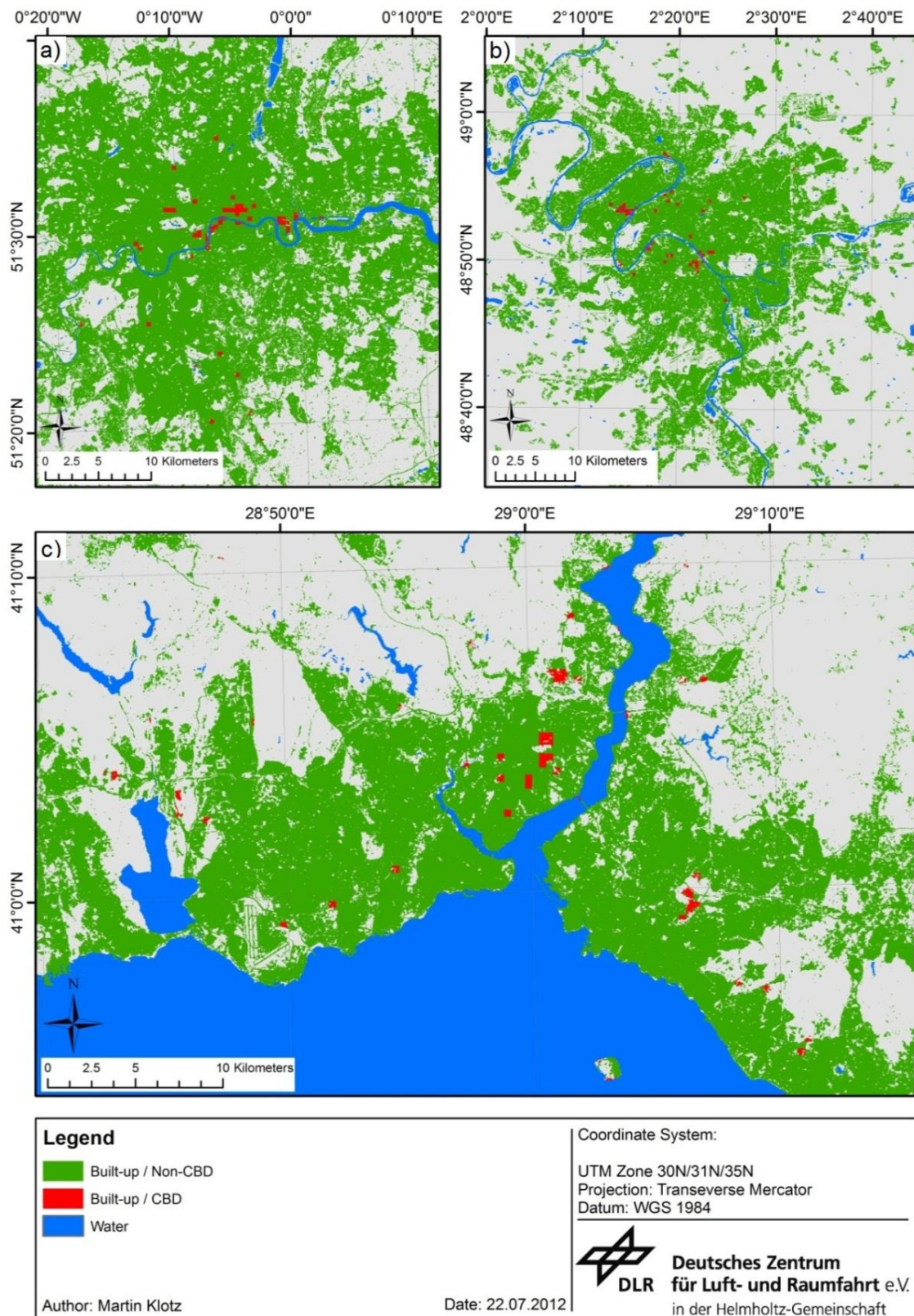
Fig. 4-7 CBD classification results for a) London, b) Paris, and c) Istanbul
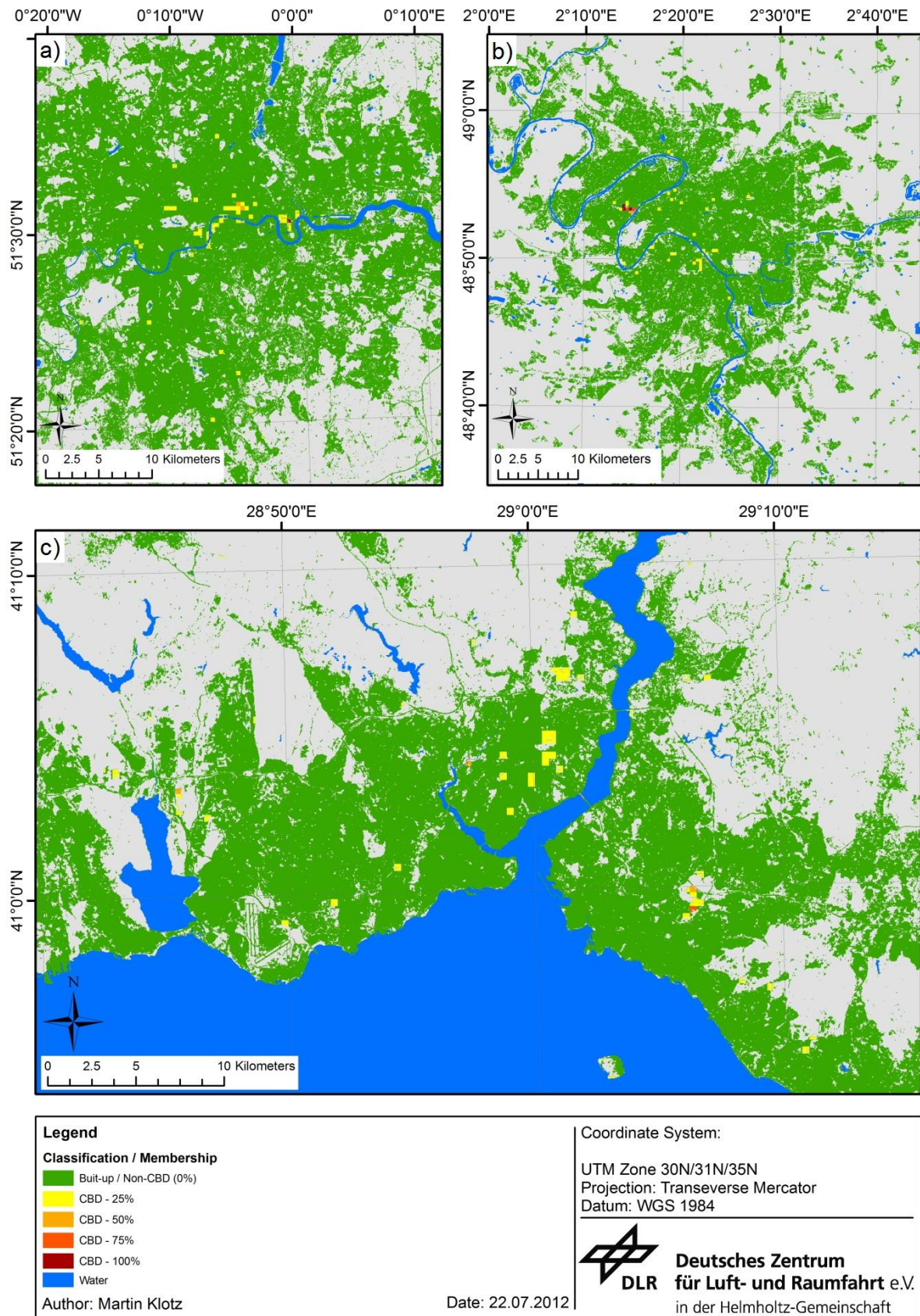
Fig. 4-8 CBD classification results including membership values for a) London, b) Paris, and c) Istanbul

4.1.3 Cross-city comparison

The interpretation of the spatial configuration of the correctly detected CBDs (section 4.3.2.3) across cities presents a difficult task due to two reasons: (1) CBDs are a type of planned formal settlements. Therefore, a comprehensive interpretation of the spatial arrangement of this UST commonly requires expert knowledge on the urban planning context of the particular city or region. (2) CBDs are defined and delineated based on purely physical characteristics. Thus, the spatial CBD configuration can only be interpreted as an arrangement of urban structure types indicating city-internal centres but cannot be directly related to functional arrangement of urban land use.

Across cities, the number of CBDs is relatively similar ranging between 22 detected districts for London and 25 for Istanbul (Figure 4-9). The total CBD area is averaging at around 6km² for all cities. When looking at the relative CBD coverage, a higher value is found for Istanbul compared to the other cities, contrasting its lower *LPI* of CBDs. Thus, Istanbul does not feature an extensive dominant CBD such as La Defense in Paris or the financial district in the City of London which in turn, indicate the supremacy of these global cities with regard to international business. Although Istanbul features the largest number, a dominant CBD cannot be identified indicating the coexistence of multiple centres in the polycentric urban landscape (Ciraci and Kundak, 2000).

Comparing the spatial configuration of CBDs, Istanbul exhibits the highest mean CBD-to-CBD distance but the lowest nearest neighbour distance. Thus, Istanbul's urban footprint level is characterised by disperse spreading of spatially clustered centres, whereas London and Paris show a more regular distributions of CBDs. Furthermore, Istanbul exhibits the lowest building density by CBDs within the urban core area and a high mean CBD-to-centre distance. In contrast, CBDs in London and Paris are located geographically more central with moderate mean distances to the historic centre.

Overall, these values reflect the nature of urban growth in the investigated cities. London and Paris, as rather monocentric and marginally growing metropolitan regions (Halbert, 2006; Taubenböck *et al.*, 2012), exhibit a more regular planned distribution of CBDs in geographically central locations with dominant and specialised centres. In contrast, the sprawling nature of

urban growth and the high-density building including informal settlements (Seger and Palencsar, 2010) in Istanbul directs construction of CBDs to the remaining open spaces of the polycentric urban landscape. The spider chart clearly reveals these differences and analogies across cities.

Legend:

n(CBDs) =	number of CBDs;
AA =	absolute area covered by CBDs (km²);
RA =	relative area covered by CBDs (‰);
LPI =	largest patch index (%);
MD =	relative mean CBD-to-CBD distance (%);
MNND =	relative mean CBD-to-CBD nearest neighbor distance (%);
CBD-D5 =	CBD density in relation to the built-up area in a 5km circle around the centre (%);
MDC =	relative mean CBD-to-centre distance (%)
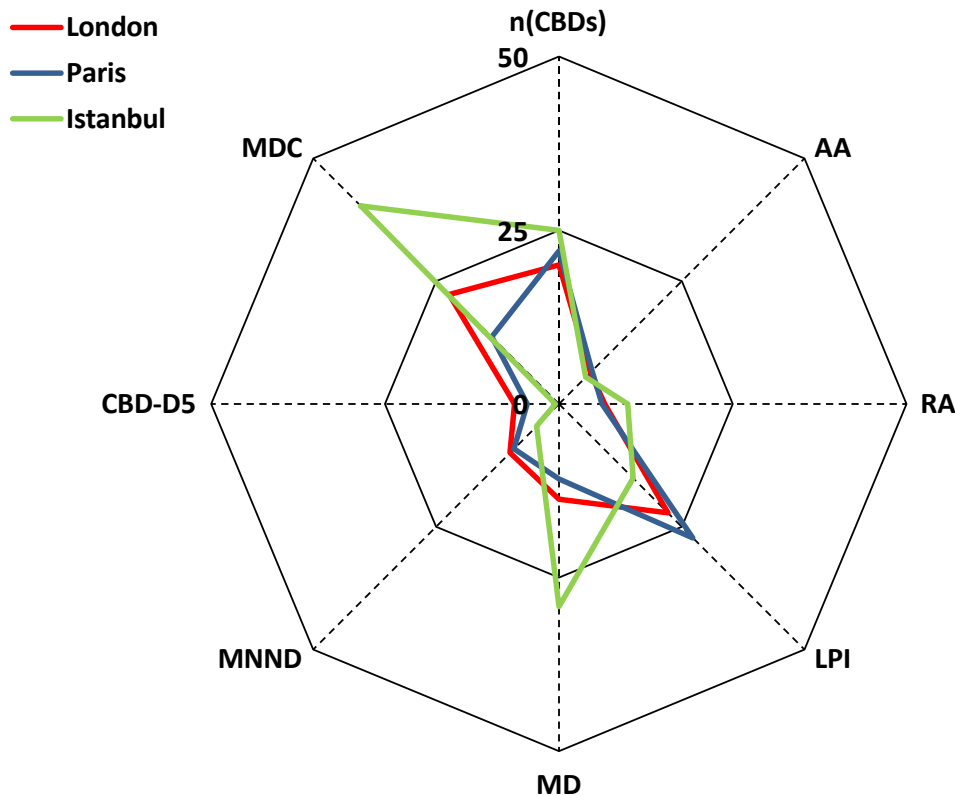
Fig. 4-9 Spider-charts presenting spatial metrics for cross-city comparison

4.2 Methodological evaluation

4.2.1 Accuracy of urban footprint classifications

The accuracy assessment of Landsat TM classifications (Figure 4-10) provides a degree of confidence about the employment of the urban footprint as a spatial reference for CBD delineation. For all classified images high overall accuracies between 88% and 95% were achieved. Furthermore, the Kappa-Index as a more robust measure ranges from 0.83 to 0.92

indicating that the obtained results are significantly better than chance (Table 4-2). Overall, the final urban footprint classifications allow for a correct delineation of built-up areas as a reliable spatial frame for CBD delineation despite their limited geometric potential.
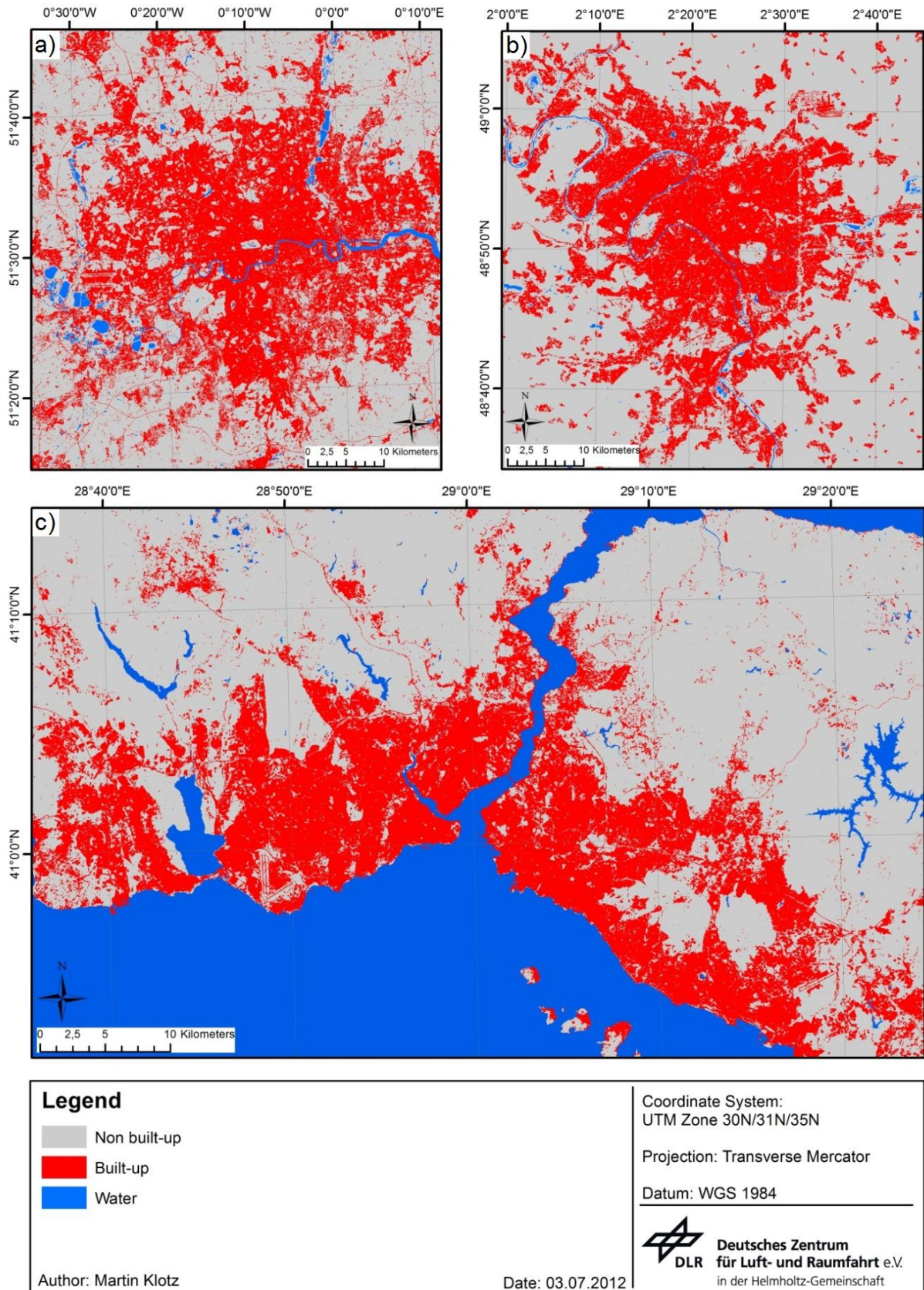
Fig. 4-10 Urban footprint classifications for a) London, b) Paris, and c) Istanbul

Tab. 4-2 Confusion matrices of urban footprint classifications

a) London 2011	Built-Up	Non Built-Up	Water	Row Total
Built-Up	94	6	0	100
Non Built-Up	15	83	2	100
Water	0	1	99	100
Column Total	109	90	101	300

Overall Accuracy	92.00		Kappa-Index	0.88
Producer Accuracy			**Omission**	
Built-Up	86.24		Built-Up	13.76
Non Built-Up	92.22		Non Built-Up	7.78
Water	98.02		Water	1.98
User Accuracy			**Commission**	
Built-Up	94.00		Built-Up	6.00
Non Built-Up	83.00		Non Built-Up	17.00
Water	99.00		Water	1.00

b) Paris 2006	Built-Up	Non Built-Up	Water	Row Total
Built-Up	83	15	2	100
Non Built-Up	9	88	3	100
Water	0	5	95	100
Column Total	92	108	100	300

Overall Accuracy	88.67		Kappa-Index	0.83
Producer Accuracy			**Omission**	
Built-Up	90.22		Built-Up	9.78
Non Built-Up	81.48		Non Built-Up	18.52
Water	95.00		Water	5.00
User Accuracy			**Commission**	
Built-Up	83.00		Built-Up	17.00
Non Built-Up	88.00		Non Built-Up	12.00
Water	95.00		Water	5.00

c) Istanbul 2006	Built-Up	Non Built-Up	Water	Row Total
Built-Up	94	6	0	100
Non Built-Up	7	93	0	100
Water	0	3	97	100
Column Total	101	102	97	300

Overall Accuracy	94.67		Kappa-Index	0.92
Producer Accuracy			**Omission**	
Built-Up	93.07		Built-Up	6.93
Non Built-Up	91.18		Non Built-Up	8.82
Water	100.00		Water	0.00
User Accuracy			**Commission**	
Built-Up	94.00		Built-Up	6.00
Non Built-Up	93.00		Non Built-Up	7.00
Water	97.00		Water	3.00

4.2.2 Evaluation of morphological filtering results

Beside urban footprint classification, a further important working stage is presented by the generation of nDSMs as a representation of the above-ground building volume for CBD delineation. In this context, DTMs as the decisive subproduct of the morphological filtering process are assessed. For this purpose, a 5m digital terrain model of 1.5m vertical accuracy provided by Bluesky (2012) for the test site in London was used. Table 4-3 exhibits measures of error from the difference image (Filtered DTM - Reference DTM) including RMSE with regard to different kernel sizes tested. The results show the minimum deviations for a kernel window size of 10x10 pixels. Although minimum and maximum deviations range between -14m and 12m, the RMSE of 2.81 in combination with a close-to-zero mean error reveals that the filtering results are good enough for the representation of the above-ground building volume in its correction dimension.

Tab. 4-3 Statistical evaluation of the produced DTM in relation to varying kernel size, Carnary Wharf

Kernel	Min.	Max.	Mean	Std. Dev.	RMSE
3	-9.45	24.25	4.22	2.64	4.98
5	-10.11	17.54	3.23	2.43	4.04
10	-14.02	12.43	0.23	2.48	2.81
20	-18.81	7.59	-0.57	2.91	2.97
30	-26.32	7.06	-2.19	3.45	4.09
40	-26.33	4.76	-3.42	3.88	5.20
50	-26.67	3.67	-4.43	4.16	6.08
75	-26.33	3.07	-6.93	4.80	8.43
100	-26.32	3.02	-8.60	5.19	10.05
150	-28.29	2.87	-12.13	5.36	13.23
200	-28.29	2.87	-14.66	5.15	15.52

In addition to these descriptive statistics, profile graphs of the filtered and the reference DTMs are displayed in figure 4-11 for the optimum kernel size. With respect to Cartosat's geometric capabilities, the profiles show that the algorithm is generally able to detect bare-earth surface from the input DSM and in turn, allow for the generation of reliable nDSMs in spite of local deviations of up to 5m. To gain further confidence about the selected kernel size, an advanced DTM evaluation for all test sites has been carried out with regard to reference DTMs generated using hierarchical image filtering from Cartosat-1 stereo images by Arefi *et al.* (2009). In this context, similar optimum kernel sizes ranging between 5 and 10 pixels and very consistent profiles were found confirming the accuracy of the proposed method.
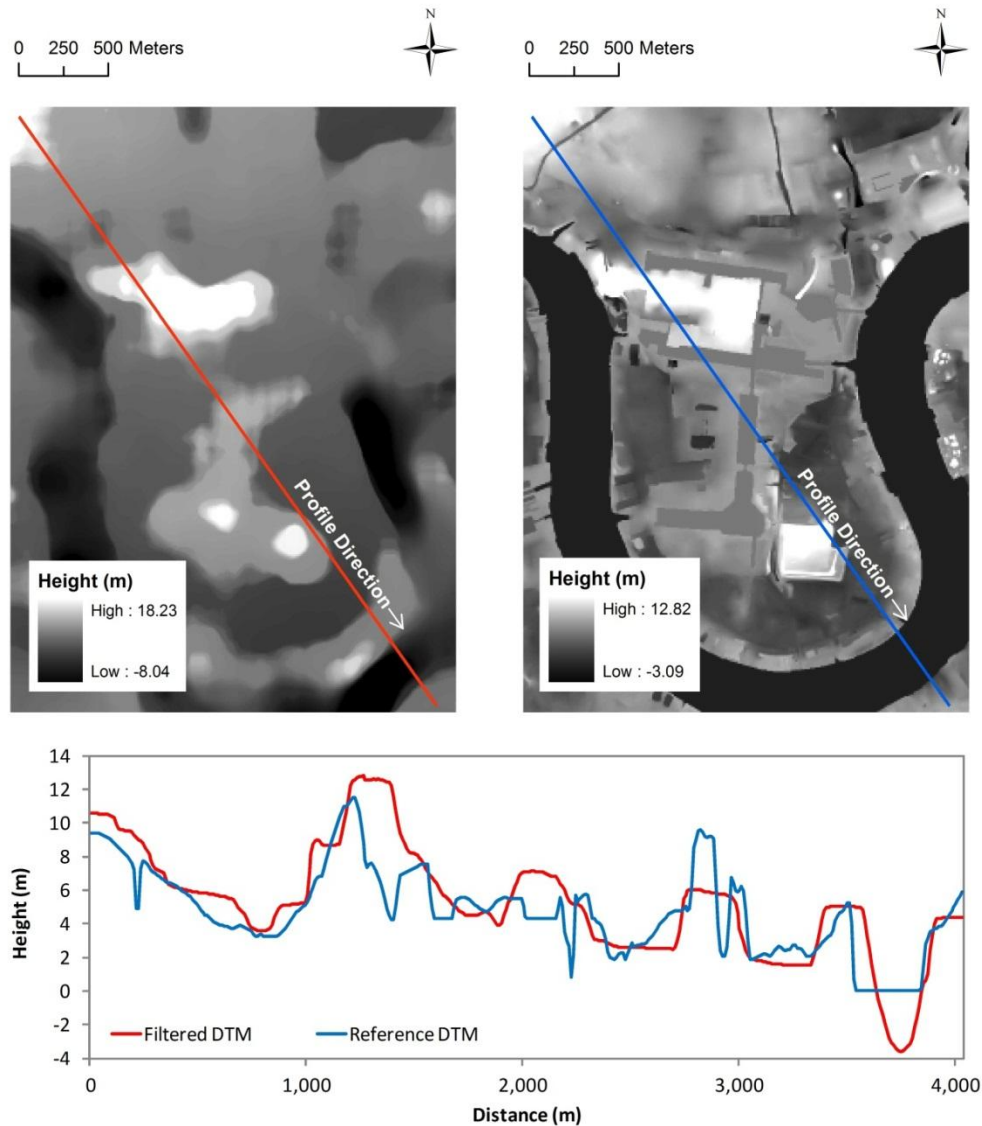
Fig. 4-11 DTM quality assessment by profile lines, Carnary Wharf (kernel size: 10x10 pixel)

4.2.3 Accuracy of object-based CBD delineation

4.2.3.1 Spatial delineation accuracy

The spatial delineation accuracy is assessed to determine the precision of the final CBD classification within the selected test sites compared to the statistical delineation of CBDs by dissimilarity clustering. Across test sites, the overall accuracies range between 83% and 86% (Table 4-4). Furthermore, the Kappa-Index constantly exceeds a value 0.38 in comparison to a chance agreement. These numbers indicate a high accuracy of the overall classification on test site level. However, delineation results feature increased errors of omission, especially for CBDs, resulting in considerable lower producer accuracies ranging between 63% and 77%. Furthermore,

relatively high errors of commission across test sites lead to low user accuracies between 31% and 67%. These shortcomings in terms of spatial precision result predominantly from the choice of square units as building blocks and emphasise a distinct problem of scale inherited in the designation of suitable statistical reference units for parameters aggregation. Although the delineated areas are not found to be overly precise regarding their form, CBDs are generally correctly delineated from the surrounding urban environment.

Tab. 4-4 Confusion matrices of spatial CBD delineation for a) Carnary Wharf, b) La Defense, and c) Levent

a) London	CBD	Non-CBD	Row Total
CBD	12,873	28,528	41,401
Non-CBD	3,942	189,062	193,004
Column Total	16,815	217,590	234,405
Overall Accuracy	86.15	Kappa-Index	0.38
Producer Accuracy		Omission	
CBD	76.56	CBD	23.44
Non CBD	86.89	Non CBD	13.11
User Accuracy		Commission	
CBD	31.09	CBD	68.91
Non CBD	97.96	Non CBD	2.04

b) Paris	CBD	Non-CBD	Row Total
CBD	47,145	23,687	70,832
Non-CBD	22,507	190,216	212,723
Column Total	69,652	213,903	283,555
Overall Accuracy	83.70	Kappa-Index	0.56
Producer Accuracy		Omission	
CBD	67.69	CBD	32.31
Non CBD	88.93	Non CBD	11.07
User Accuracy		Commission	
CBD	66.56	CBD	33.44
Non CBD	89.42	Non CBD	10.58

c) Istanbul	CBD	Non-CBD	Row Total
CBD	9,528	12,661	22,189
Non-CBD	5,510	78,991	84,501
Column Total	15,038	91,652	106,690
Overall Accuracy	82.97	Kappa-Index	0.41
Producer Accuracy		Omission	
CBD	63.36	CBD	36.64
Non CBD	86.19	Non CBD	13.81
User Accuracy		Commission	
CBD	42.94	CBD	57.06
Non CBD	93.48	Non CBD	6.52

4.2.3.2 Detection accuracy

The spatial detection accuracy presents a check whether the blocks classified as CBDs reflect the typical physical feature of CBDs based on a visual comparison. Overall, 134 of 177 blocks detected across cities reflect structures in line with the physical features of CBDs resulting in a total user accuracy of 76% and an error of omission of 24% (Table 4-5). Examples of correctly detected blocks from this aerial evaluation and include the Milbank Centre (2), the City (3), and St George Wharf (5) for London (Figure 4-12), the commercial centre (2), the national library (3), and the shopping district at the Tour Monteparnasse (5), for Paris (Figure 4-13), as well as the high-rise residential district Atasehir (3), Sisli Plaza (4), and Maslak CBD (5) for Istanbul (Figure 4-14). Between cities, constantly high accuracies are evident in London and Paris whereas Istanbul features a higher error of commission of 33%. This can be attributed to the more complex urban terrain in Istanbul inducing morphological errors. However, the overall high detection accuracies confirm the transferability of the presented method and the applied thresholds across cities.

Tab. 4-5 Aerial evaluation of the detection accuracy

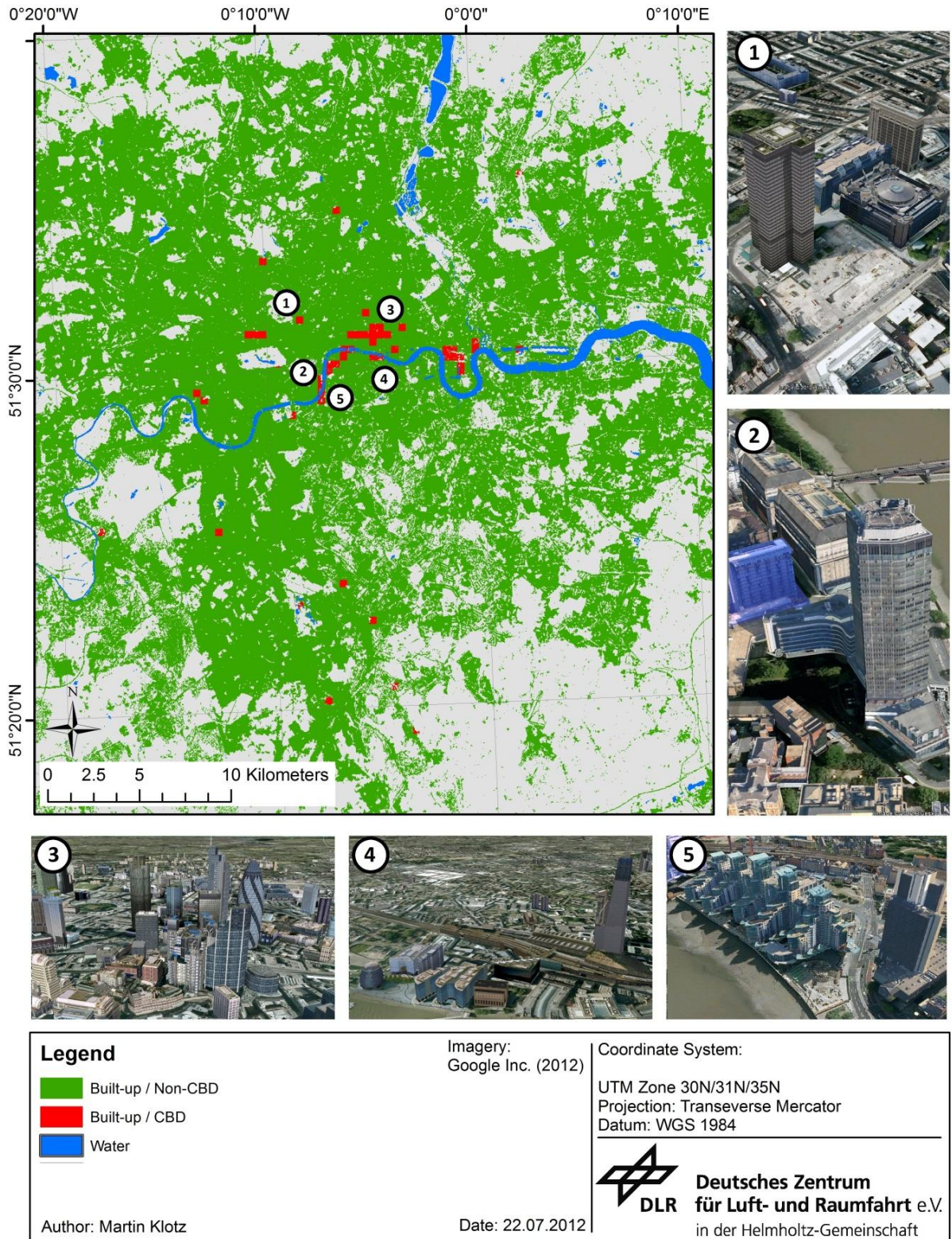|	London		Paris		Istanbul		Total	
	Absolute	Percentage (%)	Absolute	Percentage (%)	Absolute	Percentage (%)	Absolute	Percentage (%)
Number of blocks detected	57	100.00	54	100.00	66	100.00	177	100.00
User Accuracy	45	78.95	45	83.33	44	66.67	134	75.71
Erros of commission	12	21.05	9	16.67	22	33.33	43	24.29

Fig. 4-12 Aerial evaluation map, London

Fig. 4-13 Aerial evaluation map, Paris
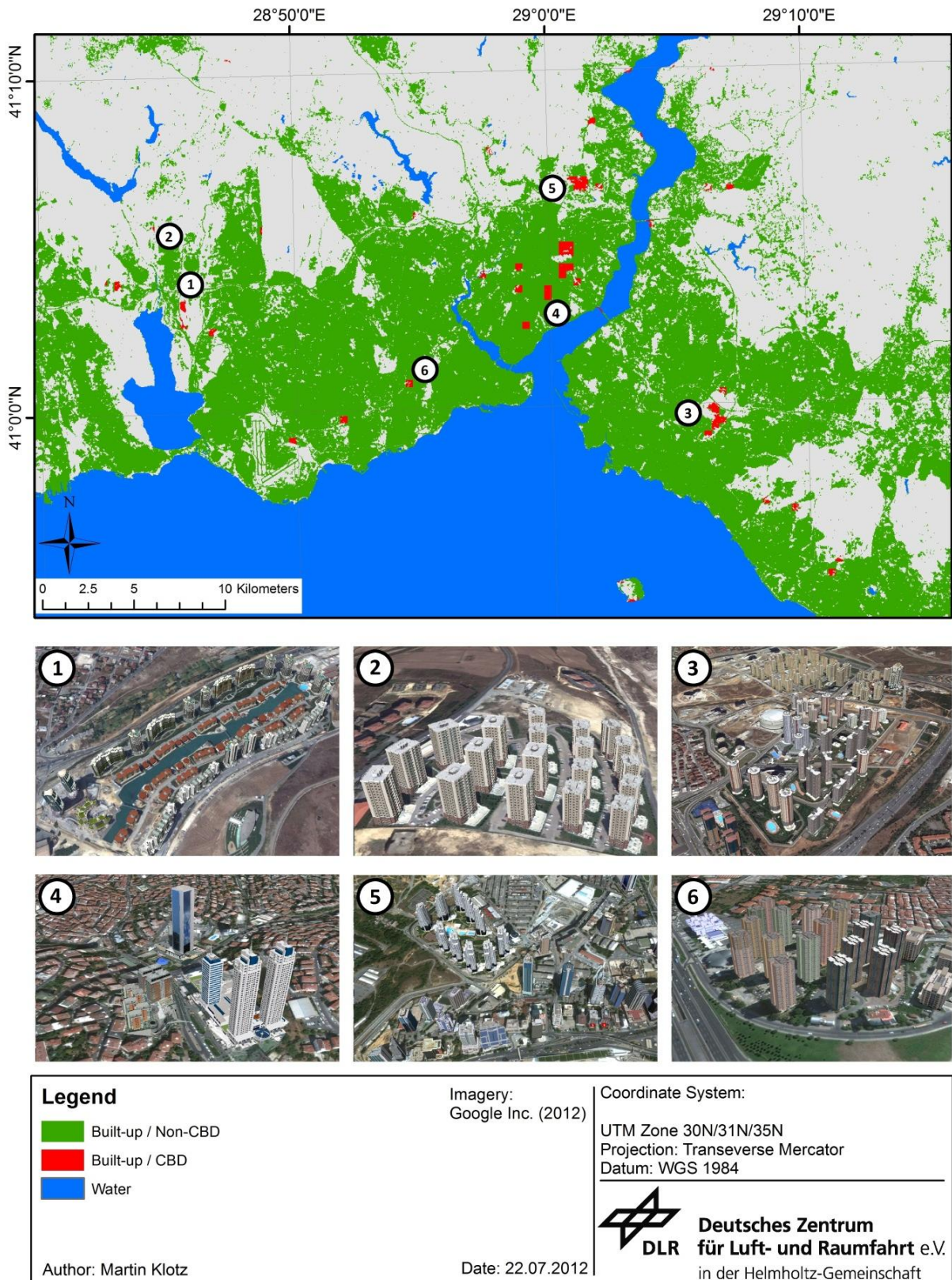
Fig. 4-14 Aerial evaluation map, Istanbul

5. MAIN FINDINGS

In order to present the main findings of this study, it is referred to the research questions defined in section 1.3 of this dissertation.

(1) For the delineation of CBDs as an UST from the surrounding urban morphology, physical parameters were logically derived from qualitative statements of the published literature. This parameter set includes average and maximum values of building height and volume, building density of high-rise buildings, as well as floorspace density. This holistic approach of parameter combination allows for a comprehensive representation of the physical face of CBDs across cities.

(2) Structural analyses by comparison of CBDs and Non-CBD areas derived from 3D city models on district level reveal significant differences regarding the classes' physical features. With regard to all selected parameters, the analysis of within- and between-group variance clearly shows that CBDs are – across cities - more similar to each other than to the more homogenous urban environment. This confirms that CBDs can be differentiated from the surrounding urban morphology due to its physical characteristics and thus, the central hypothesis of this study.

(3) In order to delineate CBDs from the surrounding urban morphology based on physical parameters, the combination of multispectral Landsat images and HR DSMs provide the required physical features. Cartosat-1 stereo sensors have proofed to be particularly suitable for the generation of large-scale and high-resolution DSMs covering extensive urban agglomerations. Although the extraction of individual buildings is beyond the data's geometric capabilities, the above-ground building volume is presented in its correct dimension on pixel level for the spatial delineation of CBDs.

(4) The remote sensing analysis of this study presents a method for CBD delineation in large-scale urban environments. This method includes the extraction of the urban footprint from multispectral Landsat scenes as a spatial frame for CBD delineation, followed by a stepwise semi-automatic procedure of morphological filtering, hierarchical segmentation and fuzzy-logic classification of Catosat-1 DSMs. Using the same set of physical parameters, a straight-forward classification rule, and comprehensive class thresholds across cities, this method

provides a transferrable approach towards CBD detection and delineation for large-scale and complex urban environments.

(5) By applying the presented method to three European megacities, CBDs are detected with a producer accuracy of 75.71% and spatially delineated with overall accuracies exceeding 82.97%. Furthermore, delineation results are significantly better than chance indicated by the Kappa Index ranging between 0.38 and 0.56. However, due to the choice of artificial square reference unites for the aggregation of physical parameters, classification results are not highly precise which is reflected by relatively high errors of commission and omission. Nevertheless, for applications of urban risk analysis or large-scale urban planning, CBDs are generally correctly delineated. Furthermore, the high overall accuracies confirm the transferability of the applied method and thresholds.

(6) Spatial metrics paint a characteristic picture of the spatial configuration of CBDs across cities which can be attributed to the nature of urban growth. London and Paris exhibit regular distributions of CBDs in geographically central locations and comparatively large dominant CBDs in line with the coordinated way of urbanisation. In contrast, the sprawling nature of urban growth and high-density building of fast-changing Istanbul, forces the construction of clustered CBDs to remaining open spaces in non-central locations of the polycentric urban landscape.

In this context, also the limitations of datasets and the presented method must be discussed. First, as Cartosat-1 DSMs do not allow for an analysis of the built environments on the level of individual buildings, substitute physical parameters are employed on pixel level that are associated with a certain degree of information loss. Nevertheless, these parameters reflect the distinct physical features of CBDs in their correct dimension relative to the urban surrounding. Second, a considerable limitation is presented by the use of artificial square blocks as statistical reference units as street network data do not present a feasible databasis for transferable CBD delineation in large-scale cities due to consistency and availability of data. Consequently, the alternative choice for grid-based structuring induces scale-dependent errors of precision of the final classification. However, this approach presents the best possible practice at the current state of data availability. Finally, a decisive limitation is related to the basic conceptual approach of this study. By the definition of the CBD as an UST based on purely physical characteristics a direct relation to the urban land use cannot be established. This decision is based on the capabilities of remote sensing measuring the physical face of cities and justified by limited data availability of

socioeconomic variables from large-scale land use surveys. In fact, this very lack of data is the reason for a distinct research gap towards delimitation of CBDs and the main motivation of this study.

6. CONCLUSION

Definitions of CBD as a mental construct are fuzzy and mostly qualitative. This study has introduced a conceptual framework to classify and define measurable physical parameters to delineate CBDs from a morphological point of view. In this context, remote sensing has proved to be an up-to-date and area-wide data provider capable for the structuring of large-scale, dynamically changing, and complex urban areas. For CBD delineation based on physical parameters, HR DSMs from the Indian satellite Cartosat-1 have proven to be particularly useful as they feature large aerial coverage and availability at a high geometric resolution and thus, allow for the extraction of the decisive physical attributes.

With regard to urban risk analysis and land use based disaggregation of exposure data, the presented approach can be seen as a reasonable step forward to support CBD delineation, especially in combination with more widely available spatial datasets such as socioeconomic variables on postcode level in the future. Furthermore, large-scale urban planning can benefit from the presented method and results as they indicate an important part of the functional arrangement of cities. However, to gain further confidence about the transferability of this approach, the presented method and the applied thresholds need to be evaluated for a larger number of test sites.

The study at hand clearly reveals that further research for urban structuring is on demand. The structural reflection of urban areas by remote sensing is one perspective of urban analysis. As a visual representation of socio-economic influence, population pressure, political actions and many more, the physical structure is a distinct indicator for urban land use. However, due to the number and diversity of influencing variables, interdisciplinary approaches may allow for a deeper insight and understanding of the functional arrangement of cities in the future.

REFERENCES CITED

Abelen, S., Taubenböck, H., and Stilla, U. (2011) Interactive classification of urban areas using decision trees. *In*: Proceedings of the Joint Urban Remote Sensing Event (JURSE), Munich, China, 11-13 April. Munich: JURSE.

Abelen, S. (2009) *Development of a user interface for optimizing urban area classification from Landsat data.* Thesis (MSc): Technical University of Munich.

Albertz, J. (2007) *Einführung in die Fernerkundung. Darmstadt*: WBG.

Alonso, W. (1960) A theory of the urban land market. *Papers in Regional Science*, 6, 149-157.

Angel, S., Sheppard, S.C., and Civco, D.L. (2005) *Thy dynamics of global urban expansion.* Washington: Transport and Urban Development Department, World Bank.

Arefi, H., d' Angelo, P., Mayer, H., and Reinartz, P. (2009) Automatic generation of digital terrain models from Cartosat-1 stereo images. *In*: Proceedings of the International Society for Photogrammetry and Remote Sensing workshop 2009, Hannover, 2-5 June 2009. Hannover: ISPRS.

Baerwald, T.J. (1978) The emergence of a new downtown. *Geographical Review*, 68, 308-318.

Batty, M., and Longley, P., (1994) *Fractal Cities.* London: Academic Press.

Benenson, I., and Torrens, P.M. (2004) *Geosimulation – Automata-based modeling of urban phenomena.* London: John Wiley & Sons.

Benner, J., Geiger, A., and Leinemann, K. (2005) Flexible generation of semantic 3D building models. *In*: Gröger, G., Kolbe, T., eds. *International ISPRS/EuroSDR/DGPF-Workshop on Next Generation 3D City Models.* Bonn: EuroSDR, 2005, 17-22.

Benz, U., Hoffman, P., Willhauck, G., Lingenfelder, I., and Heynen, M. (2004) Multi-resolution, object-oriented, fuzzy analysis of remote sensing data for GIS-ready information. *ISPRS Journal of Photogrammetry and Remote Sensing*, 58, 239-258.

Berry, P., and Allen, P. (1961) *Central place studies: A bibliography of theory and applications.* Philadelphia: Regional Science Research Institute.

Blaschke, T. (2010) Object based image analysis for remote sensing. *Journal of Photogrammetry and Remote Sensing*, 65. 2-16.

Bluesky (2012) 5m Digital Terrain Model, England and Wales (DTM). *Licensed by The GeoInformation Group, received and distributed by the Landmap service of Mimas at the University of Manchester* [Online]. Available from: http://www.landmap.ac.uk/index.php/Datasets/

Bluesky-DTM/Key-Facts-Bluesky-DTM/menu-id-100331.html [Accessed: 18 April 2012].

Bochow, M. (2010) *Automatisierungspotential von Stadtbiotopkartierungen durch Methoden der Fernerkundung.* Thesis (PhD). University of Osnabrück.

Bochow, M., Segl., K., and Kaufmann, H. (2007) Automating the built-up process of feature-based fuzzy logic models for the identification of urban biotopes from hyperspectral remote sensing. *In*: Proceedings of the Joint Urban Remote Sensing Event, Paris, France, 11-13 April 2007. Paris: URS/URBAN.

Borruso, G., and Porceddu, A. (2009) A Tale of Two Cities: Density Analysis of CBD on Two Midsize Urban Areas in Northeastern Italy. *In*: Murgante, B., Borusso, G., and Lapucci, A., eds. *Geocomputation and Urban Planni*ng. Berlin: Springer, 2009, 37-56.

Brenner, C. (2000) *Dreidimensionel Gebäudekonstruktion aus digitalen Oberflächenmodellen und Grundrissen.* Thesis (PhD). University of Stuttgart.

Breunig, M., Taubenböck, H., Wurm, M., and Roth, A. (2009) Changing urbanity in Istanbul - Analysis of megacity developments using synergistic potentials of multi-temporal SAR and optical data. *In*: Proceedings of the Joint Urban Remote Sensing Event, Shanghai, 20-22 May 2009. Shanghai: URS/URBAN.

Burgess, E.W. (1929) Urban areas. *In*: Smith, T.V., and White, L.D., eds. *Chicago: An Experiment in Social Science Research.* Chicago: The University of Chicago Press, 1929, 113-138.

Carol, H. (1960) The hierarchy of central functions within the city. *Annals of the Association of American Geographers*, 50, 419-438.

Chander, G., Markham, B.L., and Helder, D.L. (2009) Summary of current radiometric calibration coefficients for Landsat MSS, TM, ETM+ and EO-1 ALI sensors. *Remote Sensing of the Environment,* 113, 893-903.

Chuvieco, E., and Huete, A. (2010): *Fundamentals of satellite remote sensing.* Boca Raton: CRC Press.

Ciraci, H., and Kundak, S. (2000) Changing urban pattern of Istanbul: From monocentric to polycentric urban structure *In*: 40th European Regional Science Conference, Barcelona, 29 August – 1 September 2000. Barcelona: European Regional Science Association.

Coffey, W.J., Polese, M., and Drolet, R. (1994) Examining the thesis of central business district decline: evidence from the Montreal metropolitan area. *Environment and Planning*, 28, 1795-1814.

Congalton, R.G., and Green, K. (2009) *Assessing the accuracy of remotely sensed data: Principles and practices.* 2nd ed. Boca Raton: CRC Press.

Couclelis, H. (1992) People manipulate objects (but cultivate fields): Beyond the raster-vector debate in GIS, Theories and Methods of Spatio-Temporal Reasoning in Geographic Space. *In*: Frank, A.U., Campari, I., and Formentini, U. (editors) *Lecture Notes in Computer Science*. Berlin: Springer, 2010, 65–77.

CTBUH – Council on Tall Buildings and Urban Habitat (2011) CTBUH Height Criteria – what is a tall building? *CTBUH* [Online]. Available from: http://www.ctbuh.org/TallBuildings/ HeightStatistics/Criteria/tabid/446/language/en-US/Default.aspx [Accessed: 2 April 2012].

D'Angelo, P., Schwind, P., Krauss, T., Barner, F., and Reinartz, P. (2009) Automated DSM based georeferencing of Cartosat-1 stereo scenes. *In:* Proceedings of International Archives of Photogrammetry, 39.

D'Angelo, Uttenthaler, A., Carl, S., BArner, F., and Reinartz, P. (2010) Automatic generation high quality DSM based on IRS-P5 Cartosat-1 stereo data. *In:* ESA Living Planet Symposium, Bergen, 28 June – 2 July 2010. Bergen: ESA.

Donnay, J.P., and Barnsley, M.J. (2001) *Remote sensing and image analysis*, 2nd ed. Boca Raton: CRC Press.

Drozdz, M., and Appert, M. (2010) Re-understanding the CBD: a landscape perspective. *In*: Naik, D., and Oldfield, T., eds. *Critical Cities*. London: Myrdle Court Press, 2010, 1-14.

Dulong, C., Filip, D., Früh, C., Lafon, S., Lyon, R., Ofab, A., Vincent, L., and Weaver, J. (2010) Google Street View: Capturing the World at Street Level. *IEEE Computer*, 43, 32-38.

Erteking, O. (2008) Spatial distribution of shopping malls and analysis of their trade areas. *European planning studies*, 16, 143-155.

ESRI (2011) ArcGIS Desktop (Release 10) *ESRI* [Software]. Redlands, CA: Environmental Systems Research Institute.

ESRI (2012) Basemap – World Imagery. *ESRI* [Online]. Available from: http://www.arcgis.com/home/item.html?id=10df2279f9684e4a9f6a7f08febac2a9 [Accessed: 4 August, 2012].

Fogelston, R.M. (2001) *Downtown: its rise and fall*. New Haven: Yale University Press.

Ford, L.R. (1976) The urban skyline as a city classification system. *Journal of Geography*, 75, 154-164.

Fritsch, D. (1999) Virtual Cities and Landscape Models - what has Photogrammetry to offer? *In*: Fritsch, D., and Spiller, R., eds. *Photogrammetric Week `99*. Heidelberg: Wichmann Verlag, 1999, 3-14.

Frueh, C., and Zakhor, A. (2003) Constructing 3D City Models by Merging Ground-Based and Airborne Views. *In*: IEEE Conference on Computer Vision and Pattern Recognition, Madison, WI, June 2003, Madison, WI: IEEE.

Frug, G.E., and Barron, D.J. (2008) *City bound: How states stifle urban innovation*. New York: Cornell University Press.

Galster, G., Hanson, R., Woman, H., Coleman, S., Frirebage, J., (2000) *Wrestling Sprawl to the Ground: Defining and Measuring an Elusive Concept*. Washington, DC: Fannie Mae Foundation.

Gianinetto, M. (2008) Automatic digital terrain model generation using Cartosat-1 stereo images. *Sensor Review*, 28, 299-310.

GLA - Greater London Authority (2008) *London's Central Business District: Its global importance.* London: Greater London Authority.

GLCF - Global Land cover Facility (2004) Landsat technical guide. *GLCF* [Online]. Available from: http://ftp.glcf.umd.edu/library/guide/techguide_landsat.pdf [Accessed 08 May 2011].

Goodchild (2007) Citizens as sensors: the world of volunteered geography. *GeoJournal*, 69, 211–221.

Google Inc. (2012) Google Earth (Version 6.2.2.6613) *Google Inc.* [Software]. Mountain View, CA: Google Inc.

Grohman, G., Kroenung, G., and Strebeck, J. (2006) Filling SRTM voids: The delta surface fill model. *Photogrammetric Engineering and Remote Sensing*, 72, 213–216.

Guillain, R. (2006) Changes in spatial and sectoral patterns of employment in Ile-de-France. 1978-97. *Urban studies,* 43, 2075-2098.

Haggett, P. (2001) *Geograhy: a global synthesis*. Harlow: Pearson Education Limited.

Haklay, M., and Weber, P. (2008) OpenStreetMap: User-Generated Street Maps. *IEEE Pervasive Computing*, 7, 12-18.

Halbert, L. (2006) The Paris region: polycentric spatial planning in a monocentric metropolitan region. *In*: Hall, P., and Pain, K., eds. *The Polycentric Metropolis: Learning from Mega-city Regions in Europe.* London: Earthscan Publications, 2006, 180-186.

Hall, P.G., and Pain, K. (2006) *The polycentric metropolis: Learning from mega-city regions in Europe.* Oxon: Routledge.

Haralick, R.M., Stanley, S.R., and Zhumang, X. (1987) Image Analysis Using Mathematical Morphology. *IEEE Transactions on pattern analysis and machine intelligence,* 9, 532-550.

Harris, C.D., and Ullman, E.L. (1945) The nature of cities. *Annals of the American Academy of Political and Social Science*, 242, 7-17.

Heiken, G., Fakundiny, R., and Sutter, J. (2003) *Earth Science in the City*. Washington D.C.: American Geophysical Union.

Heikkila, E., Gorden, P., Kim, J.I., Peisel, R.B., Richardson, H.W., and Dale-Johnson, D. (1989) What happened to the CBD-distance gradient. *Environment and Planning*, 21, 221-232.

Heineberg, H. (2001) *Stadtgeographie*. 2nd ed. Paderborn: UTB.

Herold, M., Couclelis, H., and Clarke, K.C. (2005) The role of spatial metrics in the analysis and modeling of land use change. *Computers, Environment and Urban Systems*, 29, 369-399.

Herold, M., Liu., C, and Clarke, K. (2003) Spatial metrics and image texture for mapping urban land use. *Photogrammetric Engineering and Remote Sensing*, 69, 991-1001.

Herold, M., Scepan, J., and Clarke, K. C. (2002) The use of remote sensing and landscape metrics to describe structures and changes in urban land uses. *Environment and Planning*, 34, 1443-1458.

Hirschmüller (2008) Stereo processing by semi-global matching and mutual information. *IEEE Transactions on pattern analysis and machine intelligence*, 30, 328-341.

Hoch, I., and Waddel, P. (1993) Apartment rents: Another challenge for the monocentric model. *Geographical analysis*, 25, 20-34.

Holt, J.B., and Lua, H. (2011) Dasymetric mapping for population and sociodemographic data redistribution. *In*: Yang, X., ed. *Urban Remote Sensing*. John Wiley & Sons, 2011, 195-208.

Hoyt, H. (1939) *The Structure and Growth of Residential Neighbourhoods in American Cities*. Washington: U.S. Government Printing Office.

Huang, J., Lu, X.X., Sellers, J.M. (2007) A global comparative analysis of urban form: Applying spatial metrics and remote sensing. *Landscape and urban planning*, 82, 184-197.

INSPIRE – Infrastructure for spatial information in the European Community (2012) Inspire Roadmap. INSPIRE [Online]. Available from: http://inspire.jrc.ec.europa.eu/index.cfm/pageid/44 [Accessed: 19 August 2012]

IPHS – International Planning History Society (2010) 14th IPHS Conference, 12-15 July 2012, Istanbul, Turkey: Urban transformation: Controversies, contrasts and challenges. *IPHS* [Online] Available from: http://www.iphs2010.com/img/image0021.jpg [Accessed 28 July, 2012].

Jensen, J.R. (2007) *Remote sensing of the environment: An earth resource perspective*. 2nd ed. London: Pearson Prentice Hall.

Jensen, J.R., and Cowen, D. (1999) Remote sensing of urban/suburban infrastructure and socioeconomic attributes. *Photogrammetric Engineering and Remote Sensing*, 65, 611-622.

Kaufman, L., and Rousseeuw, P.J. (1990) *Finding Groups in Data: An Introduction to Cluster Analysis:* Hoboken, NJ: John Wiley & Sons.

Kitmitto, K., Colin, C.V., Venters, C., Cooper, M.D., Muller, J.P., Morley, J.G., Walker, A.H., Rana, S. (2000) LANDMAP: Serving Satellite imagery to the UK academic. *University of Manchester* [Online]. Available from: http://tutor.nmmu.ac.za/uniGISRegisteredArea/ Intake13/Unit%204/kitmitto.pdf [Accessed 14 September 2011].

Knos, D.S. (1962) *Distribution of land values in Topeka, Kansas*. Lawrence: Center for Research in Business.

Kron, W. (2005) Flood risk = Hazard x Values x Vulnerability. *Water International*, 30, 58-68.

Longley, P.A., and Mesev, V. (2000) Measuring urban morphology using remotely-sensed imagery. *In:* Donnay, J.P., Barnsley., and Longley, P.A., eds. *Remote Sensing and Urban Analysis,* 2nd ed. Boca Raton: CRC Press, 2000, 148-168.

Marguilos, H.L. (2007) Commercial sub-markets in suburban Cuyahoga County, Ohio. *Urban Studies*, 44, 249-274.

Mas, J.F. (1999) Monitoring land cover changes: A comparison of change detection techniques. *International Journal of remote sensing*, 20, 139-152.

McColl, R.W. (2005) *Encyclopedia of World Geography*. New York: Infobase Publishing.

McDonald, J.F., and McMillen, P. (2010) *Urban economics and real estate: Theory and policy.* 2nd ed. Hoboken: John Wiley & Sons.

McGarigal, K., and Marks, B. (1995) FRAGSTATS: Spatial pattern analysis program for quantifying landscape structure. *University of Massachusetts Amherst* [Online] Available at: http://www.umass.edu/landeco/pubs/mcgarigal.marks.1995.pdf [Accessed 11 August 2011].

Miller, S.B. (2004) Photogrammetric products. *In:* McGlone, J., ed. *Manual of Photogrammetry*, 5th ed. Bethesda: ASPandRS, 847-854.

Muphey, E.M., and Vance, J.E: (1954b) A comparative study of nine Central Business Districts. *Economic Geography*, 30, 301-336.

Murphey, E.M., and Vance, J.E. (1954a) Delimiting the CBD. *Economic Geography*, 30, 189-222.

Murphey, R.E. (1971) *The Central Business District – a study in urban geography*. London: Aldine Transaction.

Murphey, R.E., Vance, J.E., and Epstein, B.J. (1955) Internal structure of the CBD. *Economic Geography*, 31, 21-46.

Netzband, M., and Rahman, A. (2009) Physical characterisation of deprivation in cities: How can remote sensing help to profile poverty (slum dwellers) in the megacity of Delhi/India. *In*: *In*: Proceedings of the Joint Urban Remote Sensing Event, Shanghai, China, 20-22 May 2009. Shanghai: URS/URBAN.

Netzband, M., Banzhaf, E., Höfer, R., and Hannemann, K. (2009) Identifying the poor in cities: how can remote sensing help to profile slums in fast growing cities and megacities? *IHDP Update*, 1, 22-28.

Netzband, M., Stefanov, W.L., and Redman, C. (2007) *Applied remote sensing for urban planning, governance and sustainability*. Berlin: Springer.

Ning, Y. (1984) An approach to shopping center location of Shanghai's urban area. *Acta Geographica Sinica*, 39, 163-172.

OSM – Open StreetMap (2012) OSM shapefile data – downloaded via QuantumGIS for the testsites Carnary Wharf, La Defense, and Istanbul. Open StreetMap [Online] Available at: http://www.openstreetmap.org/ [Accessed: 13 April 2012]

Pacione, M. (2005) *Urban geography: a global perspective*. 2nd ed. Oxon: Routledge.

Pan, X.Z., Zhao, Q.G., Chen, J., Liang, Y., and Sun, B. (2008) Analyzing the variation of building density using high spatial resolution satellite images: the example of Shanghai City. *Sensors*, 8, 2541-2550.

Pitzl, R.P. (2004) *Encylopedia of human geography*. Westport: Greenwood Press.

Radberger, S. (2001) *Monitoring der Verstädterung im Großraum Istanbul mit den Methoden der Fernerkundung und der Versuch einer räumlich-statistischen Modellierung*. Thesis (PhD). University of Göttingen, Faculty for Science of Forestry and Forest Ecology.

Reynolds, A.P., Richards, G., De La Iglesia, B., and Rayward-Smith, V.J. (2006) Clustering rules: a comparison of portioning and hierarchical clustering algorithms. *Journal of mathematical modeling and algorithms,* 475-504.

Richards, J.A., and Jia, C. (2006) *Remote Sensing Digital Image Analysis – An introduction*. Berlin: Springer.

Ridd, M.K. (1995) Exploring V-I-S (vegetation – impervious surfaces . soil) model for urban ecosystem analysis through remote sensing; comparative anatomy of cities. *International Journal of Remote Sensing*, 16, 2165-2185.

Roy, D., Borak, J., Devadiga, S.,Wolfe, R., Zheng, M., and Descloitres, J. (2002) The MODIS land product quality assessment approach. *Remote Sensing of Environment*, 83, 62−76.

Sassen, S. (2001) *The global city: New York, London, Tokyo*. 2nd ed. Princeton: Princeton University Press.

Sassen, S. (2002) Locating cities on global circuits. *In*: Sassen, S., ed. *Global Networks, Linked Cities*. London: Routledge, 2002, 1-38.

Schweitzer, F., and Steinbrink, J. (1998) Estimation of mega-city growth. *Applied Geography*, 18, 69-82.

Seger, M. (2012) Istanbul's Backbone - A Chain of Central Business Districts (CBDs). *In*: Serafeim, P. ed. *Urban Development*, InTech, 2012, 201-216.

Seger, M., and Palencsar, F. (2006) *Istanbul - Metropole zwischen den Kontinenten*. Borntraeger: Stuttgart/Berlin.

Shin, S.W. (2008) High-density spaces and living: Sustainable compact cities and high-rise buildings. *In*: Ng, E., ed. *Designing high-density Cities for Social and Environmental Sustainability*. London: Earthscan, 2010, 293-308.

Sirmacek, B., Taubenböck, H., Reinartz, P., and Ehlers, M. (2012) Performance evaluation for 3-D city model generation of six different DSMs from air- and spaceborn sensors. *IEEE Jounral of selected Topics in Applied Earth Observations and Remote Sensing*, 5, 59-70.

Sirmacek, B., D'Angelo, P., Kraus, T., and Reinartz, P. (2010) Enhancing Urban Digital Elevation Models Using Automated Computer Vision Techniques. *In*: ISPRS Commission VII Symposium, Vienna, 5 - 7 July 2010. Vienna: ISPRS.

Sliuzas, R., Mboup, G, and de Sherbinin, A. (2008) Report of expert group meeting on slum identification. Enschede: CIESIN/UN-Habitat.

Stolz, R. (1998) *Die Verwendung der Fuzzy Logic Theorie zur wissensbasierten Klassifikation von Fernerkundungsdaten*. Munich: Geobuch.

Streutker, D.R. (2002) A remote sensing study of the urban heat island of Houston, Texas. *International Journal of Remote Sensing*, 23, 2595–2608.

Sukopp. H., and Wittig, R. (1998) *Stadtökologie*. Stuttgart: Gustav Fischer Verlag.

Taubenböck, H. (2008c) Vulnerabilitätsabschätzung der erdbebengefährdeten Megacity Istanbul mit Methoden der Fernerkundung. Thesis (PhD). University of Würzburg.

Taubenböck, H. (2011) The global issue 'mega-urbanization': An unsolvable challenge for stakeholders, researchers and residents? In: International Archives of the Photogrammetry, Remote Sensing and Spatial Information Sciences (UDMS) - Urban Data Management Symposium, Delft, 28-23 September 2011. Delft: UDMS.

Taubenböck, H., Esch, T., Felbier, A., Wiesner, M., Roth, A., and Dech, S. (2012) Monitoring urbanization in mega cities from space. *Remote Sensing of the Environment*, 117, 162-176.

Taubenböck, H., Esch, T., Wurm, M., Roth, A., and Dech, S. (2010) Object-based feature extraction using high spatial resolution satellite data of urban areas. *Journal of Spatial Science*, 55, 117-132.

Taubenböck, H., Esch, T., Wurm, M., Thiel, M., Ullmann, T., Roth, A., Schmitdt, M., Mehl, H., and Dech, S. (2008a) Urban structure analysis of mega city Mexico City using multisensoral remote sensing data. *In:* Proceedings of SPIE Europe Remote Sensing, Cardiff, Wales, 15-18 September 2008. Cardiff: SPIE.

Taubenböck, H., Wegmann, M., Berger, C., Breunig, M., Roth, A., and Mehl, H. (2008b): Spatiotemporal analysis of Indian megacities. *In*: Proceedings of the International Archives of the Photogrammetry - Remote Sensing and Spatial Information Sciences (ISPRS), Beijing, China, 3 July 2008. Beijing: ISPRS.

Taubenböck, H., Wegmann, M., Roth, A., Mehl, H., and Dech, S. (2009) Urbanization in India – spatiotemporal analysis using remote sensing. *Computers, Environment and Urban* Systems, 33, 179-188.

Thieken, A.H., Müller, M., Kleist, L., Seifert, I., Borst, D., and Werner, U. (2006) Regionalisation of asset values for risk analysis. *Natural Hazards and Earth System Sciences*, 6, 167-178.

Thomas, R.W., and Hugget, R.J. (1980) *Modelling in Geography: a mathematical approach.* Totowa, NJ: Barnes and Noble Books.

Thurstain-Goodwin, M., and Batty, S. (1998) GIS and town centres: Exploratory environments involving experts and users. *Built Environment*, 24, 43-56.

Thurstain-Goodwin, M., and Unwin, D.J. (2000) Defining and delineating the central areas of towns for statistical monitoring using continuous surface representations. *Transactions in GIS*, 4, 305-318.

Trimble GmbH (2011a) *eCognition Deceloper 8.7 – Reference book.* Munich: Trimble GmbH.

Trimble GmbH (2011b) eCogniton Developer (Version 8) *Trimble* [Software]. Munich: Trimble Germany GmbH.

Trip, J.J. (2007) *What makes a city? Planning for "quality of Place" : the Case of High-speed Train Station Area Redevelopment.* Amsterdam: IOS Press.

Tukey, J.W. (1970) *Exploratory Data Analysis.* London: Addison-Wesley Publishing Company.

UKMap © The Geoinformation Group (2012) Building heights. *Licensed by The GeoInformation Group, received and distributed by the Landmap service of Mimas at the University of Manchester* [Online]. Available from: http://www.landmap.ac.uk/index.php/Datasets/ Building_Heights/Building-Heights-Download/menu-id-100339.html [Accessed: 11 April 2012].

UN – United Nations (2007) *World urbanisation prospects, the 2007 revision*. New York: United
      Nations.

UN – United Nations (2012a) *World urbanisation prospects, the 2011 revision*. New York: United
      Nations.

UN – United Nations (2012b) Population estimates and projections section - Online data: Urban
      agglomerations. *United Nations, Department of Economic and Social Affairs – Population Division*
      [Online]. Available from: http://esa.un.org/unpd/wup/unup/index_panel2.html
      [Accessed: 9 August 2012]

Waddel, P., Berry, J.L., and Hoch, I. (1993) Residential property values in a multinodal urban
      area: new evidence on the implicit price of location. *Journal of Real Estate, Finance and
      Economics*, 7, 117-141.

Wang, Z., and Schenk, T. (2000) Building extraction and reconstruction from lidar data.
      International Archives of Photogrammetry and Remote Sensing, 33, 958-964.

Waugh, D. (2000) *Geography – an integrated approach*. 3rd ed. Cheltenham: Nelson Thornes.

Wegmann, M., Taubenböck, H., Besser, T., Shapiro, Au., Ziegler, St., Rajashekariah, K., Esch, T.,
      and Dech, S. (2011) Sprawling crisis? Exploring crossroads of urban growth and natural
      environments with earth observation. *In:* Proceedings of the 34th International
      Symposium on Remote Sensing of Environment, Sydney, 10-15 April 2011. Sydney:
      ISRSE 2011.

Weng, Q. (2008) Remote Sensing of Impervious Surfaces: An Overview. *In:* Weng, Q., ed. *Remote
      sensing of impervious surfaces*. Boca Raton: CRC Press, 2008, xv-xvi.

Weng, Q., and Quattrochi, D. (2007) *Urban Remote Sensing*. Boca Raton: CRC Press.

Wu, C., and Murray, A.T. (2003) Estimating impervious surface distribution by spectral mixture
      analysis. *Remote Sensing of Environment*, 64, 493-505.

Wu, S., Qiu, X., and Wang, L. (2007) Population estimation methods in GIS and Remote
      Sensing: A review. *GIScience and Remote Sensing*, 42, 1548-1603.

Wünsch, A., Hermann, U., Kreibich, H., and Thieken, A.H. (2009) The role of disaggregation of
      asset values in flood loss estimation: A comparison of different modeling approaches at
      the Mulde River, Germany. *Environmental Management*, 44, 524-541.

Wurm, M., and Taubenböck, H., (2010) Fernerkundung als Grundlage zur Identifikation von
      Stadtstrukturtypen. *In:* Taubenböck, H., and Dech, S., eds. *Fernerkundung im urbane Raum*.
      Darmstadt: WBG, 2010, 94-103.

Wurm, M., Taubenböck, H., and Dech, S. (2009) Urban structuring using multisensoral remote sensing data. *In*: Proceedings of the Joint Urban Remote Sensing Event, Shanghai, China, 20-22 May 2009. Shanghai: URS/URBAN.

Wurm, M., Taubenböck, H., Schardt, M., Esch, T., and Dech, S. (2011) Object-based image information fusion using multisensor earth observation data over urban areas. *International Journal of Image and Data Fusion*, 2, 121-147.

Yager, R. (1987) *Fuzzy sets and applications: Selected Papers.* New York: John Wile and Sons.

Yigitcanlar, T., Velibeyoglu, K., and Baum, S. (2008) *Creative urban regions: Harnessing Urban Technologies to Support Knowledge City Initiatives.* London: IGI Global.

Zheng, B. (2009) Recognition of the city's centricity: density estimation in the commerce arrangement. *In*: International Conference on Management and Service Science, Wuhan 20-22 September 2009. Wuhan: MASS.

Appendix 1 – Geography Research Ethics Screening Form

Department of Geography Research Ethics Screening Form
King's College London

> **Please Note: Filling out this *Geography Research Ethics Screening Form* does NOT constitute *College Ethics Approval*.**

This *Geography Research Ethics Screening Form* will help you to determine if you must submit a *Research Ethics Application* to the *College Research Ethics Committees* before starting your research, under the guidelines for working with human participants set out by the Social Sciences, Humanities & Law Research Ethics Sub-Committee (SSHL RESC), and the Geography, Gerontology and Social Care Workforce Research Unit Panel (GGS REP).

In order to complete this process, please
(a) Familiarise yourself with the professional research ethics guidelines of *The British Sociological Association*: http://www.britsoc.co.uk/equality/ (Statement of Ethical Practice)
(b) Read "Which kinds of research require ethical approval through the KCL Research Ethics Committees?" (p. 2 of this form).
(c) Answer the questions in Table 1 below:
(d) Return the signed *Geography Ethics Screening form* to the Geography Department office and place a copy in Appendix 1 of your IGS/dissertation.
(e) If ethics approval is needed (answering 'yes' to question 2 in Table 1), you must apply for ethics approval through the appropriate *College Research Ethics* committee, and not start ANY research until ethics approval has been granted in writing.

Table 1. Department of Geography Research Ethics Screening Questions.

1) Have you read and familiarised yourself with the professional research guidelines of *The British Sociological Association*?	☒ Yes ☐ No
2) Does your research "involve human participants" and/or "raise other ethical issues with potential social or environmental implications"?	☐ Yes ☒ No

If you answered 'No' to question two, you do not need to submit your research for ethical review. If you answered 'Yes' to question two, please use the flowchart on http://www.kcl.ac.uk/innovation/research/support/ethics/about/index.aspx to establish your risk level and where you need to apply (see Table 2).

Table 2. Three levels of risk for project types, and how to obtain College Research Ethics clearance.

Project type	How to submit?
Low risk:	Can be reviewed using an on-line process. The process includes guidelines and prompts to help ensure your project is low-risk: http://www.kcl.ac.uk/innovation/research/support/ethics/committees/sshl/lowrisk/index.aspx
Moderate risk: Uncertain risk:	Should be submitted to the Geography, Gerontology and Social Care Workforce Research Unit Panel (GGS REP): http://www.kcl.ac.uk/innovation/research/support/ethics/committees/sshl/panels/gsshm.aspx
High risk:	Should be submitted to the Social Sciences, Humanities and Law Research Ethics Sub-Committee (SSHL RESC): http://www.kcl.ac.uk/innovation/research/support/ethics/committees/sshl/highrisk/index.aspx

In all cases, even if 'no' risk, you **MUST** sign and return this *Geography Research Ethics Screening Form* to be kept on file with the Department Office, and if an Undergraduate or Masters student, submit a copy of this at the end (as part of Appendix 1) of your IGS or Dissertation. In cases where there is low, moderate or high risk, **you MUST complete the *College Research Ethics Application* at least one month before you intend to start your research** and obtain written approval from them BEFORE carrying out any research.

> Carrying out research without ethical approval by the College Ethics Committee may result in a charge under misconduct regulations as "*action that deviates from accepted institutional, professional, academic or ethical standards will be regarded as misconduct and an infringement of these regulations*" "Academic regulations, Regulations concerning students & General regulations" B3 – 1.1, King's College London. You should note that your research will not be covered by the College's insurance until you have completed the College ethical review process. This means that unless you receive ethical approval for your research, if a participant makes a legal claim regarding the research, then you would be personally liable. It is your responsibility to submit your research for *College Ethical Review* in good time to carry out any research.

Name: _~~Kt. Ulotz~~ Martin Klotz_ Student Card No: _1162118_

Provisional IGS/dissertation title: _Analysis of physical building parameters from high resolution remotely sensed DSMs to support CBD delineation_

Signature: _M. Ulotz_ Date: _11/04/2012_

Appendix 2 – Geography Risk Assessment Form

KCL Department of Geography: Risk Assessment form (Individual Research and Fieldwork) [This form updated 8 April 2012]

Page **2** of **9**

3 RISK ASSESSMENT FORM AND ASSOCIATED DOCUMENTATION

This page <u>must be completed</u> for all fieldwork taking place outside the Department of Geography, any laboratory work inside the College premises and ALL student dissertation projects, whether human or physical, and whether undergraduate, postgraduate taught or postgraduate research.

AFTER reading through ALL risk categories, please sign RISK TYPE A or B below, which applies to you.

RISK TYPE A. I have considered ALL categories in this form and I declare that I am undertaking a student project/dissertation where NONE of my research will be outside of college premises or home, and will not involve any of the risks identified in ANY of the categories of this risk assessment form. For example, the research wholly involves library/archival research or analysis of existing on-line/other data. None of the risks of my project/dissertation are greater than in everyday life and normal activities. Should my research project change, such that there risks involved, it is my responsibility to fill out this form appropriately and obtain the appropriate signatures for Risk Type B.

SIGNATURES OF PERSON FILLING IN A RISK ASSESSMENT AND COUNTERSIGNATURE.
A. Person filling in this risk assessment
Name (Typed or printed in BLOCK letters):
Signature:
Date:
B. Countersignature and date
(Students – Research Supervisor; Research Staff – Project Leader; Academic Staff – Head of Department)
Name (Typed or printed in BLOCK letters):
Signature:
Date:

Print this page in triplicate; the three copies signed and countersigned, and lodged with:
  (1) Your supervisor.
  (2) The Department Office.
  (3) One for retention by yourself.
For UGT and PGT students, this signatures page of your risk assessment must be included in Appendix 1 of your dissertation.

RISK TYPE B. I have considered ALL categories in this form, indicated which risks apply to me that are greater than in everyday life and normal activities (writing yes/no for every section), for those sections where I have answered 'yes' I have indicate the degree of risk from 1–5 (1=low, 5=high), where appropriate added notes and indicated other additional risks in the final section.

SIGNATURES OF PERSON FILLING IN A RISK ASSESSMENT AND COUNTERSIGNATURE.
A. Person filling in this risk assessment
Name (Typed or printed in BLOCK letters): Martin Klotz
Signature: *M. Klotz*
Date: 11 April, 2012
B. Countersignature and date
(Students – Research Supervisor; Research Staff – Project Leader; Academic Staff – Head of Department)
Name (Typed or printed in BLOCK letters): Dr Martin Wooster
Signature: *MJW*
Date: 13/4/12

All pages in this form except for p. 1 should be printed in triplicate, the three copies signed and countersigned, and lodged with:
  (1) Your supervisor.
  (2) The Department Office.
  (3) One for retention by yourself before fieldwork commences.
For UGT and PGT students, this signatures page of your risk assessment must be included in Appendix 1 of your dissertation.

For work outside of the UK, please do not forget to obtain insurance in accordance with College regulations (application form http://www.kcl.ac.uk/about/structure/admin/finance/staff/insurance/travel.html).

Appendix 3 – Landsat datasets

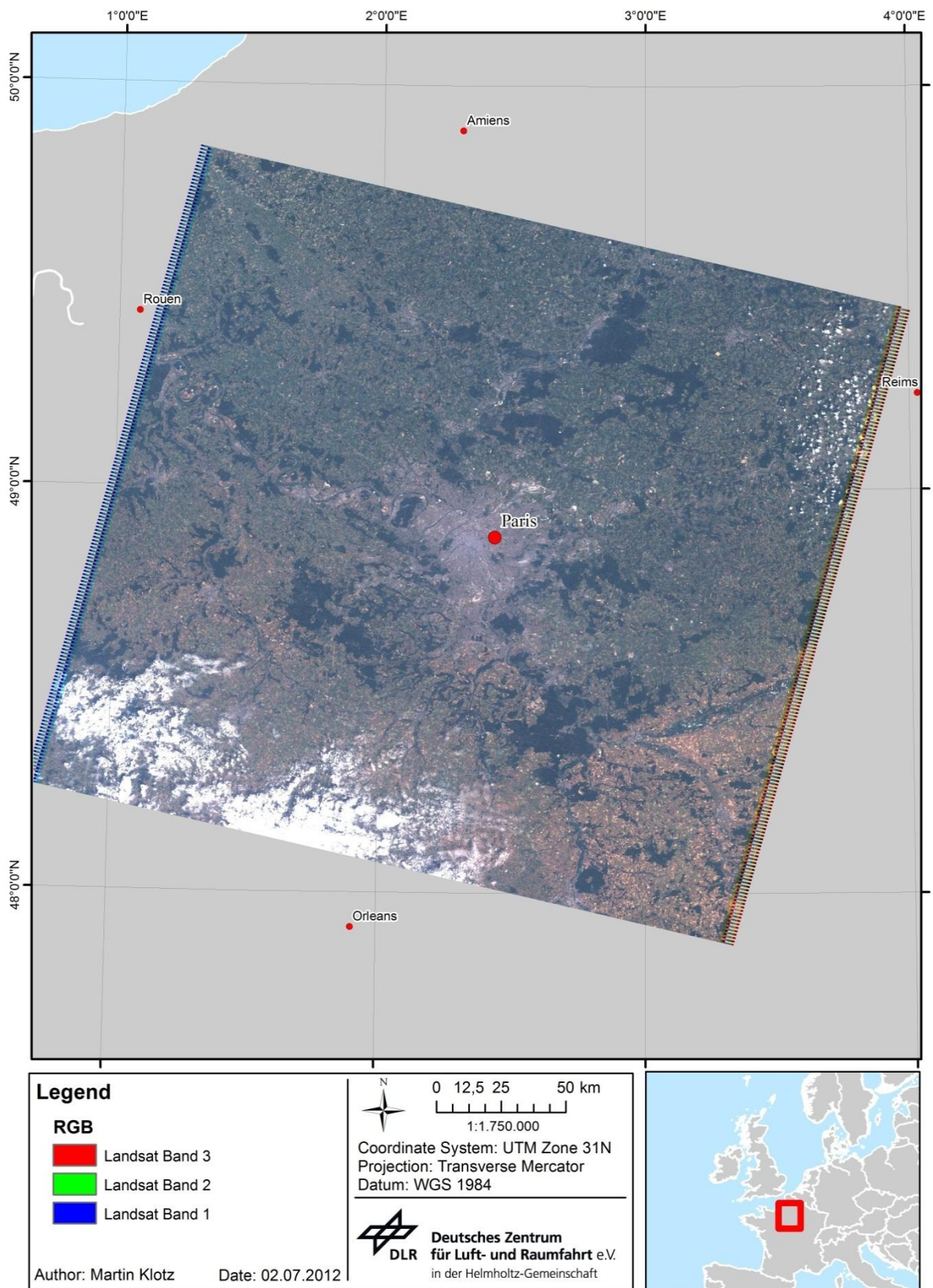**Fig. A3-1** Landsat TM scene, London, 2011

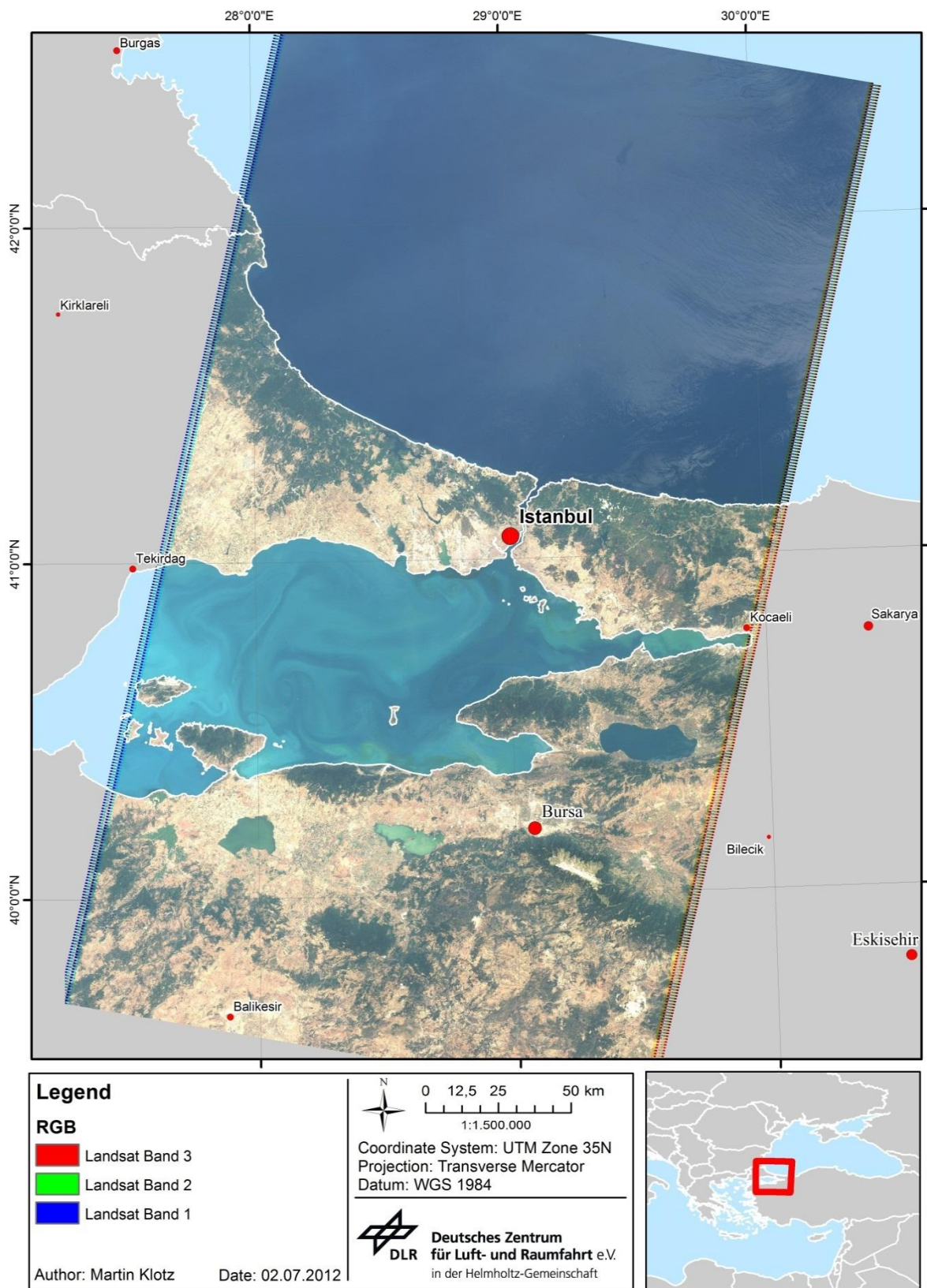**Fig. A3-2** Landsat TM scene, Paris, 2006

Fig. A3-3 Landsat TM mosaic, Istanbul, 2003
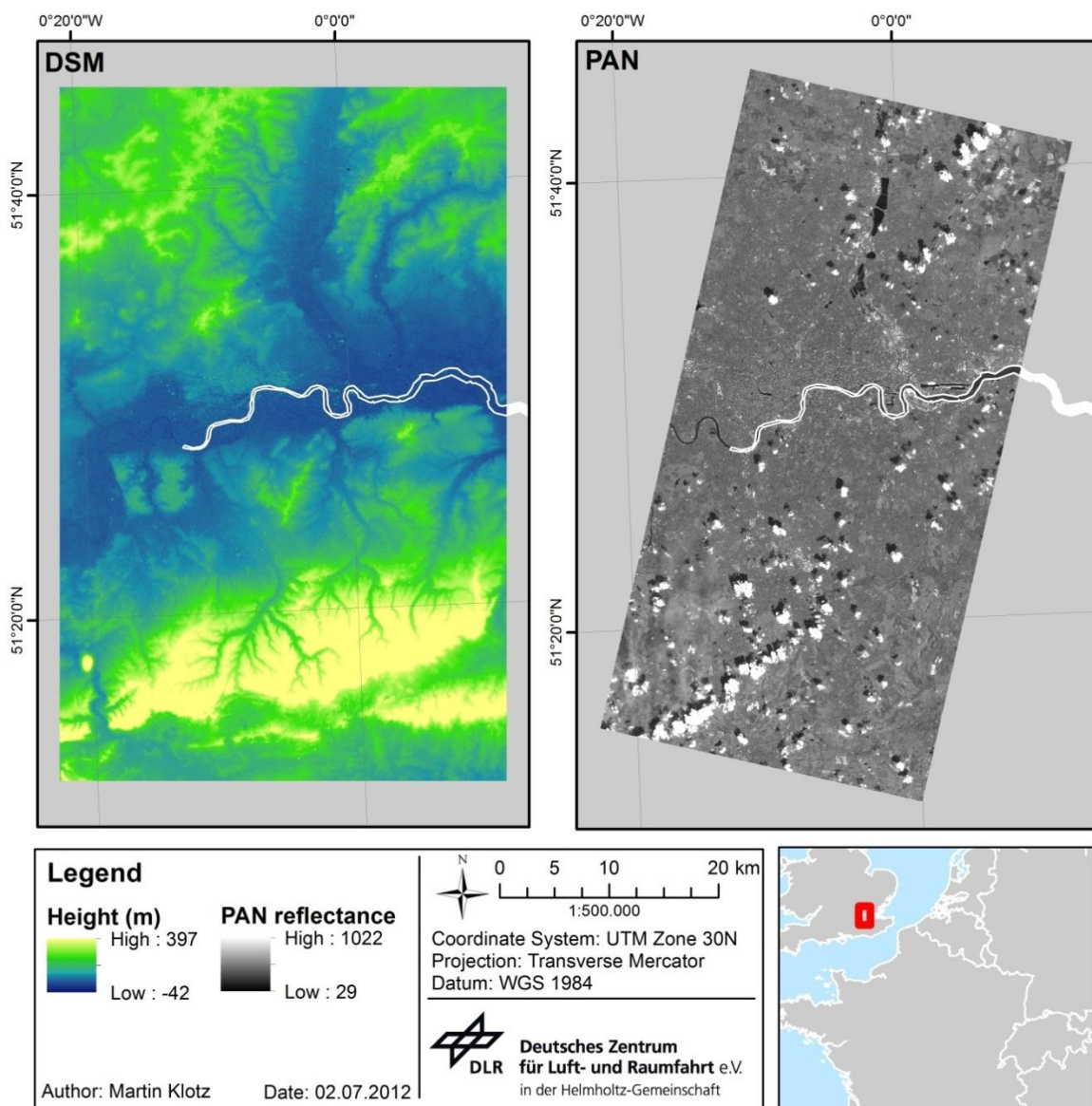
Appendix 4 – Cartosat-1 datasets

Fig. A4-1 Cartosat-1 DSM and PAN Fore image mosaic, London

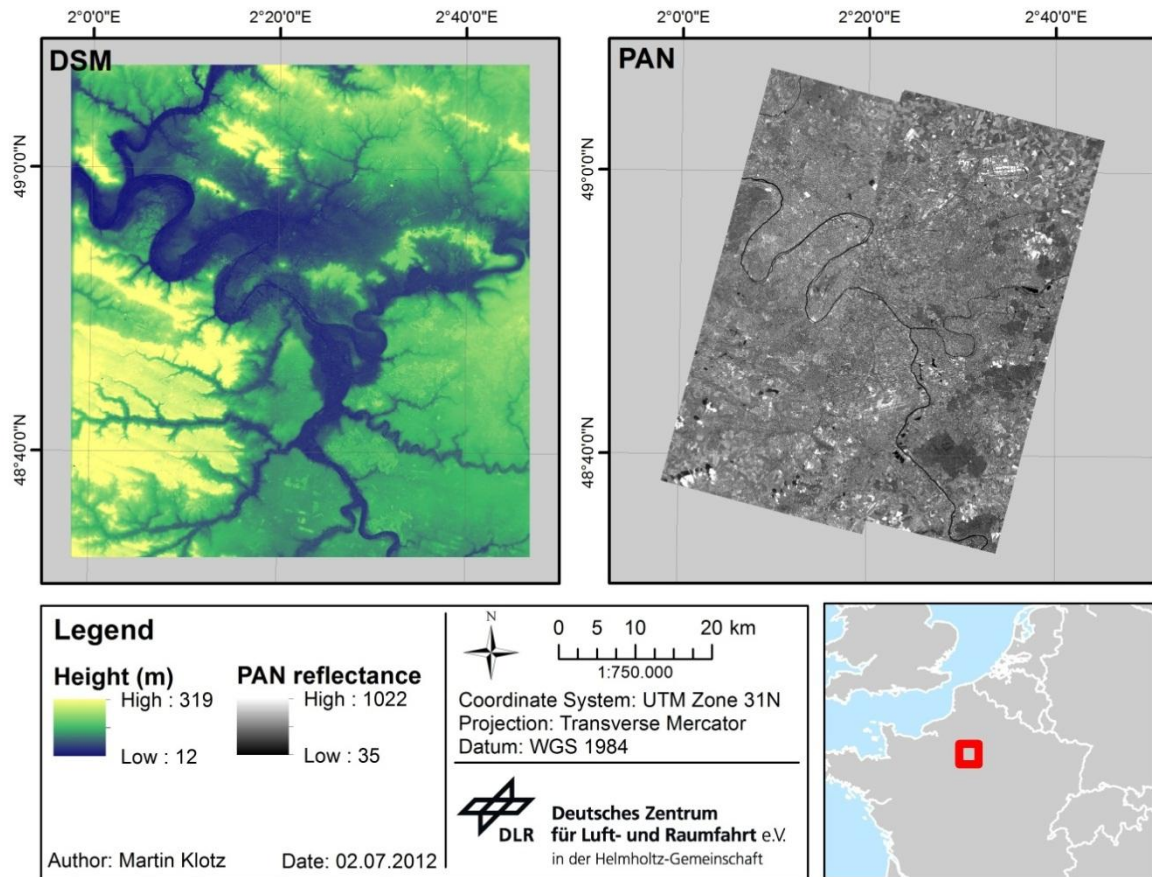**Fig. A4-2** Cartosat-1 DSM and PAN Fore image mosaic, Paris

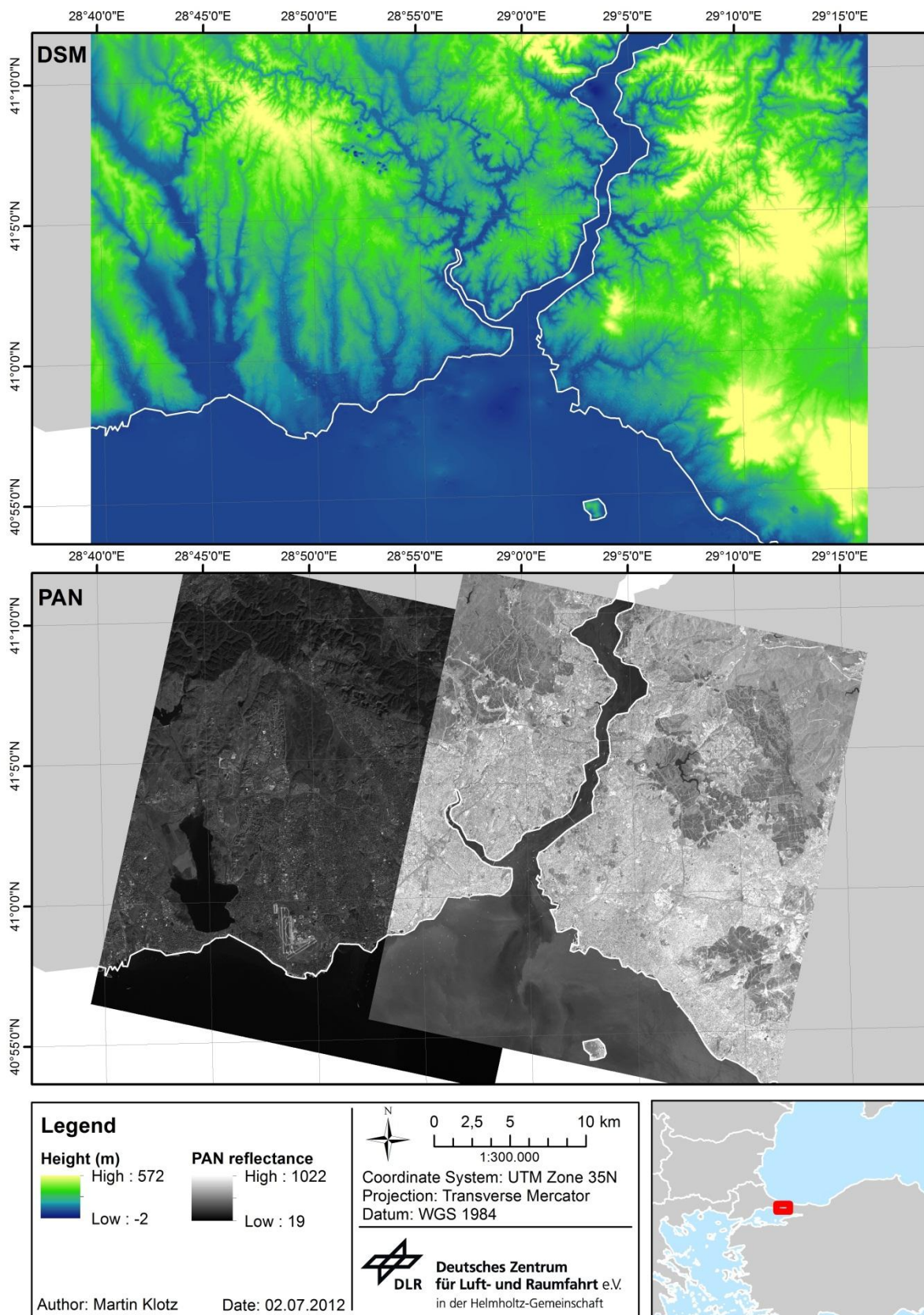**Fig. A4-3** Cartosat-1 DSM and PAN Fore image mosaic, Istanbul

Fig. A4-3 Cartosat-1 DSM and PAN Fore image mosaic, Istanbul

Appendix 5 – Partitioning around medoids (R: source code)

```r
install.packages("foreign")
install.packages("Cairo")
install.packages("vegan")
install.packages("cluster")
install.packages("tree")
install.packages("QuantPsyc")

library(foreign)
library(Cairo)
library(vegan)
library(cluster)
library(tree)
library(QuantPsyc)

# Set working directory
setwd ("E:/klotz_martin/Dissimilarity")

# Read input table
data <- read.table("E:/klot_ma/08_Dissimilarity/BuildingParamters.csv", header=TRUE, sep=";")

# Z-Transformation of variables
data.z <- as.data.frame(Make.Z(data[,c(3:ncol(data))]))

# Generate subset (Building parameters in columns 1-6)
data.sub <- as.data.frame(data.z[,c(1:6)])


### Cluster analysis ###

# Generate Dissimilarity Matrix
data.diss <- daisy(data.sub, metric="euclidean", stand=T)

# Clustering (PAM)
data.pam <- pam(data.diss, 2, diss=T, metric="euclidean", stand=F)

# Join clustering results with input data
data$dispam <- data.pam$clustering

### Visualistation (Boxplots) ###

boxplot(data$Max_height~data$CITY, ylab = "Maximum height (m)")
boxplot(data$Max_vol~data$CITY, ylab = "Maximum volume (m³)")
boxplot(data$Avg_vol~data$CITY, ylab = "Average volume(m³)")
...


### Export ###
write.dbf(data, file="BuildingParameters_clustered.dbf")
```

Appendix 6 – Advanced DTM evaluation

Kernel	Min.	Max.	Mean	Std. Dev.	RMSE
3	-28.32	28.27	0.74	3.41	3.49
5	-31.23	28.22	-0.25	3.17	3.17
10	-33.97	27.19	-1.62	2.92	3.34
20	-36.21	24.21	-4.06	3.10	5.10
30	-40.44	24.16	-5.67	3.47	6.65
40	-43.89	24.03	-6.91	3.93	7.94
50	-43.89	24.02	-7.91	4.27	8.99
75	-42.89	19.69	-10.41	5.11	11.58
100	-43.89	19.42	-12.10	5.60	13.30
150	-43.89	15.25	-15.61	5.89	16.67
200	-43.89	5.80	-18.14	5.58	18.97

**Tab. A6-1** Advanced statistical evaluation of the produced DTM in relation to varying kernel size, Carnary Wharf
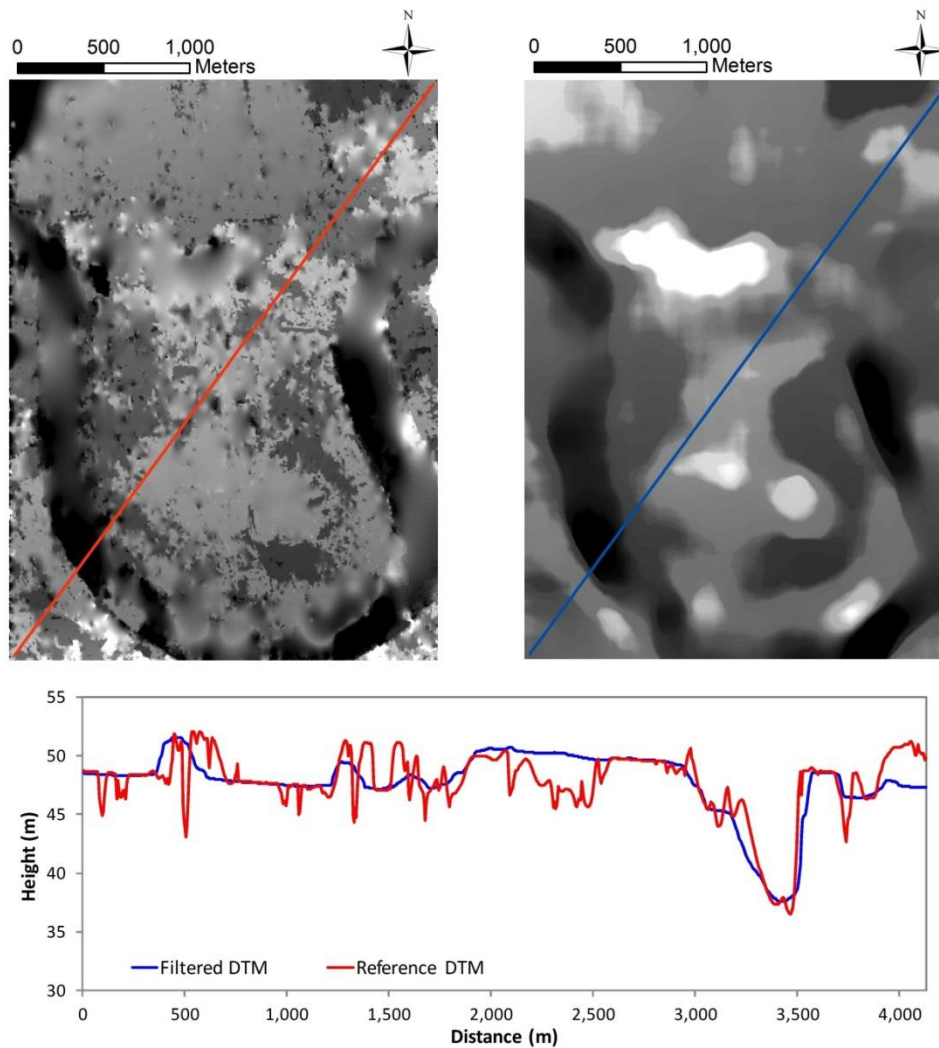
Fig. A6-1 Advanced DTM quality assessment by profile lines, Carnary Wharf (kernel size: 5x5 pixel)

Kernel	Min.	Max.	Mean	Std. Dev.	RMSE
3	-18.58	68.11	1.51	4.36	4.61
5	-21.25	68.04	-0.23	4.19	4.18
10	-26.23	68.01	-2.14	4.20	6.64
20	-30.20	64.97	4.87	4.51	8.23
30	-30.39	64.27	-6.59	4.93	9.58
40	-39.18	60.50	-7.86	5.48	9.54
50	-45.78	60.38	-9.14	6.16	11.00
75	-47.28	52.94	-11.99	7.19	13.96
100	-49.98	45.44	-14.31	8.08	16.40
150	-51.48	34.91	-17.87	9.60	20.27
200	-52.80	26.39	-21.57	10.54	24.00

Tab. A6-2 Advanced statistical evaluation of the produced DTM in relation to varying kernel size, La Defense
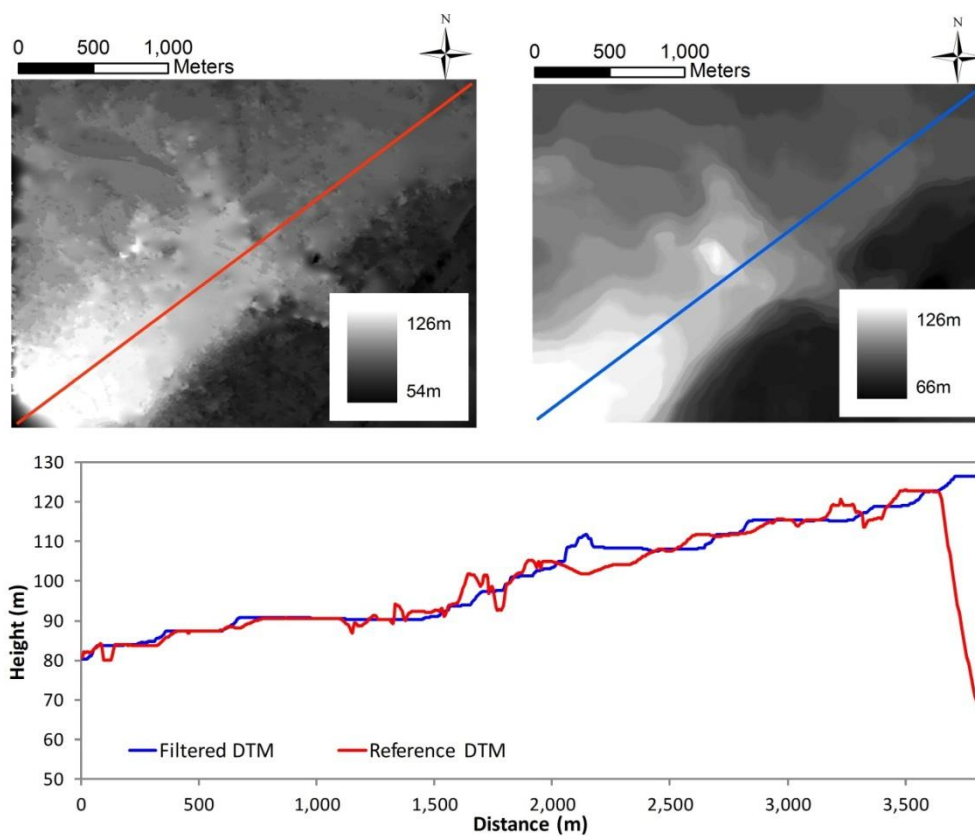
Fig. A6-2 Advanced DTM quality assessment by profile lines, La Defense (kernel size: 5x5 pixel)

Kernel	Min.	Max.	Mean	Std. Dev.	RMSE
3	-51.04	49.07	0.47	5.60	7.67
5	-53.55	48.69	-1.36	5.58	8.93
10	-56.71	44.92	-4.05	5.89	7.14
20	-63.73	34.13	-8.83	7.36	11.49
30	-67.70	30.63	-12.84	8.99	15.67
40	-76.86	24.25	-16.28	10.30	19.26
50	-79.59	21.88	-19.22	10.88	22.07
75	-79.59	19.64	-24.90	11.76	27.53
100	-83.79	19.64	-29.43	12.59	32.00
150	-84.06	19.64	-38.11	13.48	40.41
200	-102.83	19.64	-45.70	15.94	48.39

Tab. A6-3 Advanced statistical evaluation of the produced DTM in relation to varying kernel size, Levent
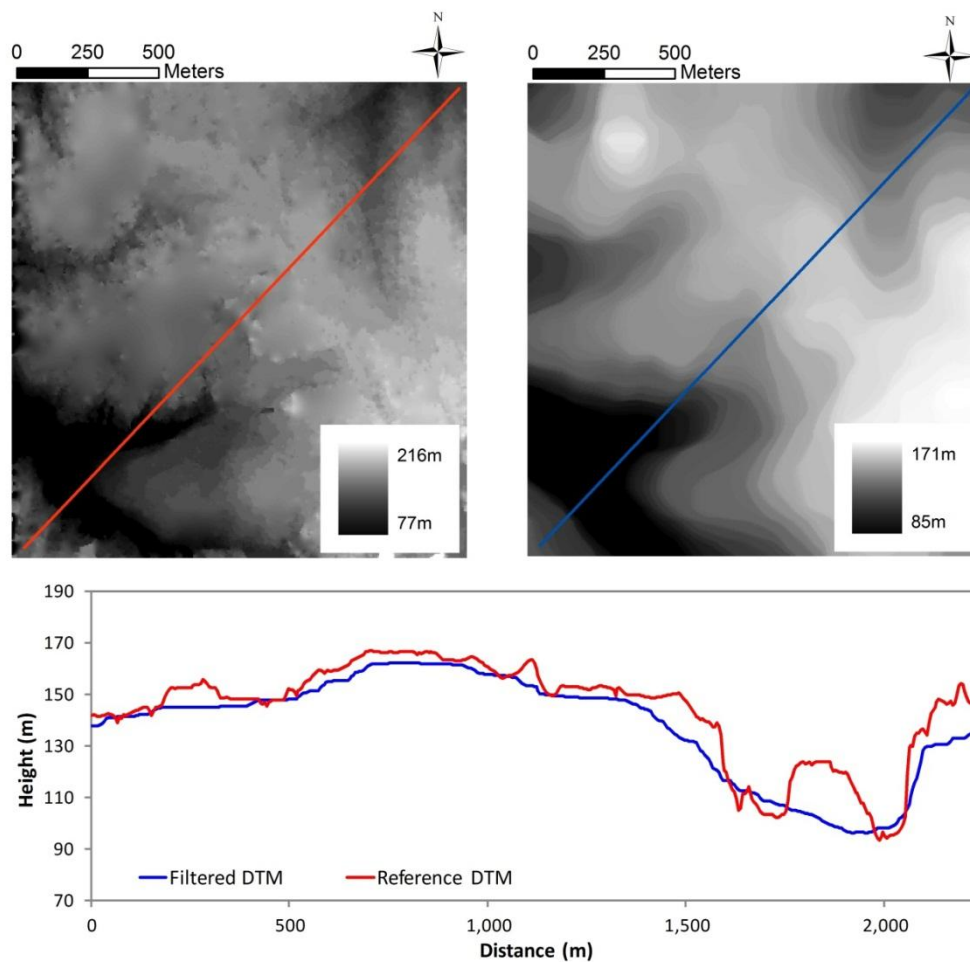

Fig. A6-3 Advanced DTM quality assessment by profile lines, Levent (kernel size: 10x10 pixel)